To the Graduate Council:

I am submitting herewith a dissertation written by Jay Gregory entitled "NMR Studies of the Active Site Geometry of Yeast Phosphoglycerate Kinase." I have examined the final copy of this dissertation for form and content and recommend that it be accepted in partial fulfillment of the requirements for the degree of Doctor of Philosophy with a major in Biochemistry.

Engin Serpersu

Engin H. Serpersu, Major Professor

We have read this dissertation
and recommend its acceptance:

Daniel W. Bolen

Jack B. Chaudhuri

Salon Georghiou

Accepted for the Council:

Lewis Winkel

Associate Vice Chancellor
and Dean of The Graduate School

NMR STUDIES OF THE ACTIVE SITE GEOMETRY OF YEAST PHOSPHOGLYCERATE KINASE

A Dissertation
Presented for the
Doctor of Philosophy
Degree
The University of Tennessee, Knoxville

Jay Gregory
August, 1993

DEDICATION

Dedicated to my wife,
Donna Goodwin-Gregory,
and to my daughter, Emma Gregory,
with deep appreciation for
their love and support.

ACKNOWLEDGEMENTS

I would like to express my sincere appreciation to my major professor, Dr. Engin Serpersu, for patient guidance throughout the course of my research, and for recognizing the best times for letting me find my own way. I would also like to thank Dr. Craig Barnes and the members of my commitee, Drs. Dan Roberts, Jorge Churchich, and Solon Georghiou, for their fresh perspectives and their encouragement.

No list of acknowledgements would be complete without thanking those alongside whom I have lived the "graduate school experience". In particular, I am grateful to Celeste Shibata for showing me that any situation where poetry is inappropriate is indeed a bad situation. Also, I thank Amanda Dion for recognizing when I was full of bull, and for telling me so. I am also particularly indebted to Dave Weaver for encouraging me to take out my mind and dust it off, and for not recoiling in horror at what occasionally fell out.

Finally, I would like to attempt to express my gratitude to those people whose gifts to me are greater than anything I could give in return. I am deeply grateful to Ann for changing my life in ways I am only beginning to recognize. I thank my mother, Phyllis Marie Burk, and my father, Drenon Dwain Gregory, for their love, and for giving me ability and motivation. Above all, I would like to thank my wife Donna and my daughter Emma for making it all worthwhile, every day.

Abstract

The active site geometry of yeast phosphoglycerate kinase (PGK) was investigated using various nuclear magnetic resonance methods. β,γ-bidentate CrATP, a stable, exchange-inert metal-nucleotide analog, was used as a probe of the conformation of 3-phospho-D-glycerate (3PGA) at the active site of PGK. The paramagnetic effects of Cr^{3+} on the longitudinal relaxation rates ($1/T_{1p}$) of the ^{1}H, ^{31}P and ^{13}C nuclei of 3PGA were examined in order to determine the distances between enzyme-bound CrATP and the nuclei of 3PGA in the ternary PGK·CrATP·3PGA complex. Kinetic studies indicated that K_i^{CrATP} was dependent on the concentration of 3PGA, and the dependence was abolished in the presence of activator sulfate ion. Similarly, NMR studies showed that the environment of CrATP bound at the active site was altered by the presence of sulfate ion.

The metal nucleus distances determined from paramagnetic NMR studies show the close proximity of the substrates at the active site of PGK, which is consistent with a hinge-bending conformational change of the enzyme for bringing the two substrates together. Additionally, the presence of an activating concentration of sulfate was observed to cause significant changes in both the relative Cr^{3+}-3PGA distances and the overall conformation of 3PGA when compared to the findings in the absence of sulfate. This is consistent with

the active site being in a "less closed" configuration when sulfate is present. Under both conditions, models can be constructed which allow for direct transfer of a phosphoryl group between the bound substrates.

Two-dimensional studies of the nuclear Overhauser effect (TRNOESY) between the protons of 2'deoxy-ATP (dATP) were used to delineate the ribose conformation and the glycosidic angle of the nucleotide bound in a ternary PGK·MgdATP·glycerol-3-phosphate complex. The resulting structure indicated an O4'-endo conformation for the ribose ring and a glycosidic angle of 59°. Additionally, the dependence of the observed NOE intensities and the corresponding calculated distances was analyzed as a function of the mixing time for NOE development and of the [substrate]/[protein] ratio. It was observed that no single mixing time was adequate for reliable estimation of initial cross-relaxation rates for all interproton NOE's observed, and that although spin diffusion can be effectively circumvented for longer periods at higher [substrate]/[protein] ratios, the lack of NOE constraints under these conditions make distance calculations unreliable. The results suggest that an in-depth analysis of this type should be performed for NOE conformational studies in order to obtain the best possible structure. The results suggest that the use of a perdeuterated enzyme system as described in this study is essential for accurate estimation of cross-relaxation rates at low [substrate]/[protein] ratios.

TABLE OF CONTENTS

LIST OF TABLES

LIST OF FIGURES

LIST OF ABBREVIATIONS

A-D, analog to digital; ADP, adenosine 5′-diphosphate; **AMP**, adenosine 5′-monophosphate; **Arg**, arginine; **ATP**, adenosine 5′-triphosphate; **1,3-bisPGA**, 1,3-bisphosphoglycerate; **CD**, circular dichroism; **cpm**, counts per minute; **CrATP**, β,γ-bidentate $CrATP(H_2O)_4$; **2D**, two-dimensional; **dATP**, 2′deoxyadenosine 5′-triphosphate; **DNA**, deoxyribonucleic acid; **DNAse**, deoxyribonuclease; **DSS**, 3-(trimethylsilyl) propanesulfonic acid; **EDTA**, ethylene diamine-tetraacetic acid; **EPR**, electron paramagnetic resonance; **G-3-P**, glycerol-3-phosphate; **GAPDH**, glyceraldehyde-3-phosphate dehydrogenase; **His**, histidine; **^{2}HPGK**, perdeuterated yeast phosphoglycerate kinase; **Lys**, lysine; **MES**, 2-(N-morpholino) ethanesulfonic acid; **MgADP**, bidentate complex of Mg^{2+} with ADP; **MgATP**, bidentate complex of Mg^{2+} with ATP; **MgATPβS**, bidentate complex of Mg^{2+} with ATP which is sulfur-substituted at the β-position; **MW**, molecular weight; **NAD^+**, nicotinamide adenine dinucleotide; **NADH**, nicotinamide adenine dinucleotide, reduced form; **NMR**, nuclear magnetic resonance; **NOE**, nuclear Overhauser effect; **NOESY**, nuclear Overhauser effect spectroscopy; **PDB**, Protein Data Bank; **2PGA**, 2-phospho-D-glycerate; **3PGA**, 3-phospho-D-glycerate; **PGK**, yeast phosphoglycerate kinase; **RF**, radio frequency; **RMS**, root mean square; **RNAse**, ribonuclease; **SDS**, sodium dodecyl sulfate; **S_N1**, unimolecular nucleophilic substitution; **S_N2**, bimolecular nucleophilic substitution; **TCA**,

trichloroacetic acid; **Tris**, Tris(hydroxymethyl)aminoethane; **TRNOESY**, transferred nuclear Overhauser effect spectroscopy; **UV**, ultraviolet.

Chapter I

Introduction

Phosphoglycerate kinase (PGK; EC 2.7.2.3) catalyzes the reversible phosphoryl transfer reaction (1):

$$\text{1,3-bisphospho-D-glycerate} + \text{ADP} \underset{}{\overset{Mg^{2+}}{\rightleftharpoons}} \text{3-phospho-D-glycerate} + \text{ATP}$$

This reaction is the first ATP-generating step of the glycolytic pathway. As a result of its vital metabolic role, PGK has been the subject of extensive study, and major research efforts have focused on the enzyme's structure, catalytic mechanism, and kinetic behavior.

In its catalytically active form, PGK exists as a monomer of molecular weight approximately 47,000. The enzyme is arranged in a "dumbell" shape, wherein two globular domains (corresponding to the amino- and carboxy- terminal halves) of approximately equal size are connected by a narrow waist region (2). Previous structural studies of phosphoglycerate kinase have been ambiguous regarding the locations and relative orientation of the substrates bound at the active site. Crystals of yeast PGK suitable for X-ray crystallographic studies were grown in solutions containing high concentrations of ammonium sulfate, but would not grow in

the presence of MgATP or MgADP (3). Attempts to locate the metal·nucleotide and triose binding sites by soaking PGK crystals in high concentrations of substrates yielded very low occupancy with MgATP, but allowed for a tentative assignment of the MgATP binding site location on the inner surface of the C-terminal domain, near the waist region (an assignment which has since been substantiated by affinity labelling experiments (4), among others). No electron density attributable to 3PGA was observed in these experiments; therefore, the location of the binding site for 3PGA was deduced to be in an area of positively charged amino acid side-chains near the waist portion of the amino terminus, the so-called "basic patch" region, which is located opposite the proposed MgATP binding site. This region was found to be highly conserved among PGK's from different species (5). The results of the X-ray crystallographic studies therefore suggested an orientation of the bound substrates in which the γ-phosphoryl group of MgATP was 10-12 Å away from 3PGA (6). The X-ray structure of a binary pig muscle PGK·3PGA complex crystallized from polyethylene glycol solution has been recently published (7). The crystallographic data from this study confirmed that the binding site for 3PGA is located in the basic-patch region as earlier suggested. However, two residues (His-62 and Arg-170) which were thought to interact with 3PGA based on site-directed mutations in yeast PGK (8,9) were found not to be involved in 3PGA binding in the pig muscle binary complex.

Therefore, the results of the study with the pig muscle enzyme do not unequivocally support the proposed location of the 3PGA binding site suggested from experiments with yeast PGK.

Previous mechanistic studies have shown that phosphoryl transfer catalyzed by PGK occurs with inversion of configuration at phosphorous, a result which implies a direct transfer mechanism (10). Hinge bending was proposed as a mechanism for bringing the substrates of PGK together based on structural similarities with hexokinase; small angle X-ray scattering measurements of yeast hexokinase showed that the radius of gyration of the enzyme in solution decreased by 0.95 ± 0.24 Å upon binding glucose (11). This result fits well with the observation from crystallographic studies of a 12° rotation of one of the lobes of hexokinase relative to the other upon glucose binding (12). In a similar manner, the radius of gyration of PGK was observed to decrease by 1.09 ± 0.34 Å upon formation of the ternary complex in solution (13). This change could be brought about by by an 8-14° rotation of one lobe relative to the other. The structure of the closed active site and the relative conformations of the bound substrates are not known; indeed, it has yet to be demonstrated that the bound substrates approach one another closely enough to allow for direct phosphoryl transfer to take place.

PGK has a number of interesting kinetic properties which have been the subject of numerous studies. The enzyme exhibits

substrate activation as evidenced in the downward curvature seen in double reciprocal (Michaelis-Menten) type plots (14). Millimolar concentration of sulfate has been observed to abolish these substrate activation effects (15). Sulfate anion has also been found to be an effector of this enzyme, with millimolar levels acting to increase V_{max} as well as K_m for both substrates (15). Higher sulfate concentrations have an inhibitory effect (16). The mechanisms responsible for substrate activation and for the effects of sulfate are unknown. PGK binds two moles of ATP per mole of enzyme (17), one of which exhibits much higher affinity for divalent metal ions, and is bound at the enzyme active site (18). The binding sites and stoichiometries for other multivalent anions, including sulfate and 3PGA, have not been clearly established. Furthermore, analysis of the effects of site specific mutations of several residues has failed to confirm their specific roles in sulfate activation or metal binding as suggested by X-ray studies (3,9).

The proposed hinge bending mechanism of PGK has been investigated by Dryden et al. (19). Earlier work by this group (20) and others (21) had shown that the waist region of PGK mediates cooperativity between the two globular domains; the binding of ATP to the C-terminal domain of the molecule acts to stabilize both domains, and is accompanied by a stiffening of the waist region. Binding of 3PGA to this complex induces destabilization of the waist region, a "loosening of the

hinge". This has been interpreted as evidence for a "permissive" model for hinge bending, wherein binding of the triose substrate leads to conformational changes which permit, rather than direct, the hinge to bend.

The structural motif of two lobes separated by a deep substrate-binding cleft is common not only to PGK and hexokinase, but is a general feature of a number of kinases whose structures are known. Adenylate kinase, in the absence of substrates, has a deep cleft which closes somewhat when substrates are diffused into the crystals (22). Phosphofructokinase, when crystallized in the presence of its sugar substrate fructose 6-phosphate, is in a closed conformation with the sugar buried in the interdomain region (23). Thus, hinge bending is suspected to be a general feature of catalysis by kinases.

The β,γ-bidentate complex of Cr^{3+} with ATP (CrATP) is an exchange-inert analog of MgATP which is stable at pH 5.9 (24). Additionally, Cr^{3+} is paramagnetic, a property which makes it useful for a variety of binding and structural studies based on magnetic resonance techniques. CrATP is not a substrate for PGK (25), and has been shown to competitively inhibit catalytic activity with respect to MgATP in a number of enzymes which utilize metal·ATP as a substrate, including hexokinase, pyruvate kinase, and PGK (26). Metal·ADP complexes have been used with 3PGA and PGK in paramagnetic metal-to-phosphorus distance measurements (27) and in EPR studies (28);

the findings suggested that the resulting dead-end complex formation did not induce active site closure. Studies from our laboratory have also shown that a fluorescent ATP analog, adenosine diphosphate pyridoxal, specifically labeled Lys 385 instead of lysines 213 or 217 which were suggested by crystallographic studies to interact with the polyphospho-chain of ATP (29). Clearly, the description of the active site geometry of PGK is far from complete, and structural information about the closed, catalytically active form of the enzyme is needed in order to gain further insight into its catalytic mechanism.

The goal of the research outlined in this document is to delineate the geometries of the substrates bound at the active site of yeast phosphoglycerate kinase, and to investigate the effect of sulfate on the active site structure. The research described makes extensive use of kinetic analysis of PGK activity; additionally, much of the binding work, and all of the structural work utilizes nuclear magnetic resonance spectroscopic techniques. It is hoped that the results of these studies add some insight into the mechanism of action of phosphoglycerate kinase, and in some way add to the body of knowledge describing catalysis by kinases in general.

Chapter II

Kinetic Characterization of Yeast PGK at pH 5.9

A. Introduction

Despite a large body of data in the literature describing the kinetic behavior of yeast phosphoglycerate kinase, many questions remain unanswered, particularly regarding the substrate activation and anion binding effects that have been observed. Early work with this enzyme clearly showed substrate activation effects, manifested as downward curvature in double-reciprocal (Lineweaver-Burk) plots at high concentration of either substrate (14). This effect has been variously interpreted, but is generally taken as evidence of two types of binding sites for each of the substrates; a "high affinity" site, which has since been shown to correspond to the catalytic or active site, and a "low affinity" site, which is postulated to perform a regulatory function (30). In experiments performed at near-physiological pH, Larsson-Raznikiewicz determined the kinetic constants for PGK under low and high substrate concentration conditions, corresponding to the occupation of either the high-affinity site or both sites, and reported that the K_m values for either substrate at either the low or high affinity site were independent of the concentration of the other substrate, a finding that suggested

a random kinetic mechanism (14). Working in a substrate concentration range that allowed characterization of the high affinity site, Janson and Cleland reported K_m^{MgATP} = 140 μM, K_m^{3PGA} = 80 μM, and V_{max} = 200 units/mg from experiments performed at pH 7 (31).

The inclusion of sulfate in the reaction medium has been shown to activate PGK, increasing V_{max} and K_m for both substrates; maximal activation is seen in the range of 5-40 mM sulfate, depending on the concentration of substrates present (15). Increases in V_{max} of up to five-fold have been reported in the presence of sulfate (32). Sulfate also acts to eliminate the substrate activation effects observed with this enzyme. These sulfate activation experiments are complicated by the fact that the ionic strength of the reaction mixtures was not strictly controlled; thus, it is difficult to separate out sulfate-specific activation effects from general anionic strength effects. Scopes has shown that release of 1,3-bisphosphoglycerate is the rate limiting step in the catalytic mechanism, and proposed that the release of 1,3-bisphosphoglycerate is accelerated when sulfate is present (15). Interestingly, studies by M. Cohn and co-workers showed that although sulfate activates catalysis by PGK, the actual rate of transfer of phosphate from MgATP to 3PGA is reduced by 15% in the presence of sulfate (33).

The theories which have been proposed to explain the mechanism of activation of PGK by substrates and by sulfate

adhere to two basic models (15,30). In the model described by Fairbrother et al. (30), two anion binding sites are proposed: 1) a primary general anion binding site, which shares at least two residues involved in 3PGA binding, and is believed to mediate activation effects, and 2) a secondary general anion binding site, whose occupation at very high anion concentration leads to inhibition. Scopes presents a different model (15), in which he suggests a two-step dissociation for the product 1,3-bisphosphoglycerate, with both substrates and sulfate activating catalysis by accelerating the dissociation of 1,3-bisphosphoglycerate. Both of these models will be analyzed in greater detail in the General Discussion section (Chapter V), regarding both how well they explain previously observed properties of PGK, and how well they fit with the results of the present studies.

The inhibition of PGK by the MgATP analog CrATP was found to be linear competitive versus both MgATP and 3PGA in experiments performed at pH 7 (26). From that data, K_i^{CrATP} versus MgATP was found to be 700 μM, and K_i^{CrATP} versus 3PGA was found to be 370 μM. However, several technical points render this data suspect, including the presence of a large excess of free Mg^{2+} (which has been shown to have an inhibitory effect on this enzyme) and the fact that the experiments were carried out at a pH where the stability of CrATP is significantly reduced (since the exchange of Cr^{3+} ligands is both acid and base catalyzed (34)).

One of the stated goals of this research was to use β,γ-bidentate CrATP as an NMR probe of the active site geometry of PGK. To allow for this, a complete kinetic chracterization of the enzyme at pH 5.9 was necessary. This is a pH at which CrATP is stable for long periods, and since the NMR experiments proposed would sometimes cover periods of up to 60 hours, it first had to be shown that the kinetic behavior of PGK was unchanged at this pH as compared to observations at pH 7.5-8. This would demonstrate that no drastic structural changes were induced at the pH of the NMR studies, therefore showing that structural information obtained in this way applied to the physiologically relevant form of the enzyme, not an artifactual conformation induced by pH.

B. Experimental Procedures

1. *Materials*

Yeast phosphoglycerate kinase and rabbit muscle glyceraldehyde phosphate dehydrogenase (GAPDH) used in these studies were obtained as ammonium sulfate precipitates from Boehringer-Mannheim. PGK was further purified by gel filtration using a Sephacryl HR-200S column equilibrated with 5 mM MES-NaOH pH 5.9 and was stored at -80°C as a lyophilized powder. The enzyme was homogeneous as determined by SDS-polyacrylamide gel electrophoresis, with a specific activity

of 250 μmoles/min/mg protein at pH 5.90. GAPDH was separated from ammonium sulfate either by dialysis or by gel filtration using a Sephadex G-25 column equilibrated with 10 mM Tris-HCl pH 7.5, and was stored frozen at -20°C. 3-Phosphoglycerate was obtained as a barium salt from Sigma, and was converted to the sodium form using the following procedure: the barium salt was dissolved in HCl, treated with a near-stoichiometric amount of H_2SO_4 to precipitate the barium, neutralized with NaOH, and passed through a column of Chelex 100 resin to remove remaining trace metals. The concentration of the resulting 3PGA solution was determined enzymatically. Vanadate-free ATP was obtained from Sigma as a disodium salt; $CrCl_3$ was from Morton Thiokol. All other reagents were of the highest purity commercially available. Buffers and ATP solutions were passed over Chelex 100 resin to remove trace metals prior to use; the concentration of ATP solutions was determined spectrophotometrically at 260 nm, using an extinction coefficient of ε_{260} = 15,400 M^{-1} cm^{-1}.

2. *Preparation of CrATP*

β,γ-bidentate $CrATP(H_2O)_4$ was prepared basically as described by Dunaway-Mariano and Cleland (24). On ice, 10 ml of a 20 mM aqueous solution of $CrCl_3$ was added to 10 ml of 20 mM ATP at pH 3.0; the resulting solution was heated to 80°C and maintained at that temperature for ten minutes. The solution was then cooled to 4°C and loaded (at 4°C) onto a 0.5

x 10 cm column of Dowex-50W cation exchange resin (2% cross-link; Sigma Biochemicals) which had been pre-washed with 0.1 N HCl followed by sufficient de-ionized water to return the effluent to pH 6. After sample application the column was washed with sufficient de-ionized water to elute any unreacted ATP and to resolve the CrATP from unreacted $Cr^{3+}(H_2O)_6$, which remained at the top of the resin. The $Cr^{3+}(H_2O)_6$ layer was carefully removed with a pasteur pipette and discarded; the intense green CrATP band was then removed with a clean pasteur pipette and loaded onto the top of a small (1 cm x 1 cm) Dowex-50W (2% cross-link) column which had been freshly treated by washing with 6 N HCl followed by enough de-ionized water to return the effluent to aqueous pH. CrATP was eluted from this column with a solution of 0.3 M aniline, and was collected in 0.5 ml fractions. The final fractions were discarded to reduce the presence of excess aniline in the CrATP. The CrATP solution was then immediately extracted four times with diethyl ether to remove any contaminating aniline, and residual ether was removed by passing a stream of nitrogen through the solution. Finally, the pH of the CrATP solution was set in the range of 4-5, and the solution was diluted to a final concentration of 8-15 mM. The concentration of the CrATP was spectrophotometrically determined as previously described (24). Solutions were stored at 4°C and used within 5 days of preparation.

3. *Assay Method*

Kinetic assays were performed by measuring spectrophotometrically the decrease in absorbance at 340 nm associated with the oxidation of NADH in a coupled-enzyme assay system using GAPDH as the coupling enzyme. Although the equilibrium of the PGK reaction lies in favor of ATP formation, the enzyme activity is usually assayed in the direction of gluconeogenesis (due to the instability of 1,3-bisPGA under the assay conditions), so that reaction progress can be monitored through the coupling enzymatic activity, as shown below:

$$\text{3-Phosphoglycerate} + \text{MgATP} \underset{}{\overset{\text{PGK}}{\rightleftharpoons}} \text{1,3-Bisphosphoglycerate} + \text{MgADP}$$

and

$$\text{1,3-Bisphoglycerate} + \text{NADH} + \text{H}^+ \overset{\text{GAPDH}}{\rightleftharpoons} \text{Glyceraldehyde 3-phosphate} + \text{NAD}^+ + \text{P}_i$$

Assay mixtures contained 0.052-3.44 mM ATP, 0.076-1.58 mM 3PGA, 120 mM NaCl, 50 mM MES-NaOH pH 5.90, and $MgCl_2$ in 1 mM excess of total nucleotide concentration. MgATP concentrations were calculated based on a K_D for MgATP of 80 μM (35). In all assays, the NADH concentration was sufficient to give 1-1.3 absorbance at 340 nm, and at least 150 μg coupling enzyme was used, which was found to be not rate limiting at double the PGK concentration with the highest substrate concentration

used. The effect of varying both substrates was examined, both in the presence or the absence of 40 mM sulfate ion. In order to maintain a constant ionic strength, NaCl was omitted when sulfate ion was used. Measurements were taken using 1 cm quartz cuvettes thermostatted to 25°C in a Beckman DU-70 spectrophotometer, with a 1 ml reaction volume. 0.25 μg of PGK was added to start the reaction.

C. Results

1. *Kinetics of PGK at pH 5.9*

Lineweaver-Burk plots of PGK activity exhibited downward curvature at high substrate concentrations when either substrate was varied (Figure II-1; data shown only for MgATP as varied substrate). This is similar to previous observations at pH 7.5-7.8 (32,36). When extrapolated back to infinite velocity, the regions corresponding to high substrate concentration (greater than 600 μM 3PGA or MgATP) yielded the V_{max} and K_m values for the low affinity site for each substrate (Table II-1). The high affinity regions were examined more closely in separate experiments (Figure II-2), which yielded the substrate K_m values listed in Table II-1. These values were similar to those reported in the literature for the pH range 7.5-7.8. The results also showed that the K_m for each substrate was independent of the concentration of the other

substrate, a result which is consistent with the random bi-bi kinetic scheme that has been proposed for this enzyme (14).

Substrate activation effects were absent when 40 mM sulfate anion was included in the reaction mixture (Figure II-3). The presence of sulfate raised the K_m 3.5 fold and 15 fold for MgATP and 3PGA, respectively, and V_{max} increased 2 fold (Table II-1). As was the case seen in the absence of sulfate, K_m for each substrate was independent of the concentration of the other substrate. When compared with the kinetic data in the literature, these findings clearly show that the kinetic behavior of PGK at pH 5.90 is unchanged when compared to that observed at pH 7.5-7.8 (32,36).

2. *Inhibition by CrATP*

Kinetic analysis of the inhibition of PGK by CrATP was performed at several different (constant) concentrations of the second substrate 3PGA, and showed that CrATP is a linear competitive inhibitor with respect to MgATP at pH 5.90 (Figure II-4 and inset). Interestingly, however, extrapolation of plots of slope vs. [CrATP] to determine K_{iapp} for each of the experiments revealed that the apparent K_i^{CrATP} increased as the concentration of the fixed substrate (3PGA) was increased between 70-700 μM 3PGA (Figure II-5). Linear extrapolation of the apparent K_i^{CrATP} values observed in the presence of various concentrations of 3PGA yielded a K_i^{CrATP} of 70 ± 14 μM in the absence of 3PGA (Figure II-5). In the presence of 40 mM

sulfate, CrATP was still a linear competitive inhibitor of the enzyme with respect to MgATP (Figure II-6 and inset) with a K_i value of 725 ± 178 μM. However, the observed K_i for CrATP was found to be independent of the concentration of 3PGA over the concentration range used (Figure II-5). It was not possible to extend this work to higher 3PGA concentration due to the fact that the high concentration of CrATP needed for inhibition under these conditions was found to have adverse effects on the activity of the coupling enzyme (GAPDH) used in these assays. The implications of the differential inhibition of PGK by CrATP in the absence and presence of sulfate, as they pertain to active site geometry, will be discussed later.

The inhibition of CrATP versus 3PGA was analyzed at three different concentrations of MgATP, in the absence and presence of sulfate. Figure II-7 shows the mixed-inhibition pattern that was observed at all MgATP concentrations when 3PGA was the variable substrate in the absence of sulfate (data shown for only one concentration of MgATP). Replots of K_i(slope) vs. [MgATP] and K_i(intercept) ($=\beta K_i$) vs. [MgATP] yielded K_i(slope) = 40 ± 20 μM and K_i(intercept) = 600 ± 150 μM (Table II-1). In the presence of 40 mM sulfate, the inhibition was non-competitive (Figure II-8; data shown for only one concentration of MgATP), with K_i(slope) = 570 ± 130 μM and K_i(intercept) = 450 ± 100 μM (Table II-1). Previous studies of this type, conducted by Dunaway-Mariano and Cleland (26), had suggested that CrATP was a competitive inhibitor of PGK with

respect to both substrates; however, detailed analysis of the type described here was not performed by that group. Considering the relation K_i(intercept) = βK_i(slope), and knowing that β represents the factor by which the dissociation constant for 3PGA is changed by the binding of CrATP, it is clear that in the absence of sulfate K_i(slope) $\neq$ K_i(intercept), that is, $\beta \neq 1$. β values which deviate from unity are indicative of mixed-type inhibition, wherein saturating amounts of the non-varied substrate are not sufficient to overcome inhibition. In the presence of sulfate, K_i(slope) = K_i(intercept) (within experimental error), that is, $\beta = 1$, indicating purely non-competitive inhibition.

D. Discussion

As shown in Table II-1, the kinetic constants for the formation of 1,3-bisphosphoglycerate and MgADP from 3-phosphoglycerate and MgATP by PGK indicate no significant changes in the kinetics of PGK at pH 5.9, a pH at which the metal-nucleotide analog CrATP is stable for extended periods of time. The effects of sulfate on enzyme kinetics which have been previously observed at pH 7.5-7.8 (32,36), namely enzyme activation and loss of substrate activation, were also observed under the conditions of the present study.

When 3PGA was the variable substrate, the inhibitory

behavior of CrATP was found to be dependent on the presence or absence of sulfate. When sulfate was excluded, mixed-type inhibition was observed; detailed analysis of this phenomenon showed that the dissociation constant of 3PGA was significantly affected by the binding of CrATP under these conditions. We have interpreted this in terms of a physical interaction of CrATP and 3PGA at the active site mediated by exchange-inert water ligands in the coordination sphere of Cr^{3+} upon formation of the ternary PGK·3PGA·CrATP complex. Although enzyme active site closure may bring 3PGA and CrATP into close proximity under these conditions, the presence of exchange-inert water ligands in the Cr^{3+} coordination sphere may prevent the approach of 3PGA to CrATP, thereby creating an "overlap" interaction between the substrates. On the other hand, when sulfate is present, CrATP was purely non-competitive with respect to 3PGA; under these conditions, the active site may adopt a conformation that does not necessitate such a close approach of CrATP and 3PGA. The bound sulfate may physically prevent complete active site closure, or may induce active site conformational changes that create a more open arrangement. The observed inhibitory patterns may simply reflect this difference in active site geometry when sulfate is present. An alternative explanation is that binding of 3PGA occurs at a second site and creates the observed effects through propagated conformational changes. A model to explain the observed effects is shown in Figure II-9. These effects

would be unobservable with metals such as Mg^{2+} and Mn^{2+}, which have much higher ligand exchange rates than Cr^{3+}.

CrATP is a linear competitive inhibitor of PGK with respect to MgATP under the conditions of the present study, indicating that CrATP binds to the MgATP binding site. Further insight is gained by examining the effect of sulfate on the K_m of both substrates as well as its effect on CrATP inhibition. Table II-1 shows that the K_m for both substrates is increased when sulfate is present in the reaction mixture. The affinity of the enzyme for CrATP is also greatly reduced in the presence of sulfate; furthermore, the dependence of K_i^{CrATP} on the concentration of 3PGA is abolished. It has been suggested that binding of sulfate to PGK causes conformational changes which result in lowered affinity for both substrates (15,16). This idea is supported by the present study, and a further effect of sulfate binding is also suggested, namely that the substrate binding sites change orientation relative to one another such that the closed form of the enzyme no longer has the 3PGA and metal-ATP binding sites in a relative geometry that necessitates close approach of 3PGA to the metal ion, as also suggested from previous studies in this laboratory (37). Similarly, the activation effect of sulfate could be explained on the basis of this model, wherein a less closed form of the enzyme allows more rapid release of 1,3-bisPGA product, which is the rate limiting step in the catalytic mechanism; the studies by Scopes cited earlier suggested that this may indeed

be the case (15). Additionally, the observation of Cohn and co-workers that the actual rate of transfer of phosphoryl from MgATP to 3PGA was reduced in the presence of activating concentration of sulfate (33) is consistent with a conformationally-altered active site under those conditions. These findings are in excellent agreement with the sulfate effect found in this study.

The kinetic data described here show no significant deviation from previous observations in other laboratories obtained under conditions that were more closely physiological. Therefore, the conclusion that structural studies performed at this pH will directly apply to the native form of PGK appears justified. In preparation for the NMR measurements, the next step in the project was to characterize the binding affinity and stoichiometry of the various ligands to PGK under the current pH conditions. This will allow for the quantitation of the amounts of the various complexes present in the NMR samples, making analysis of paramagnetic relaxation data useful for distance determinations.

Chapter III

Analysis of Ligand Binding to PGK at pH 5.9

A. Introduction

Investigation of the stoichiometry and dissociation constants of binary and ternary complexes of enzymes with paramagnetic metal ions, paramagnetic substrate analogs, and diamagnetic substrates is a field of study in which magnetic resonance techniques have proven extremely useful. In particular, the measurement of the longitudinal relaxation rates ($1/T_1$) of water protons in the coordination sphere of paramagnetic metal ions has provided much structural, kinetic, and thermodynamic information on such complexes (38,39). Additionally, metal coordination schemes (40) and the exchange rates of substrates into and out of paramagnetic environments on enzymes (41) have been determined. Estimation of ligand stoichiometries and dissociation constants has also been accomplished through the use of various other techniques, including equilibrium dialysis with radiolabelled ligands (42) and non-equilibrium binding methods such as Penefsky's centrifuged-column procedure (43).

Understanding how stoichiometries and dissociation constants can be obtained from water proton relaxation data requires some familiarity with the principles of NMR. The

theory describing the physical basis of the nuclear magnetic resonance phenomenon has been comprehensively reviewed (44,45) and will only be briefly described here. Spin 1/2 nuclei (among which ^{1}H, ^{13}C, and ^{31}P are of chief biological interest) possess net magnetic moments which, when placed in an external magnetic field, will equilibrate by aligning themselves with respect to the direction of the applied field. The magnetic vectors also experience a torque that will cause them to precess about the axis of the applied field at a frequency called the Larmor frequency, which is characteristic for a given nucleus. This system can be perturbed away from equilibrium by the application of a radio frequency (RF) pulse, resulting in an excited state wherein the direction of the net magnetic vector has been tilted away from its equilibrium alignment in the external field (by an amount determined by the power and duration of the RF pulse), and where the nuclear magnetic vectors have aligned to precess in phase with each other. The mechanisms that modulate the return of this system to the ground state are collectively termed relaxation. Specifically, longitudinal relaxation, with its associated first-order rate constant $1/T_1$, governs the return of the net magnetic vector to alignment with the external magnetic field; loss of RF-induced phase coherence occurs via a process known as transverse relaxation, with a first order rate constant $1/T_2$.

The measurement of water proton $1/T_1$ values as a tool for investigating binding to macromolecules depends on mechanisms by which water proton relaxation rates are enhanced. In order for longitudinal relaxation to occur, the excited nuclei must lose magnetic energy to their surroundings (the "lattice"). For this to happen, the lattice must be capable of absorbing magnetic energy at the Larmor frequency of the excited nucleus. The magnetic interaction between a nucleus and the lattice is governed by molecular tumbling in solution. For protons of small molecules like water, transfer of magnetic energy to the lattice is inefficient due to the fast rate of tumbling of the water molecule as compared to the proton Larmor frequency (10^{11} sec^{-1}, versus 6.3×10^8 sec^{-1} at a field strength of 2.35 Tesla, respectively). The association of a water molecule with a macromolecule or a macromolecule·paramagnet complex can enhance $1/T_1$ by two mechanisms. First, upon immobilization of a water molecule on a macromolecule, the spin-lattice interaction of the water protons is modulated by the slower tumbling time of the macromolecular complex (~10^8 sec^{-1}), increasing its efficiency. Second, paramagnetic species contain unpaired electrons which give them much stronger magnetic moments than protons, making them more efficient acceptors of magnetic energy; exchange of water molecules into and out of the coordination sphere of a paramagnetic ion can therefore increase the $1/T_1$'s of water protons through increased interaction with the paramagnet.

As will be seen in the next chapter, the measurement of paramagnetic-metal to nucleus distances using NMR methods relies on accurate characterization of all complexes present in the NMR samples. Since the experiments proposed for this system involved NMR analysis of the ternary PGK·3PGA·CrATP complex, it was vital that the stoichiometries and dissociation constants of the ligands to all possible binary and ternary complexes be determined. This was accomplished through a combination of techniques, utilizing NMR examination of binary and ternary complex formation, as well as the binding of radiolabelled substrate analogs to the enzyme. The results of the experiments presented in this section allow for precise quantitative treatment of the paramagnetic distance measurement data.

B. Experimental Procedures

1. *Materials*

Yeast phosphoglycerate kinase used in these studies was obtained as an ammonium sulfate precipitate from Boehringer-Mannheim, and was further purified as described in the "Experimental Procedures" section of Chapter II. The enzyme was homogeneous as determined by SDS-polyacrylamide gel electrophoresis, with a specific activity of 250 μmoles/min/mg protein at pH 5.9. β,γ-bidentate CrATP was synthesized as

previously described (Experimental Procedures, Chapter II), and was used as a diastereomeric mixture. ATP was obtained from Sigma; [γ-^{32}P] ATP was obtained from Amersham. All other reagents were of the highest purity commercially available. All buffers and nucleotide solutions were passed over Chelex 100 resin to remove trace metals prior to use.

2. *Preparation of [γ-^{32}P] CrATP*

[γ-^{32}P]-labelled CrATP$(H_2O)_4$ was prepared in the same way as was the unlabelled compound (24), with the following modifications (46). The reaction was scaled down by a factor of ten, such that 1 ml of 20 mM $CrCl_3$ and 1 ml of 20 mM ATP (unlabelled) were mixed on ice to give 2 ml reaction volume. To this was added 10 μl of 25 μCi/μl [γ-^{32}P] ATP (not more than 0.08 pmoles total [γ-^{32}P] ATP). The yield of the reaction was 1 ml of 14 mM [γ-^{32}P] CrATP (14 μmoles), with a specific activity of 12.6 cpm/pmole as determined by scintillation counting.

3. *Analysis of CrATP Binding via Circular Dichroism (CD) Spectroscopy*

Analysis of the preferential binding of either the Δ or Λ isomer of CrATP to PGK was performed through inactivation of PGK with racemic CrATP, followed by removal of PGK-bound CrATP by filtration and analysis of the unbound fraction by CD spectroscopy. The inactivation mixture consisted of 3.24 mM

CrATP, 0.146 mM PGK, 100 mM NaCl, and 50 mM MES-NaOH pH 5.9 in a total volume of 9 ml. Progress of inactivation was monitored by taking 1 μl aliquots from the inactivation mixture, diluting it into 50 μl of 50 mM MES-NaOH 100 mM NaCl mixture, and then analyzing a 5 μl aliquot of the diluted enzyme in a PGK activity assay as described in Chapter II, "Experimental Procedures". The enzyme was found to be 90% inactivated after 90 minutes of incubation at 25°C. The inactivated PGK, together with the bound CrATP, was separated from the unbound CrATP by filtration through a collodion membrane (MW cutoff 25,000, Schleicher & Schuell) using a vacuum collodion filtration apparatus at 4°C. The composition of the filtrate was analyzed between 450 nm and 700 nm using a Jasco J40A spectropolarimeter, with a 10 cm path length quartz cuvette. A sample consisting of 3.24 mM racemic CrATP in 100 mM NaCl and 50 mM MES-NaOH pH 5.9 was used to calibrate the baseline.

4. *Binding Studies with [γ-^{32}P] CrATP*

Binding experiments were carried out using a centrifuged-column procedure (47). Pre-incubation mixtures containing 50 mM MES-NaOH pH 5.90, 120 mM NaCl, and 145 μM PGK were incubated for 1 minute at room temperature. Varying amounts of [γ-^{32}P] CrATP, along with de-ionized H_2O sufficient to give a final volume of 100 μl, were added to the pre-incubation mixture, and the samples were incubated for 3 minutes at room temperature. 90 μl aliquots were then loaded onto freshly spun

Sephadex G-50 (fine) columns (60 seconds pre-spin at 900 rpm in a Clay-Adams Dynac II centrifuge) and centrifuged for 90 seconds at 900 rpm (180 x g). Column effluent was taken up in 8 ml aqueous counting scintillant (Amersham) for scintillation counting. The experiment was repeated including 4.43 mM 3PGA and/or 40 mM sulfate ion in the pre-incubation mixture.

5. *Magnetic Resonance Measurements.*

NMR studies of water proton relaxation rates were carried out using a Seimco pulsed NMR spectrometer as previously described (48,49). Titrations were performed at 24.3 MHz at a probe temperature of 21°C. Longitudinal relaxation rates were measured using the 180°-τ-90° pulse sequence of Carr and Purcell (50), with a delay of $5T_1$ to allow for complete relaxation. T_1 values were calculated from

$$T_1 = \tau(\text{null})/\ln 2 \qquad \text{(Equation III-1)}$$

where τ(null) is the delay between the 180° and 90° pulses. The paramagnetic contribution to the relaxation rate ($1/T_{1p}$) was taken as the difference between the observed relaxation rate in the presence ($1/T_{1(obs)}$) and absence ($1/T_{1(o)}$) of CrATP:

$$1/T_{1p} = 1/T_{1(obs)} - 1/T_{1(o)} \qquad \text{(Equation III-2)}$$

The observed enhancement (ε^*) of the relaxation rate is

defined as the ratio of the paramagnetic contribution in the presence of the enzyme (denoted by *) to that in the absence of the enzyme:

$$\varepsilon^* = \frac{1/T_{1p}^*}{1/T_{1p}} \qquad \text{(Equation III-3)}$$

C. Results

1. *Stereoselectivity of Phosphoglycerate Kinase*

When the γ-phosphate of ATP becomes coordinated to chromium, the phosphorous becomes prochiral but not asymmetric. However, asymmetry is introduced at the β-phosphorous upon coordination of the β-phosphate. The remaining two oxygen ligands of the β-phosphorous present two different possible points of attachment for the AMP moiety, one leading to right hand screw sense (the Δ isomer) and the other leading to left hand screw sense (the Λ isomer). Inactivation of PGK with a racemic mixture of CrATP, followed by removal of PGK and bound nucleotide by filtration, resulted in enrichment of the Λ isomer of CrATP in the remaining solution as determined by CD spectroscopy (data not shown).

This result indicates preferential binding of the Δ diastereomer by the enzyme.

2. *Binding of [γ-^{32}P] CrATP to PGK*

The binding of [γ-^{32}P] CrATP to PGK was investigated in the presence or absence of 3PGA and/or sulfate (Figure III-1). Formation of the binary enzyme·CrATP complex in the presence and absence of sulfate could not be detected with the centrifuge column method used in these studies. This is probably due to fast off rates of CrATP from the enzyme, which is presumably in the "open" conformation when 3PGA is absent. As the figure shows, in the presence of 4.43 mM 3PGA, 1:1 mol/mol binding of CrATP to PGK was observed, with a dissociation constant of 550 ± 120 μM. This value agrees well with the K_i values in the kinetic studies in the presence of 70-700 μM 3PGA. The presence of both 3PGA and sulfate in the pre-incubation mixture resulted in biphasic binding of CrATP to PGK under these conditions. The data is shown with a fitted curve which assumes two types of non-interacting binding sites for CrATP. The observed stoichiometries of 0.85 ± 0.06 and 3.0 ± 0.38, with dissociation constants of 900 ± 70 μM and 6000 ± 450 μM respectively, suggest that the affinity of CrATP to the enzyme is lowered when sulfate is present. The high affinity site for CrATP probably represents the active site; the low affinity sites may represent non-specific binding of CrATP to the enzyme·3PGA complex, since very high concentrations of

CrATP were required in order to achieve high occupancy of the high affinity site. These findings are consistent with the kinetic data and with the hypothesis that the active site may not be tightly closed when sulfate is present. The resulting binding constants from all Scatchard analyses are summarized in Table III-1.

3. *Water Proton Relaxation Enhancement Studies*

Binding of CrATP to the enzyme increased the observed relaxation rates of water protons. Experiments were performed with different PGK/CrATP ratios which allowed extrapolation to infinite enzyme concentration in order to determine the binary enhancement factor (ε_b) in the binary PGK·CrATP complex (Table III-1). The results of such experiments are shown in Figure III-2, which yielded ε_b of 1.46 ± 0.12. Since the observed enhancement (ε^*) includes the contributions of relaxation rates due to free and bound CrATP, the determined ε_b, together with the observed enhancements, were then used to calculate the concentration of free and bound CrATP in the solutions of enzyme and CrATP according to the equation (51):

$$\varepsilon^* = \frac{[P]_f}{[P]_T}\varepsilon_f + \frac{[P]_b}{[P]_T}\varepsilon_b \qquad \text{(Equation III-4)}$$

where $[P]_f$, $[P]_b$, and $[P]_T$ are free, bound, and total

concentrations of paramagnetic species, respectively. ε_f is the enhancement due to free paramagnet, which equals one by definition. Scatchard analysis of this data is shown in Figure III-3, which yielded a dissociation constant of 60 ± 19 μM for the enzyme·CrATP complex, with a stoichiometry of 1.2 ± 0.4 mole CrATP per mole enzyme (Table III-1). The determined values are in agreement with the kinetic data, despite the fact that the data in Figure III-3 has considerable noise because of low enhancement values.

The formation of ternary PGK·CrATP·3PGA complex was monitored by titrating PGK·CrATP complex with 3PGA. Figure III-4 shows the results of such titrations starting from various CrATP/PGK ratios (from 1/3 to 4/3). The enhancement of the observed relaxation rates (ε^*) increased at low 3PGA concentration, and began to decrease at higher 3PGA concentration. Similar titrations performed in the presence of sulfate yielded curves which are almost mirror image of those observed in the absence of sulfate (Figure III-5), where an initial de-enhancement at low 3PGA concentration was followed by enhancement as 3PGA concentration increased. These results clearly show the formation of the ternary PGK·CrATP·3PGA complex in both cases. The results further suggest that the environment of metal at the active site is different in the presence and absence of sulfate. Attempts were made to obtain an enhancement factor for the ternary complex (ε_t) by curve fitting as described earlier (48,52). The data could not be

explained by a single ε_t value, suggesting multiple conformational changes during the formation of the ternary complex or multiple binding of 3PGA to the PGK·CrATP complex.

D. Discussion

Inactivation experiments showed preferential binding of the Δ isomer of CrATP to PGK as measured by CD spectroscopy of the inactivation supernatant. This observation agrees with the results of earlier studies using MgATP analogs which had sulfur substituted for the β-phosphorous (MgATPβS)(25); these studies showed specific binding of the S_p isomer, which corresponds to the Δ screw sense isomer of CrATP (53). However, this is in contrast to observations with hexokinase, which exclusively binds the Λ isomer of CrATP (54).

Binding experiments showed that the presence of 3PGA was necessary to bring about tight binding of CrATP to the enzyme. Since the dissociation constant of CrATP from the binary complex is much lower compared to the ternary complex (Table III-1), this observation suggests that binding of 3PGA is necessary for active site closure, which may trap the substrates at the "closed" active site, thereby reducing the off rate of CrATP significantly. Similarly, Williams and co-workers found that binding of 3PGA to PGK caused structural changes in the enzyme even in the absence of nucleotide (30). Inclusion of sulfate in the pre-incubation mixture resulted in

an increase in the dissociation constant for CrATP. Fitting of the data by assuming two types of independent sites yielded a K_d^{CrATP} of 900 ± 70 μM for the high affinity site, which is in good agreement with the kinetic findings, and 0.85 stoichiometry of CrATP to PGK. Additional CrATP binding sites observed under these conditions are probably the result of non-specific interactions between CrATP and the enzyme, since much higher γ-^{32}P-CrATP concentrations were necessary due to the presence of sulfate.

The binding of CrATP to PGK in the absence of 3PGA was studied by measuring the $1/T_1$ of water protons. The results showed a 1.46 fold enhancement of the paramagnetic effect of CrATP on the observed relaxation rates of water protons when compared to free CrATP, clearly indicating the formation of a binary PGK·CrATP complex. Titration of the binary PGK·CrATP complex with 3PGA yielded multiphasic curves (Figures III-4 and III-5). Net enhancement or de-enhancement of observed relaxation rates results from changes in the correlation time for the electron-nuclear dipolar interaction (τ_c) and/or altered solvent accessibility of bound paramagnet (48). Given this, the ternary titration data can be explained in terms of a model which involves two binding sites for 3PGA, a high affinity site (presumably the catalytic site) and a low affinity "anion binding site". In the absence of sulfate, an initial enhancement upon binding 3PGA to the active site could reflect a conformation in which an increase in τ_c overcomes a

loss of solvent accessibility to Cr^{3+} due to closure of the active site. At higher 3PGA concentration, the anion site becomes populated, and a new interplay of τ_c and solvent accessibility is observed, which represents a different conformation around the metal ion at the active site. However, this experiment is complicated by the fact that the affinity of CrATP to the enzyme is decreased in the presence of 3PGA. Therefore, the observed decrease in ε^* may be due in part to the increased dissociation of CrATP from the enzyme.

In the presence of sulfate the initial complex presumably has the anion site occupied by a sulfate molecule. Low 3PGA concentration would therefore populate the active site, and the observed net de-enhancement reflects an altered environment for bound CrATP under these conditions. Higher 3PGA concentration induces further changes at the active site which are evident from the observed enhancements. Since the K_i of CrATP is independent of 3PGA concentration when sulfate is present (as shown in the kinetic studies), these observations suggest the binding of a second 3PGA molecule to the PGK·CrATP·3PGA complex. Whether 3PGA displaces sulfate at the anion site or binds to another site cannot be distinguished with our data.

The results of the ternary titrations indicate that the initial ternary complex is conformationally different in the absence or presence of sulfate, which is shown by the changes in ε^* in opposite directions. ε^* reaches a maximum or minimum

in the presence or absence of sulfate, respectively (Figures III-4 and III-5), thus indicating two different ternary complexes in which the metal is exposed to different environments. The effect of sulfate observed in the present studies cannot be attributed to a salt effect since the ionic strength was kept identical in both systems by the inclusion or omission of NaCl. Furthermore, although two nucleotide binding sites are present, the above observations can not be attributed to redistribution of ATP between enzyme sites and metal, since CrATP is an exchange-inert complex.

Chapter IV

Determination of the Geometry of Substrates Bound at the Active Site of PGK

A. Introduction

Understanding enzymatic catalysis in terms of the underlying principles of organic reaction mechanisms requires precise structural knowledge of the reacting species. X-ray crystallography of various enzyme·substrate complexes has yielded a wealth of information that in many cases has led to the elucidation of catalytic mechanisms (55,56). Such an approach has thus far proven to be of only limited usefulness in the case of phosphoglycerate kinase, due to the difficulties encountered in attempts to crystallize binary and ternary complexes of the enzyme with its substrates or with substrate analogs. In addition, large conformational changes observed in PGK in solution studies upon the binding of substrates have led many to question the applicability of X-ray structures to understanding catalysis by PGK. Certainly, the X-ray structure of the apoenzyme, obtained in the presence of a high concentration of sulfate, cannot automatically be assumed to represent the catalytically competent form of PGK.

Of the techniques available to study molecular structure in solution, only NMR has proven to have the resolution necessary for characterization of active site geometry. During

the 1970's, NMR measurement of the distances of substrate nuclei to a proximal paramagnetic reference point emerged as a prominent field of structural study. The technique has been successfully applied to the elucidation of the conformation of substrates and substrate analogs bound at the active site of adenylate kinase (57), pyruvate kinase (58), staphylococcal nuclease (59), and yeast metalloaldolase (60), to name but a few. In addition, nuclear Overhauser effect (NOE) studies have been used to delineate active site geometry of enzymes such as creatine kinase (61) and the Klenow fragment of DNA polymerase I (62), among others.

Determination of distances between paramagnetic metal centers and substrate nuclei relies on evaluation of $1/T_{1p}$, the effect of the paramagnet on $1/T_1$ values of those nuclei; the magnitude of this effect exhibits a $1/r^6$ dependence on the distance between the paramagnetic metal center and the substrate nucleus of interest. More precisely, $1/T_{1p}$ of the magnetic nuclei (^1H, ^{13}C, ^{31}P, etc.) of a substrate molecule that is exchanging into and out of a paramagnet·enzyme complex depends ultimately on five parameters: the correlation time for the electron-nuclear dipolar interaction, τ_c; the relative stoichiometry of the substrate and paramagnet in the complex, q; the lifetime of the complex, τ_M; the outer sphere contribution to the relaxation rate due to ligand molecules beyond the inner coordination sphere, $1/T_{o.s.}$; and the distance r between the nucleus and the metal center. It can be seen

that evaluation of the first four of these will allow for quantitative assessment of the fifth, r, which is the goal of the present application of this method. τ_c can be thought of as a measure of the efficiency of transfer of magnetic energy between the excited nucleus and the paramagnet, in the sense that it represents a combination of motional functions which govern this interaction; its magnitude can be evaluated through analysis of the frequency dependence of the $1/T_{1p}$ of ligand nuclei, as described in the "Magnetic Resonance Methods" section of "Experimental Procedures". The stoichiometry (q) can be evaluated by methods discussed in the previous chapter, among others. A numerical value for the lifetime of the complex (τ_M), or more precisely, the rate of dissociation of the substrate from the paramagnetic complex ($1/\tau_M$), need not be quantitatively assessed; it need only be shown that the observed relaxation rates are not exchange-limited; that is, that the ligand exchange rates are much faster than the relaxation rates ($1/\tau_M \gg 1/T_{1p}$). This can be shown by establishing that the observed $1/T_{1p}$ values decrease as temperature is increased, since ligand exchange rates would be expected to increase at higher temperature. Thus, positive slope of $1/T_{1p}$ vs. 1/temperature plots indicates that the rates being monitored are actually longitudinal relaxation rates; also note that this condition need only be established for the fastest relaxing nuclei to be observed (in this case, ^1H). The outer sphere contribution to the relaxation rate ($1/T_{o.s.}$) can

be shown to be negligibly small by displacing the paramagnetic ligand through the addition of excess diamagnetic ligand, which should remove the paramagnetic effect on the observed $1/T_1$. Once q and τ_c have been determined, fast exchange conditions have been satisfied, and outer sphere contributions have been assessed, measurements of $1/T_{1p}$ can be used for distance determinations as described in "Results", section 5, of this chapter.

Although the process of longitudinal relaxation can be reasonably well represented in terms of the behavior of the net magnetization vector in an applied magnetic field (as described in the introduction to Chapter III), understanding the basis of the nuclear Overhauser effect (NOE) is less straightforward. The NOE is defined as the change in intensity of one resonance upon perturbation of the transitions of another resonance. If we perturb one resonance in a system (for example, through saturation of that resonance), we have disturbed the energy of the entire system away from its thermal equilibrium position, and the rest of the system will compensate for that change. This effect is more easily visualized through examination of an energy level diagram of an isolated two spin system. Consider two spins i and s in an applied magnetic field; the orientation of those spins (aligned either with ($\uparrow$, or α) or against ($\downarrow$, or β) the

direction of the applied field) can be diagrammed as follows:

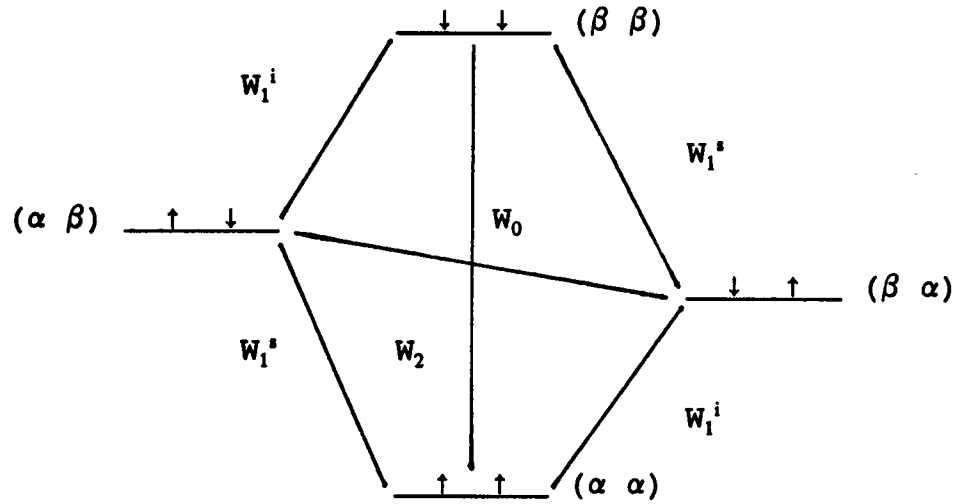

The population of these energy levels will follow a Boltzmann distribution at thermal equilibrium. The energy difference between (α β) and (β α), although exaggerated in the diagram, can be assumed to be negligible, so that these two levels will be essentially equally populated. The (α α) level, being lowest in energy, will have the highest population.

As can be seen from the diagram, there are six transitions available to this system upon perturbation: (α α)$\rightarrow$(β α) and (α β)$\rightarrow$(β β) (termed the W_1^i transitions, for net single spin transitions involving nucleus *i*); (α α)$\rightarrow$(α β) and (β α)$\rightarrow$(β β) (W_1^s transitions); (α β)$\rightarrow$(β α) (W_0 transitions) and (α α)$\rightarrow$(β β) (W_2 transitions). If we consider the selective perturbation of spin *i*, the transitions described above are available to spin *i* as relaxation mechanisms. It can be seen that the W_1 transitions involve only *i* or *s*, and therefore do

not reflect any interaction between the two spins. The W_0 and W_2 transitions involve both spins; therefore, relaxation of the perturbed spin *i* through either of these pathways affects the orientation of spin *s*, illustrating how a change in the energy of one spin can alter the energy of the other. The interaction is mediated through the coupling of the magnetic fields of the two nuclei (dipolar coupling), which behave as magnetic dipoles due to their net nuclear spin. The W_0 and W_2 transitions together are termed cross-relaxation (denoted by σ), and they represent the transfer of magnetic energy between dipolar-coupled nuclei. Cross-relaxation manifests itself as a change in the intensity of the resonance of spin *s* when spin *i* is perturbed, which is the nuclear Overhauser effect. This change can be either positive or negative, and the magnitude as well as the sign of the NOE are subject to many physical influences. Finally, it should also be noted that all of the transitions described above contribute to the observed longitudinal relaxation rate $1/T_1$.

The above treatment is useful in understanding the source of the NOE, but the practical aspects of NOESY spectroscopy, including how to get structural information from NOE data, are not evident from such an idealized description. In fact, the magnitude of the NOE observed between two spin 1/2 nuclei exhibits the same $1/r^6$ dependence on the distance separating those nuclei as was seen in the paramagnetic relaxation enhancement technique. Complications arise, however, when we

consider that the isolated two-spin system is a poor approximation of the actual situation, wherein an excited nucleus has not one but multiple simultaneous pathways for relaxation, through cross-relaxation to all neighboring nuclei on the substrate molecule, and through the many other pathways that contribute to longitudinal relaxation. In addition to the fact that multiple relaxation processes are occurring simultaneously, there is the added complication that once spin has been transferred from one nucleus to another through cross-relaxation (the primary NOE), the second nucleus will then proceed to transfer that newly acquired magnetic energy to its nearest neighbors, resulting in the generation of secondary and higher-order NOE's which carry no information about the distance between the two nuclei in the original interaction. This higher-order spin-transfer process is aptly called spin-diffusion, as it describes the process by which the NOE becomes completely non-specifically distributed. Spin-diffusion has been treated in theoretical fashion by Redfield (63), among others, as well as being first demonstrated in a real system by Kalk and Berendsen (64).

Spin-diffusion is a serious technical problem in NOE distance studies, and overcoming it to the extent where NOESY data can be used to determine conformations of bound substrates presents a formidable challenge. Indeed, if one considers the number of protons in an average sized protein molecule (an estimated 4000 protons per PGK molecule, for

example), and the fact that as many as 60% of those protons are in methylene groups (and are thus in very close proximity to other protons (65)), the number of spin diffusion pathways quickly becomes staggering, and it is amazing that the technique can give any useful distance information at all. However, careful analysis of the time-dependence of the development of NOE intensity can in many cases still provide a good estimate of the true cross relaxation rates that would be observed in the absence of any competing processes. A practical ramification of all of these competing processes is to place an upper limit of about 4 Å on the distances which can be reliably measured in this way.

One obvious way to reduce spin-diffusion is by reducing the "background" level of protons, thereby eliminating many spin-diffusion pathways. This has been attempted in various ways, and in the present studies we have used the perdeuterated PGK enzyme available in this laboratory to provide a greatly reduced proton background. Through the work described in her Master's Thesis, Celeste Shibata clearly illustrated the advantages of this system for NOESY studies of the type performed here (66). Another approach to reducing spin-diffusion is through reducing the mixing time, which is an instrumental parameter governing the time period allowed for the generation of the NOE, such that only the initial first-order processes (primary NOE's) have sufficient time to develop (this can have the undesired effect of reducing the

signal intensity, and therefore the signal to noise ratio). In the present study, this approach was also utilized, and a third parameter was also varied, that being the substrate to enzyme ratio. Lowering this ratio has the effect of reducing the residence time of the substrate at the active site of the enzyme, again resulting in a shorter time period for the development of NOE's, as will be illustrated more fully in the "Results" and "Discussion" sections of this chapter. It should be emphasized that the ligand residence time does not correspond to the time required for a single binding event (which remains unchanged at all ratios); rather, it represents the number of opportunities in a given time period that a particular substrate molecule will have to bind at the active site. It is hoped that all of this parameter optimization has the effect of demonstrating in a reliable way that the NOESY data being used for conformational analysis was acquired under conditions that minimized the contributions of secondary processes, thereby assuring that the determined conformation most closely represents the actual conformation of the substrate molecule bound at the active site of the enzyme.

B. Experimental Procedures

1. *Materials*

[U-^{13}C]Glycerol was obtained from NIH Stable Isotope Resource at Los Alamos. β,γ-bidentate $Cr(H_2O)_4ATP$ was prepared immediately before use as described in the "Experimental Procedures" section of Chapter II, and diluted with ^2H_2O for ^1H NMR experiments. 99.9 atom % and 99.96 atom % ^2H_2O was purchased from Isotec and Wilmad, respectively. Deuterium chloride and sodium hydroxide-d (both 99.9 atom %) were from MSD Isotopes. All other chemicals used were of the highest grade commercially available. Stock buffer solutions were passed over Chelex 100 resin to remove trace metals prior to use. pH of solutions in ^2H_2O (pH*) is reported as read directly from the pH meter. [U-^{13}C]3PGA was prepared from [U-^{13}C]glycerol as described (67), and was purified by Sephadex LH-20 chromatography.

Perdeuterated PGK (^{2}HPGK) used in the NOE studies was isolated from *Saccharomyces cerevisiae* strain 20B-12 containing multi-copy plasmid pCGY219 which had been grown in fully deuterated medium as described (66); Sephacryl HR200-S chromatography was run in 2 mM deuterated sodium acetate buffer at pH 7.2. ^{2}HPGK was exchanged into ^2H_2O by successive rounds of lyophilization followed by dissolution in ^2H_2O. 2'deoxy-ATP (dATP) and DL-α-glycerophosphate were purchased from Sigma. Deuterated acetic acid used in preparing the

deuterated acetate buffer was from Cambridge Isotope Laboratories.

2. *Magnetic Resonance Methods*

The paramagnetic effect of CrATP on the relaxation rates of the protons of 3PGA bound in the ternary complex were determined at 200 and 250 MHz (Nicolet NMC-200 and Bruker AC-250 instruments, respectively), using the inversion recovery method with 500 μl samples in ^2H_2O, and 16 variable delay values ranging from 2 ms to 15 s. 90° pulse widths were around 5.2 μs. Chemical shifts were referenced to external DSS. To avoid the interference of Tris protons, PGK was first exchanged into 5 mM Na^+ acetate by passage through a Sephadex G-25 column equilibrated with 5 mM acetate buffer pH 5.9. The enzyme was then exchanged into ^2H_2O by three cycles of lyophilization and redissolving in ^2H_2O. NaCl, Na_2SO_4, and 3PGA solutions were directly prepared in ^2H_2O. Samples contained 0.108 to 0.338 mM PGK, 7 to 10 mM 3PGA, and either 60 mM NaCl or 20 mM sulfate, in acetate buffer at pH 5.9.

The paramagnetic effect of CrATP on the relaxation rates of 3PGA phosphorus was measured at 161 MHz on a Bruker AMX-400 wide bore spectrometer equipped with a 5 mm quad-nuclear (^1H, ^{11}B, ^{13}C, and ^{31}P) probe. Relaxation rates were determined by inversion recovery with proton decoupling. Typically, 90° pulse widths were 8 μs, and 8 variable delays ranging from 1 ms to 30 s were used. Chemical shifts were referenced to

external phosphoric acid. Samples were composed of 0.35 to 0.45 mM PGK, 8.3 mM 3PGA, and either 60 mM NaCl or 20 mM sulfate, in 50 mM MES-NaOH buffer at pH 5.9, with 20% (v/v) ^2H_2O as the lock solvent. Transverse relaxation rates ($1/T_2$) were estimated from the widths of resonances at half-height ($\Delta\nu_{1/2}$), where $1/T_2=\pi\Delta\nu_{1/2}$.

The paramagnetic effect of CrATP on the relaxation rates of 3PGA carbon atoms was measured at 62 MHz on a Bruker AC-250 spectrometer. T_1 values were determined using the progressive saturation method (68) due to the fact that the extremely long delays needed for complete relaxation of the carbonyl carbon made the use of inversion recovery time-prohibitive. Progressive saturation experiments were carried out using a pulse program of my own design called JT1PS.AU (Figure IV-1), the language of which is compatible with Bruker AC instruments equipped with ASPECT 3000 computers and the ADACOS operating systems. Control experiments showed that T_1 values for the carbons of 3PGA were identical when determined with inversion recovery and progressive saturation (data not shown). Chemical shifts were referenced to external dioxane (67 ppm). 5 to 7 variable delays were used, ranging from 1 to 1000 s, and 90° pulses were around 6.5 μs. The binary titration sample consisted of 10.5 mM [U-^{13}C]3PGA in 50 mM MES-NaOH pH 5.9, with 20% (v/v) ^2H_2O. Samples for the ternary titrations contained 0.3 to 0.4 mM PGK, 9.9 mM [U-^{13}C]3PGA, and either 60 mM NaCl or

20 mM sulfate, in 50 mM MES-NaOH buffer at pH 5.9, with 20% (v/v) ^2H_2O.

Heteronuclear ^1H-^{13}C correlated spectroscopy was done on a Bruker AMX-400 spectrometer using standard Bruker software. The sample was composed of 150 mM 3PGA in ^2H_2O at pH 6. The temperature dependence of $1/fT_{1p}$ in the binary and ternary complexes of PGK, 3PGA and CrATP was examined at 14°, 24°, and 34°C at 200 MHz. Sample composition was as described above for analysis of the paramagnetic effect of CrATP on the protons of 3PGA.

The correlation time for the dipolar electron-nucleus interaction in the ternary PGK·CrATP·3PGA complex in the presence and absence of 20 mM sulfate was determined by studying the frequency dependence of $1/T_{1p}$ of water protons at 15, 24.3, 42, and 59 MHz with the Seimco NMR spectrometer using the null point method, and at 250 MHz on a Bruker AC-250 spectrometer and 400 MHz on a Bruker AMX-400 spectrometer using inversion recovery. Evaluation of τ_c was performed as described earlier (48,49). Samples contained 0.383 mM PGK, 0.187 mM CrATP, 5.2 mM 3PGA, and either 60 mM NaCl or 20 mM sulfate, in 40 mM MES-NaOH pH 5.9 with 20% (v/v) ^2H_2O. Corrections were made to account for the paramagnetic effect of free CrATP on the observed relaxation rates (48,49).

Two-dimensional transfer NOE spectroscopy (TRNOESY) was performed at 27°C on the Bruker AMX-400 instrument equipped with a 5 mm proton-selective probe for optimum proton

with irradiation of the residual $^2HO^1H$ peak during the relaxation delay period. The dependence of NOE intensity upon mixing time was analyzed at four mixing time values over the range 15 to 90 msec, using three different ratios of [MgdATP]/[^{2}HPGK]: 18:1, 22:1, and 55:1. Samples were composed of 0.38, 0.28, or 0.09 mM ^{2}HPGK and 7.0, 6.2, or 5 mM dATP, respectively; samples also contained 50 mM deuterated acetate buffer pH 7.2, 50 mM NaCl, 1.5-3 mM D-α-glycerophosphate, and $MgCl_2$ in 1 mM excess of nucleotide concentration, in a final volume of 0.5 ml of ^2H_2O.

3. *Calculation of Inter-proton Distances for dATP from 2DTRNOESY Data and Evaluation of the Effect of Mixing Time and [MgdATP]/[^{2}HPGK] Ratio*

The NOE intensities for all of the spectra under all conditions were quantitatively evaluated using the volume integration routine in the Bruker Instruments UX-NMR software package. These data were then analyzed using the MARDIGRAS (**M**atrix **A**nalysis of **R**elaxation for **DI**scerning the **G**eomet**R**y of an **A**queous **S**tructure) FORTRAN program developed by B.A. Borgias and T.L. James at the University of California at San Francisco. This program was designed to calculate inter-proton distances from cross-peak intensities measured from TRNOESY experiments, taking into account all of the spin-diffusion that was observed in the data. The program requires as input a Protein Data Bank (PDB) file of the structural coordinates

a Protein Data Bank (PDB) file of the structural coordinates of the molecule of interest (in our case, dATP); an intensity file containing measured NOE intensities for all observed cross-peaks, including those due to spin diffusion; and a parameter file containing information such as the correlation time for the system, the mixing time that was used to collect the data, the noise level in the measured intensities, and other factors. The program then iteratively calculates inter-proton distances using the PDB coordinates as a starting structure, and outputs those calculated distances to a separate file, along with the RMS error in the calculated distances after the last iteration. The program also allows for the input of certain fixed-distance constraints to be taken into consideration; in the present study, the H2′-H2″ distance was held constant at 1.79 Å and the H2′-H1′ distance was held constant at 2.92 Å, with the program calculating all other distances according to these constraints. These distances are known from X-ray crystallography to a very high precision (H2′-H2″ = 1.78 ± 0.01 Å, H2′-H1′ = 2.92 ± 0.20 Å). The major primary NOE interactions that are necessary for determining the conformation of bound dATP are the H1′-H4′, H2″-H4′, and H2″-H5′5″ NOE's for the pucker of the ribose ring, and the H2′-H8 and H5′5″-H8 NOE's for the determination of the glycosidic angle.

C. Results

1. *Paramagnetic Effects of CrATP on the Longitudinal Relaxation rates of the Protons of 3PGA*

A one-dimensional ^{1}H NMR spectrum of 3PGA is shown in Figure IV-2. The resonances were assigned by two-dimensional heteronuclear ^{1}H-^{13}C correlated spectroscopy (Figure IV-3). The multiplet centered at 4.24 ppm was assigned to the proton attached to carbon 2 (designated H2), and the multiplets centered at 4.01 and 4.13 ppm were designated as H3 and H3′, respectively.

Under the conditions of the present study, [3PGA]/[PGK] ratios used were sufficient to give greater than 92% of the enzyme in the binary PGK·3PGA complex at the beginning of the paramagnetic titrations. Titration of CrATP into samples containing PGK and 3PGA resulted in an increase in the $1/T_1$ values of the protons of 3PGA in the presence or absence of sulfate. Figure IV-4 shows the observed $1/T_1$ values plotted against the concentration of CrATP bound in the ternary PGK·CrATP·3PGA complex in the absence of sulfate. $1/T_1$ values varied linearly with bound CrATP concentration under these conditions, as well as when sulfate was included (Figure IV-5). Despite the multiplicity of the resonances, the inversion recovery plots were not multiphasic within the time range used to determine T_1. In order to correct for the effect of free CrATP and binary CrATP·3PGA complex on the longitudinal

relaxation rates of 3PGA protons, the same titration was performed in the absence of PGK (Figure IV-4, dashed line). Comparison of the paramagnetic effects of CrATP on $1/T_1$ of 3PGA protons in binary and ternary systems shows that the presence of PGK results in an enhancement of the paramagnetic effect of CrATP, indicating the formation of a ternary PGK·CrATP·3PGA complex. Furthermore, the presence of sulfate causes significant changes in the relative and absolute paramagnetic effect of CrATP on the three protons (note the different scales on CrATP axis in Figures IV-4 and IV-5). The corrected and normalized paramagnetic effects ($1/fT_{1p}$) of CrATP on the 3PGA protons in the ternary PGK·CrATP·3PGA complex are given in Table IV-1, and were used for distance determinations after justifying that they contain distance information as described below.

2. ***Paramagnetic Effects of CrATP on the Longitudinal Relaxation Rates of the ^{31}P of 3PGA***

The proton-decoupled ^{31}P NMR spectrum of 3PGA yields a singlet 4.17 ppm downfield from H_3PO_4 (data not shown). Addition of the enzyme caused a 3 ppm upfield shift of the 3PGA resonance, as well as significant broadening, indicating binary complex formation (data not shown). Similar to ^1H NMR studies, titration of CrATP into this sample resulted in an enhancement of the paramagnetic effects of CrATP on $1/T_{1p}$ of 3PGA phosphorus as compared to the same experiment without

enzyme (Figure IV-6). The presence of 20 mM sulfate anion reduced the paramagnetic effect of CrATP on $1/T_{1p}$ in the PGK·CrATP·3PGA complex (Figure IV-6). The addition of 5 mM ATP removed the observed paramagnetic effects indicating that the outer sphere contribution to the observed relaxation rates was negligible. Table IV-1 contains the $1/fT_{1p}$ values determined from these experiments. In the ternary complex, the $1/fT_{2p}$ values of phosphorous exceeded all of the $1/fT_{1p}$ values by more than an order of magnitude (Table IV-1), which is consistent with fast exchange conditions.

3. *Paramagnetic Effects of CrATP on the ^{13}C Longitudinal Relaxation Rates of 3PGA*

The proton-decoupled ^{13}C spectra of both natural abundance and U-[^{13}C]3PGA are shown in Figure IV-2. The resonances centered at 68, 73, and 179 ppm were assigned as C3, C2, and C1 respectively based on chemical shifts and two-dimensional heteronuclear ^{1}H-^{13}C correlated spectroscopy with the unlabelled compound (Figure IV-3). Determinations of metal to proton distances had indirectly indicated the positions of C2 and C3. Since the position of C1 was undetermined, and since this carboxyl group represents the acceptor for the transferred phosphoryl group in the reaction catalyzed by phosphoglycerate kinase, the data aquisition parameters were optimized for determination of the metal to C1 distance.

Figure IV-7 shows the effect of titrating CrATP into samples containing either 3PGA alone, or 3PGA and PGK in the presence and absence of sulfate. The enhancement of $1/T_{1p}$ in the presence of enzyme, as well as the decreased slope of the $1/T_{1p}$ versus [CrATP] curves in the presence of sulfate ion as compared to the no sulfate case, are both clearly visible. These findings agree well with the observations with the other nuclei. A much larger effect was observed with the C2 carbon, which is shown as an inset in Figure IV-7 due to large differences in T_1 values as compared to C1. This is in excellent agreement with the observed effect of sulfate on the paramagnetic effect of CrATP on H2. The C3 carbon peak was obscured by an impurity when sulfate was present and therefore the paramagnetic effect of CrATP on this resonance was not determined under these conditions. This does not have a large effect on the determination of the conformation of 3PGA since the position of this atom was determined by known distances to the directly bound protons. The $1/fT_{1p}$ values obtained from this data are given in Table IV-1.

4. *Determination of the Correlation Time and Evaluation of Temperature Dependence of $1/fT_{1p}$ of 3PGA Protons*

The temperature dependence of $1/fT_{1p}$ of the protons of 3PGA was examined in order to assure that fast exchange conditions were being met. In this experiment, fast exchange is indicated by a decrease in relaxation rate with increasing

temperature; increasing relaxation rates with increasing temperature is indicative of exchange limitation, since exchange rates ($1/\tau_M$) increase at higher temperatures. Figure IV-8 shows positive slope of $1/fT_{1p}$ versus 1000/T plots for all protons of 3PGA, indicating that the observed relaxation values can be used for distance determinations.

Determination of metal-nucleus distances from observed $1/fT_{1p}$ values requires a measurement of τ_c, the correlation time for the dipolar Cr^{3+}-nucleus interaction. τ_c was evaluated by measuring the $1/T_{1p}$ of solvent water protons of samples at six frequencies, as described under the "Experimental Procedures" section of Chapter III. The paramagnetic contribution to the relaxation rates ($1/T_{1p}$) observed at 15, 24.3, 42, 59, 250, and 400 MHz for the binary and ternary complexes of CrATP in the presence and absence of sulfate are listed in Table IV-2. The measured relaxation rates were corrected to account for the contribution of free CrATP and τ_c was determined, by using a least squares fitting computer program with an 8.8% error, according to the following equations (47):

$$1/\tau_c - 1/\tau_s = \frac{B\tau_r}{1+\omega_s^2\tau_r^2} + \frac{4B\tau_r}{1+4\omega_s^2\tau_r^2} \qquad \text{(Equation IV-1)}$$

and

$$f(\tau_c) = \frac{3\tau_c}{1 + \omega_I^2\tau_c^2} + \frac{7\tau_c}{1 + \omega_S^2\tau_c^2} \qquad \text{(Equation IV-2)}$$

where τ_c is the dipolar correlation time, ω_I and ω_s are the nuclear and electron precession frequencies, respectively, τ_s is the longitudinal electron spin relaxation time, B is the zero field splitting parameter, and τ_v is a time constant for ligand motion that modulates B.

The determined τ_c values are shown in Table IV-2; these values were used in the calculation of metal to nucleus distances, and are similar to values observed earlier for enzyme-bound CrATP (57,69). τ_c values for the various complexes were also calculated assuming τ_c to be independent of frequency; this analysis yielded slightly shorter distances, but did not affect the determined distances beyond the error limits shown in Table IV-2.

5. *Determination of Cr^{3+} to Nucleus Distances in Ternary Complexes*

Distances of the nuclei of 3PGA from Cr^{3+} of CrATP in the ternary enzyme·CrATP·3PGA complex in the presence and absence of sulfate were calculated according to the equation (70):

$$r = C[(qfT_{1p})f(\tau_c)]^{1/6} \qquad \text{(Equation IV-3)}$$

where r is the internuclear distance, C is the product of known physical constants, q is the stoichiometry, and $f(\tau_c)$ is given by Equation IV-2 (above). The C values used were 705, 522, and 445 for protons, phosphorous, and carbon, respectively (71). The results of these calculations, which represent the Cr^{3+} to 3PGA nucleus distances in the ternary complexes in the presence and absence of sulfate, are given in Table IV-1. These distances can be built into a model which allows for direct transfer of the phosphoryl group under both ionic conditions (Figures IV-9 and IV-10). The substrate arrangements shown in the figures were built using the Desktop Molecular Modeller software from Oxford University Press.

6. *Analysis of the Dependence of the Intensity of MgdATP NOE's on Mixing Time and on [MgdATP]/[^{2}HPGK] Ratio*

The spectra in Figures IV-11 and IV-12 show the NOE intensities for the 18:1 [MgdATP]/[^{2}HPGK] ratio sample at two extreme mixing times (15 and 70 msec, respectively). Comparison of these two figures shows that the longer of the two mixing times allows ample time for significant spin-diffusion to develop. This is evident in the appearance of the H2″-H8, H4′-H8, H2′-H4′, H2″-H5′5″, and H1′-H5′5″ NOE's, and especially in the appearance of NOE's from H1′ and H4′ to H2 of the adenine ring. Figure IV-13 (acquired at a [MgdATP]/[^{2}HPGK] ratio of 22:1 using 70 msec mixing time) shows that spin-diffusion is less prevalent under these

conditions, since the secondary NOE's described above are either absent or reduced in intensity. Figure IV-11 also shows that even at this short mixing time, the major primary NOE cross-peaks necessary for determination of the dATP conformation are strongly visible.

A plot of %NOE versus mixing time (where %NOE indicates NOE cross-peak intensities that have been normalized to a percent of the intensity of a diagonal peak, in this case the H1′ resonance) for the 18:1 ratio data (Figure IV-14) shows that, with the exception of the H2′-H2″ NOE, all of the observed NOE intensities have nearly converged to the same level at 70 msec mixing time. Similar analysis of the data from the 22:1 ratio experiment shows the same behavior, although the convergence is less rapid (Figure IV-15). Also, even though there are fewer NOE interactions visible in the data taken at 55:1 [MgdATP]/[^{2}HPGK] ratio, the convergence for the visible NOE's is even less pronounced, as shown by the fact that the H2′-H8 NOE is still increasing in intensity even after 90 msec mixing time, and the H2′-H2″ NOE is only beginning to level off at that point (Figure IV-16). A plot of %NOE (at 15 msec mixing time) versus [MgdATP]/[^{2}HPGK] ratio for three prominent NOE interactions (H1′-H4′, H2′-H8, and H2″-H1′) shows the effect of decreased ligand residence time on the dynamic range of the data (Figure IV-17); the error in the distances calculated from those data would be expected to increase as the dynamic range of the data decreases. The

ramifications of these effects will be more fully explored in the "Discussion" section of this chapter.

7. Determination of the Conformation of MgdATP Bound at the Active Site of PGK in a Ternary ^{2}HPGK·dATP·Glycerol-3P Complex

The interproton distances calculated from the data acquired at a [MgdATP]/[^{2}HPGK] ratio of 18:1, with a mixing time of 15 msec, are shown in Table IV-3. Included for comparison are the distances calculated from the 22:1 ratio and 15 msec mixing time experiment. The distances shown in this table were calculated as described in "Experimental Procedures", Section 3, and were then used to construct a model of dATP using the Desktop Molecular Modeller software. The resulting structure, which represents the conformation of dATP at the active site of the ternary complex, is shown in Figure IV-18. From this model, the pucker of the ribose ring is seen to be O4'-endo, and the glycosidic angle was determined to be 59° (Figure IV-19).

Figure IV-20 shows a plot of interproton distance (as calculated by MARDIGRAS) versus mixing time for the 18:1 ratio data. The plot shows that as mixing time is increased, the calculated distances appear to converge toward some average value. The distances calculated for the 22:1 ratio data exhibit the same behavior, although, as was seen for %NOE's versus mixing time, the convergence is less rapid at this higher ratio (Figure IV-21). Finally, the 55:1 ratio data, due

in part to the lack of NOE interactions observed at this ratio, and in part to the greatly decreased dynamic range in the NOE's that were observed, could not be fit by MARDIGRAS to give acceptable distances across the entire mixing time range based on the starting model (the PDB coordinates). The first two mixing times gave distances that were (marginally) acceptable under the input constraints (Figure IV-22); beyond 25 msec mixing time the program could not calculate the H2′-H8 distance from the data, and this distance is vital to the determination of the glycosidic angle. A plot of calculated distance *r* (from the data taken at 15 msec) versus [MgdATP]/[^{2}HPGK] ratio for the H1′-H4′, H2′-H8, and H2″-H1′ interactions shows that the distances as calculated by MARDIGRAS appear to diverge at higher ratios (Figure IV-23); the corresponding RMS errors increased as well, from 1.07 to 1.69. The program also calculates a cross-peak intensity based on the calculated distances; the average % error between the MARDIGRAS calculated NOE's and those observed experimentally increased from 20.8% to over 107% as the [MgdATP]/[^{2}HPGK] ratio was increased.

D. Discussion

The presence of phosphoglycerate kinase was observed to enhance the paramagnetic effect of CrATP on relaxation rates of 3PGA nuclei, showing the formation of a ternary PGK·CrATP·3PGA complex. In order to use this relaxation data for metal to nucleus distance determinations, it is necessary to estimate the contribution of τ_M, the exchange rate of the substrate from the paramagnetic complex, to the observed relaxation rates. This was done by measuring the temperature dependence of $1/fT_{1p}$. Figure IV-8 shows that $1/fT_{1p}$ values decreased as temperature increased, indicating fast exchange of 3PGA out of the ternary complex. Since $1/\tau_M$ would be expected to increase at higher temperatures, the data suggest that τ_M does not contribute to the observed relaxation rates. Additionally, frequency dependence of $1/T_{1p}$ values (Table IV-2) is indicative of fast exchange conditions since τ_M is independent of frequency. Therefore, the observed relaxation rates carry distance information and can be used in the determination of metal to nucleus distances. Table IV-1 shows the determined metal to nucleus distances for the nuclei of 3PGA in the ternary complex. The distances were determined from data collected in three different types of experiments for each ionic condition, with each experiment optimized to observe effects on the particular nuclei of interest and each one using different enzyme and CrATP preparations. Despite

this, the distances determined from these experiments all converge at a single point (corresponding to the metal center), suggesting that no systematic errors were introduced by the different experimental conditions. Models of the conformation of 3PGA at the active site of PGK with and without sulfate were constructed using these determined distances. In building the models, we arbitrarily restricted the position of the carboxyl oxygen of 3PGA such that it was optimally aligned for phosphoryl transfer. Under both sets of conditions, at least one conformation of 3PGA was found that would yield an arrangement of substrates which satisfied the determined metal to nucleus distances. The resulting models were checked to make sure that there was no van der Waals overlap between the 3PGA nuclei and the water ligands of Cr^{3+}. Figures IV-9 and IV-10 and the distances in Table IV-1 show that all 3PGA nuclei were farther from the metal when sulfate was present. In addition to an overall increase in the distance of 3PGA from Cr^{3+}, sulfate causes relative conformational changes of 3PGA. Of the 3PGA protons, H3′ is closest to the metal center, followed by H3 and H2. With sulfate present, H2 becomes the closest, followed by H3′ and H3, and all are farther from Cr^{3+} than in the sulfate-absent case. These results are confirmed by the determined metal to carbon distances that indicated significant lengthening of Cr^{3+} to C2 distance in the presence of sulfate (Figures IV-9 and IV-10; Table IV-1). Another significant change was

observed in the metal to phosphorus distance, which was also longer when sulfate was present. If sulfate ion binds at the active site, electrostatic interactions may cause displacement of the phosphoryl group by sulfate, resulting in the observed altered arrangement of substrates. However, many other explanations are also possible.

Despite significant changes in the conformation of 3PGA, the carboxyl carbon to metal distance remains fairly constant under both conditions, with only a slight increase observed with sulfate present. This suggests a small change in the distance between the attacking nucleotide and γ-phosphorus of ATP. Based on the models shown in Figures IV-9 and IV-10, we determined oxygen to phosphorus distances of 4.43 Å and 4.85 Å in the absence and presence of sulfate respectively. M. Cohn and co-workers reported a 15% decrease in the rate of phosphoryl transfer in the presence of an activating concentration of sulfate (18); the observed distance increases, possibly along with a deviation from optimum transfer alignment, could be one explanation for their findings. However, it is unlikely a change of this small magnitude would lead to a change in the reaction mechanism in the presence of sulfate.

One striking feature of the TRNOESY spectrum shown in Figure IV-11, acquired with a 15 msec mixing time and [MgdATP]/[^{2}HPGK] ratio of 18:1, is a background virtually free of interfering protein NOE cross-peaks, a result of using

perdeuterated PGK in the experiments. The low background allows for quantitative assessment of the H2′-H2″ NOE, which is swamped out by the diagonal when protiated PGK is used. This is important, since both of these protons are bonded to the same carbon, and the distance between them is necessarily fixed. Therefore, the magnitude of this NOE can be used as an additional constraint for the distance calculation program, and as a spectral ruler for determination of the unknown distances; an observed NOE of a given magnitude, developing between two protons which are separated by a known, fixed distance, can be used to ratio other inter-proton distances from their observed NOE's. In addition to the lack of interfering protein NOE's, the reduced number of protons overall allows for the receiver gain of the NMR instrument to be increased at a given concentration of dATP over when protiated PGK is used. The increased receiver gain enhances the signal to noise ratio in the spectra, reducing the error in the measured NOE intensities.

Extensive spin-diffusion in the spectrum shown in Figure IV-12 is evident from the presence of strong NOE's between the H2″-H8, H4′-H8, H2′-H4′, H2″-H5′5″, and H1′-H5′5″ proton pairs, which are probably mediated through intervening substrate protons. The extent of spin-diffusion is especially pointed out by the presence of an NOE from H4′ to H2 of the adenine ring, which is probably mediated through the H1′ and H2″ protons. The H1′-H2 NOE (representing a distance of

greater than 4 Å) would normally have to be attributed to spin diffusion; however, one consequence of the deuterated background is to allow for the measurement of longer distances with this technique, so the possibility that the 1′-H2 NOE is a result of a primary interaction can not be ruled out here. A comparison of these spectra to Figure IV-13 and (which was acquired at a [MgdATP]/[^{2}HPGK] ratio of 22:1 using 70 msec mixing time) illustrates two important points. First, one effect of increasing the ratio and therefore decreasing the residence time of the dATP at the active site is that spin-diffusion is circumvented for relatively longer at the higher ratio. Specifically, Figure IV-13 shows that none of the H2 interactions are visible, and the other higher order interactions are reduced in intensity as compared to Figure IV-12 (same mixing time, 18:1 ratio). Second, the intensity of the primary NOE's is also reduced at the higher ratio, resulting in lower signal to noise ratio, and thus larger error in the measured NOE intensities. The convergent behavior observed in plots of %NOE versus mixing time (Figures IV-14 and IV-15) is indicative of significant spin-diffusion under these conditions at mixing times greater than 15 msec.

What do the results of the NOESY data analysis presented suggest regarding the best way to acquire NOESY data for structural studies? It could be proposed that the rapid convergence observed in the %NOE versus mixing time and calculated distance versus mixing time plots using lower

ratios argues for acquiring NOESY data at higher [substrate]/[enzyme] ratios, where the decreased ligand residence time serves to counter the effects of spin-diffusion. However, the low signal to noise ratio and the relative lack of observable NOE constraints at the higher ratio led to high error in the calculated distances and a poorly defined final structure. The use of longer mixing times at the higher ratio could increase the signal to noise ratio and would allow for the observation of weaker NOE's. Unfortunately, the upper limit of the mixing time is determined by physical parameters of the system (most notably the correlation time, τ_c) making data acquisition at mixing times longer than approximately 300 msec counter-productive, due to competing processes such as the appearance of NOE's from the free substrate. Also, it seems reasonable to suspect (although it has not been shown to be the case) that as the %NOE's observed in a system reach a certain level, the extent of spin-diffusion will be the same regardless of the conditions that led to the development of those NOE's (i.e. short or long ligand residence time). Therefore, acqusition of NOESY data at high [substrate]/[enzyme] ratios does not seem to be the best solution.

The above argument points to the use of lower [substrate]/[enzyme] ratios in the acquisition of NOESY data for structural determination; other aspects of the present study reinforce this suggestion. As was shown, the increased

signal to noise ratio, wider dynamic range of the data, and larger number of input intensities all serve to lower the error in the calculated distances and to give a more well-defined determined structure. It also seems reasonable that the lower limit of the useable mixing time range would set a lower limit to the ratio at which a good estimation of initial cross-relaxation rates could be obtained. That is, I suspect that in the plot of %NOE versus [MgdATP]/[^{2}HPGK] ratio, the dynamic range of the data will begin to converge again at some point as even lower ratios are used. In other words, a ratio will be reached beyond which an accurate estimation of initial cross-relaxation rates can not be obtained at 15 msec mixing time (which represents the lower limit of mixing time due competition from through-bond as opposed to through-space connectivities); a plot of %NOE versus mixing time for this data would show no mixing time dependence, and little or no difference between the intensities of the various NOE interactions at even the shortest mixing time. It would therefore appear that NOESY structural studies could benefit from in-depth analysis of the type presented here, in order to maximize the conditions under which the data are acquired, thus giving the best possible determined structure. Also, the data presented here make it clear that there is no single mixing time that will allow for optimal estimation of initial cross-relaxation rates for all primary NOE interactions.

Chapter V

General Discussion and Conclusions

The results described here offer the first evidence that the ternary complex of PGK and its substrates in solution has the substrates located close enough to each other to allow for direct transfer of the γ-phosphoryl group of metal·ATP to the carbonyl acceptor of 3-phosphoglycerate. This arrangement is consistent with the proposed closing of the enzyme active site when both substrates are bound. Such close approach of substrates as was seen in the absence of sulfate (4.43 Å) makes the formation of a phosphoenzyme or metaphosphate intermediate unlikely as a mechanism for phosphoryl transfer by PGK, lending support to the direct transfer mechanism proposed by Webb and Trentham (10) based on studies of phosphorous stereochemistry. However, the transfer distance of 4.85 Å estimated in the presence of sulfate is near the upper limit for an associative-type (S_N2) mechanism (4.9 Å)(72), leaving open the possibility of a dissociative (S_N1) reaction mechanism under these conditions. The fact that the activating metal coordinates to the ATP phosphoryl group undergoing substitution (the γ-phosphorous) in this case strongly favors an associative mechanism under both ionic conditions, since this coordination scheme is known to profoundly inhibit dissociative mechanisms and to activate associative ones (72).

It is important to note that the data presented in the present study does not provide any direct evidence for a hinge-bending conformational change. Therefore, we do not know whether the observed proximity of the substrates is due to active site closure or is simply the result of binding of the substrates at proximal sites on the enzyme. However, consideration of our results in light of the locations of the substrate binding sites as proposed from X-ray crystallography, as well as the small angle solution X-ray evidence of a large-scale conformational shift in PGK upon the addition of substrates, lends strong credence to the notion of PGK as a hinge-bending enzyme, in the manner of hexokinase and possibly other kinases.

It has been proposed by Koshland (73) and later by Steitz and co-workers (74) that hinge-bending, if indeed it is a common mechanism among kinases, serves a dual purpose in catalysis by these enzymes, with both purposes being served through the exclusion of water from the active site upon enzyme closure. One effect of the establishment of a solvent free active site would be to provide a low-dielectric environment in the area of catalysis; this would facilitate nucleophilic attack by making it easier for nucleophiles to maintain local charge distribution. Secondly, the phosphoanhydride bonds of the nucleotide substrates are highly susceptible to hydrolysis; therefore, excluding water from the active sites of kinases would also aid in establishing their

specificity of function. A water-free active site helps these enzymes become efficient phosphotransferases rather than adenosine triphosphatases, by eliminating water as a substrate.

One of the significant results of the work described here is the observation of an altered conformation of bound 3PGA when sulfate was present. The kinetic and water proton relaxation data are consistent with the arrangement of the substrates shown in Figures IV-9 and IV-10; measurement of enhancement values clearly showed that the metal ion is in different environments in the presence and absence of sulfate, and the kinetic data raised the possibility of a close-approach interaction of 3PGA and metal-nucleotide which was abolished by the addition of sulfate. Difference Fourier maps of horse muscle PGK in sulfate and tartrate (in the absence of substrates) have revealed the presence of two bound sulfate ions (6). In the PGK crystals, one of these sulfate ions interacts with Arg 168 and His 62, which have been shown to be involved in binding 3PGA (30). The other bound sulfate is proposed to interact with Lys 217, which is the site of a crystallographically determined selenate binding site (75), and is a point of interaction between the polyphosphate chain of bound nucleotide substrate and the enzyme. These anion binding sites have been designated the primary and secondary anion binding sites, respectively; however, this proposed location of the secondary anion site is considered speculative.

In the present study, it was observed from the determined conformations of bound 3PGA that although the bulk of the 3PGA molecule experiences large conformational changes upon the addition of sulfate, the position of the 3PGA carbonyl group, which acts as the acceptor for the transferred phosphoryl group, remains fairly constant. This observation warrants some discussion since these experiments were performed with a metal (Cr^{3+}) whose coordinated water ligands are very slowly exchanged under the experimental conditions. One effect of the presence of these (essentially) non-exchangeable water ligands would be to increase the effective van Der Waals radius of the metal center, from 0.63 Å for Cr^{3+} alone to 2.5-2.8 Å for Cr^{3+} with coordinated water molecules (71). Therefore, extremely close approach of a ligand such as 3PGA may be somewhat hindered by the presence of these coordinated water molecules. Indeed, in the presence of a catalytically active metal such as Mg^{2+} or Mn^{2+} whose coordinated water ligands exchange rapidly, the hydroxyl group attached to carbon 2 of 3PGA may approach the metal center even more closely than was observed in this study, by displacing a metal-coordinated water molecule (possibly even coordinating with the metal). This suggestion is strengthened by the observations from the kinetic characterization that K_i^{CrATP} exhibited dependence on the concentration of 3PGA, whereas the K_m^{MgATP} exhibited no dependence on 3PGA concentration. Similarly, previous work in this laboratory has shown that the presence of 3PGA reduces

the rate of inactivation of PGK by CrATP, but has no effect on PGK inactivation rates when sulfate is present (37). This proposed "overlap" interaction of 3PGA and Cr^{3+} of CrATP and the absence of such an observable effect with MgATP could be investigated from a structural standpoint, using Mn^{2+} (like Cr^{3+}, also paramagnetic, but exhibiting rapid ligand exchange) with the paramagnetic distance techniques described here. Such experiments might show even closer approach of 3PGA to the metal center in the absence of sulfate. However, preliminary experiments along these lines suggested to us that this system was exchange-limited with respect to the $1/T_1$ values of substrate protons, due to the fact that Mn^{2+} is a stronger paramagnet (hence, more efficient acceptor of magnetic energy) than Cr^{3+}. A metal such as Co^{2+}, which has a much weaker magnetic moment than Mn^{2+}, could be used instead, but other unfavorable magnetic properties of Co^{2+} make it a "last choice" alternative for studies of this type. Thus Cr^{3+}, despite (or in many ways because of) its slowly exchanging water ligands, represented the best overall choice for these studies.

One possible mechanism for anion-mediated activation of PGK, proposed by Fairbrother et al. (30), involves the formation of an "in-line" intermediate complex upon substrate binding and active site closure. The formation of this complex (presumably through coordination of 3PGA to the metal center, although this is not made clear) allows for the establishment

of an equilibrium between closed and open conformations of the enzyme without dissociation of the in-line complex, which remains bound to the enzyme through the nucleotide substrate. This would lead to the presence of open forms of the enzyme which has the substrate complex intact and the anion site exposed. Binding of anions to this open form is thought to lead to activation by increasing the dissociation rate of the products or the original substrates (the internal equilibrium constant for enzyme-bound reactants is near unity (18)). Binding of anions at the secondary site (at high anion concentrations) is thought to be inhibitory through direct competition with the nucleotide substrate.

Another model for anion-mediated activation, proposed earlier by Scopes (15), concerns itself with mechanisms by which the rate of dissociation of 1,3-bisPGA, the tight binding product ($K_D \leq 50$ nM), can be increased by anion binding, thereby speeding up the rate-limiting step of the reaction. He proposes a model in which 1,3-bisPGA is bound to the active site through contacts at both phosphoryl groups: the 1-phosphoryl, through the same groups that interact with the γ-phosphoryl of ATP, and the 3-phosphoryl, through the same groups that bind the 3-phosphoryl of 3PGA. Thus, the dissociation of 1,3-bisPGA is a two-step process. High concentrations of either substrate can activate catalysis by removing one of the 1,3-bisPGA binding interactions. Sulfate can activate catalysis by breaking either of these contacts,

and raises K_M for both substrates by direct competition via the same mechanism. A secondary anion site is invoked to explain high-sulfate induced inhibition, through mechanisms not described.

Based on the results of the present studies, an alternative description of these effects is proposed, one that retains aspects of both of the previous models. In this model, activation of catalysis both by sulfate and by substrates takes place through the primary anion binding site. 3PGA is believed to bind to the active site through multiple contacts (through the phosphate oxygens, the 2-hydroxy group, and the carboxyl group (7)). Binding of sulfate or substrates at the primary site is proposed to increase catalytic activity through both of the following mechanisms: first, by displacement through steric interference, of the 3-phosphoryl group of 3PGA (hence, of 1,3-bisPGA) from its site of interaction with the enzyme. The loss of a binding interaction of 1,3-bisPGA leads to more rapid product dissociation, in the manner described by Scopes. It would also be expected to lead to an increase in the K_M of 3PGA for the same reason. Second, catalytic activation could be enhanced through the formation of a conformationally-altered active site, possibly induced by or mediated through the displaced 3-phosphoryl group of 3PGA. Features of this altered active site include a slightly more open substrate binding cleft in the closed form of the enzyme, allowing for more rapid 1,3-bisPGA dissociation, and slight

deformation of the nucleotide binding site, leading to the increased K_M for MgATP observed under these conditions. The existence of a secondary anion binding site responsible for anion-induced inhibition is still a likely hypothesis, although the location of this site as proposed by Fairbrother et al. is considered unlikely. Conjecturally, anion-induced inhibition could be mediated through interruption of ionic interactions in the hinge region which allow for hinge destabilization and permissive hinge bending, shifting the equilibrium in solution toward an open, rigid, catalytically inactive form of the enzyme.

The type of in-depth analysis of the dependence of %NOE and calculated distance on mixing time and on [substrate]/[enzyme] ratio that is described here has not been performed before on an experimental system, due to the fact that lack of a perdeuterated enzyme (hence high background of protein NOE's and rapid onset of significant spin-diffusion) made the working range of ratios and mixing times prohibitively narrow. The types of effects that are described here have therefore only been previously shown in theoretical systems, wherein the dependence of %NOE and calculated distances were derived through computer simulations with an ideal system (76). Still, the results of that theoretical treatment accurately predicted (at least qualitatively) the trends that we have observed in our experimental system; NOE intensities were predicted to converge rapidly toward some

average value as mixing time and (or) ligand residence time was increased, and the distances calculated from those intensities converged correspondingly. Quantitatively, however, the results of our work suggest that the simulations significantly under-estimated the rapid onset and full extent of the contributions of spin diffusion; we observed convergence of calculated distances to a much greater degree using a perdeuterated enzyme system than was predicted for a fully protiated protein background. The ramifications of the present results on NOE-based structural and sequence-assignment investigations found in recent literature, many of which were performed using a 10:1 [substrate]/[enzyme] ratio and mixing times of 150 to 300 msec (in fully protiated protein sytems) can be readily appreciated.

The glycosidic angle that was determined from the conformation of MgdATP bound at the active site of PGK is similar to that determined for other kinases, including rabbit muscle adenylate kinase (57) and pyruvate kinase (77). It has been suggested that a correlation exists between conformational strain of the nucleotide and substrate specificity for nucleotide-binding enzymes (78). When free in solution, the base portion of nucleotides prefer one of two general low-energy conformations, corresponding to *syn* and *anti* orientations (79). Deviations from these two general ranges, resulting in highly strained configurations, have been seen in enzymes which exhibit high specificity for the

nucleotide substrate; nucleotide bound at the active site of hexokinase, cAMP- dependent protein kinase, and RNA polymerase have χ values of 0°, 84° and 90°, respectively (80) as determined by NMR. However, pyruvate kinase and adenylate kinase exhibit lower nucleotide specifity and have correspondingly less-strained torsional angles of 30° and 65°, respectively. The value of 59° determined here for the glycosidic torsional angle of ATP bound to phosphoglycerate kinase places that enzyme in the latter, low substrate-specificity group; this is in agreement with the findings of Kuntz and Krietsch that yeast PGK can efficiently utilize alternate nucleotides as substrates (81).

Chapter VI

Partial Characterization of a 3→1 Phosphoglycerate Mutase Reaction

A. Introduction

As a side project to my main thesis research, I have been studying what appears to be a novel reaction associated with 3-phosphoglycerate, namely the transfer of a phosphoryl group from the 3-position of 3PGA to the 1-position of the same molecule, (a 3PGA mutase activity). This activity is interesting in that it represents a reaction of 3PGA that has not been described in the literature.

The activity was originally observed during an experiment to determine the effect of CrATP on the $1/T_1$ values of 3PGA protons in a ternary PGK·CrATP·3PGA complex in the presence of 20 mM sulfate. During the diamagnetic control portion of that experiment (measurement of 3PGA $1/T_1$'s in binary PGK·3PGA complex, i.e. in the absence of paramagnetic CrATP) the splitting pattern of two of the 3PGA resonances (H3 and H3′) simplified gradually over the course of about 2.5 hours of acquisition, accompanied by the "disappearance" of the H2 resonance (other spectral regions were not closely analyzed to find this "missing" peak). It was first suspected that we were witnessing an effect of sulfate; a nearly identical experiment had been performed before, with the only obvious difference

this time being the presence of sulfate. Subsequent incubation of 3PGA with sulfate in the absence of PGK failed to reproduce the previously observed changes in the 3PGA spectrum. We had also recently begun to use lab-purified PGK for experiments, with the previous experiments having been done with phosphoglycerate kinase purchased from Boehringer-Mannheim. UV analysis of the lab-purified enzyme revealed the presence of some contaminating material with an absorbance maximum at 260 nm. The addition of both a low pH precipitation step and a protamine sulfate precipitation of nucleic acids into the purification protocol was observed to remove the activity and to restore normal UV absorbance to the PGK solution. The decision was made at that time to attempt to determine exactly the nature of the reaction that 3PGA seemed to be involved in; subsequent experiments (described below) identified this as the 3→1 phosphoglycerate mutase reaction as mentioned earlier. We were also interested in identifying the factor(s) that were responsible for catalyzing this novel reaction.

It must be emphasized that the results described here represent only a preliminary investigation into this system. This chapter will not relate a complete, concise picture of the activity, its mechanism, the responsible catalytic agents, and its physiological significance; rather, I hope to convey a sense of what is currently understood about the activity, what is not understood, and what is hypothesized, through a description of the completed experiments and their results.

Hopefully, this information can serve to lay the groundwork for further investigation into this interesting chemical problem.

B. Experimental Procedures

1. *Materials*

Phosphoglycerate kinase used in these studies was isolated from yeast strain 20B-12 containing multi-copy plasmid pCGY219, using the purification procedure described below; both the yeast strain and the plasmid were kindly provided by Dr. Hitzeman of Genentech, Inc. Trichloro-acetic acid (TCA), ethylenediamine-tetraacetic acid (EDTA), 2-phosphoglycerate (2PGA), sodium phosphate, potassium pyrophosphate, and sonicated, single-stranded salmon sperm DNA Item # D-9156) were all obtained from Sigma. L-ascorbate and ammonium molybdate were obtained from Aldrich. All other chemicals (ATP, 3PGA, MES-NaOH, etc.) were obtained and/or prepared as described in the "Materials" sections of previous chapters.

2. *Isolation and Purification of PGK from Yeast*

Phosphoglycerate kinase was isolated following a procedure based on that of Scopes (82), with some modifications. Yeast cells were lysed by three successive

freeze-thaw cycles, and then taken up in an equal volume of lysis solution, containing 0.5 M ammonia, 1 mg/ml EDTA, and 1 mM PMSF. The resulting solution was stirred at room temperature for 6-8 hours, then allowed to sit overnight at room temperature without stirring. Stirring was restarted the next morning, and sufficient 0.5 M lactic acid was added to bring the pH to approximately 7.5. This solution was centrifuged at 30,000 x *g* for one hour and the pellet discarded. Contaminating nucleic acids were precipitated by the addition of 1 mg solid protamine sulfate per ml solution. This solution was stirred for 30 minutes and then centrifuged at 20,000 x *g* for one hour; the pellet was again discarded. 15 μg DNAse and 20 μg RNAse per ml of supernatant was added and allowed to incubate for 15 minutes at room temperature, followed by the addition of 30 g ammonium sulfate per 100 ml supernatant over a 15 minute period. The solution was stirred for 30 minutes and centrifuged at 20,000 x *g* for 15 minutes; the pellet was discarded. A second addition of ammonium sulfate (13 g/100 ml supernatant) was made as above and the solution was centrifuged. To the supernatant was added sufficient 5 M ammonium lactate, pH 3.5, to bring the supernatant pH to 4.3, resulting in the precipitation of the PGK. The solution was centrifuged, the pellet was dissolved in 1 ml of 10 mM Tris-HCl, pH 7.5, and this solution was purified on a Sephacryl HR-200S column (0.9 cm x 95 cm).

3. *NMR Measurements*

^{31}P NMR measurements were made on a Bruker AMX-400 wide bore spectrometer equipped with a 5 mm quad-nuclear (^{1}H, ^{11}B, ^{13}C, and ^{31}P) probe. Normally, 45° pulse widths were 3.5 μsec, and between 16 and 64 transients were summed for transformation, with 8 seconds delay for relaxation. Spectra were obtained with a 30 ppm window, and chemical shifts were referenced to external phosphoric acid (0.0 ppm). Samples were composed of 90-200 μM PGK, 5-9.8 mM 3PGA, 60 mM NaCl, 50 mM MES-NaOH pH 5.9, and 0.5 to 3 mg sonicated single-stranded DNA. NMR kinetic experiments were performed using a pulse program of my own design (Figure VI-1), the language of which is compatible with Bruker instruments using a UNIX-based operating system and the UX-NMR software package.

4. *Monitoring Mutase Activity Through Phosphate Determination*

Some experiments were performed by monitoring the timecourse of mutase activity under various conditions by analyzing the concentration of 1-phosphorylated product indirectly, following its hydrolysis to yield inorganic phosphate. Inorganic phosphate concentrations were determined using an ascorbate-molybdate procedure as described (83). Incubation mixtures contained 5.2 mM 3PGA, 20 mM MES-NaOH pH 5.9, 50 mM NaCl, and varying amounts of PGK solution and DNA as described in the "Results" section. Protein was observed to interfere with the phosphate assay and was therefore removed

from incubation mixtures by precipitating with 5% TCA, followed by centrifugation at 13,000 X *g* in a microcentrifuge prior to assaying for phosphate concentration. 3PGA was shown to be highly resistant to hydrolysis under the assay conditions, whereas acetyl phosphate was virtually completely hydrolyzed under the same conditions. Thus the rationale behind this assay, namely that any product formed would be hydrolyzed to form inorganic phosphate under the assay conditions, seems justified.

C. Results

1. *Identification of the Product*

^{31}P NMR revealed that the PGK solution (100 μM PGK, taken after the low-pH precipitation step) contained no phosphorylated species that could act as a phosphate donor for the reaction (Figure VI-2a). The addition of 3PGA to this enzyme solution showed that no reaction was observed under these conditions even after very long incubation times (Figure VI-2b). This spectrum also showed the presence of a small amount of contaminating 2PGA in the 3PGA solution (resonance at 3.55 ppm). The addition of 0.5 mg of DNA to the reaction resulted in the appearance of a new signal in the spectrum of 3PGA (Figure VI-2c,d,e). The chemical shift of this new resonance (-0.1 ppm) was coincident with that of the 1-

phosphoryl group of 1,3-bisPGA and to the phosphoryl group of acetyl phosphate (data not shown). The appearance of this new species was accompanied by a concomitant decrease in the total area under the 3PGA peak, indicating a decrease in the concentration of 3PGA in the sample (as shown by the increase in the height of the noise in the spectra as time passes; all spectra were acquired and processed identically, and were scaled such that the 3PGA peak was plotted to be 8cm tall. Therefore, an increase in the height of the noise level under these conditions indicates a decrease in the absolute intensity of the 3PGA peak.) The reaction was also accompanied by the appearance of a new resonance centered at 3.35 ppm, identified as inorganic phosphate based on identical chemical shifts (data not shown); a broad resonance centered at 1.95 ppm associated with the added DNA was also visible. The experiment was repeated using 3 mg of DNA (Figure VI-3); this experiment showed clearly that the DNA resonance is not changed during the course of this reaction. Very long incubations showed that the hydrolysis of all phosphorylated species to form inorganic phosphate occurred essentially to completion (Figure VI-4). Control samples of 3PGA and DNA showed no activity visible by NMR assay, even after 48 hour incubation (data not shown).

2. *Localization of the Activity*

The ability of PGK solution, taken at the various steps in the purification procedure, to catalyze the mutase reaction was analyzed. Initial cell lysate contained the activity to a high degree without the addition of DNA, as did the PGK solution taken after the protamine sulfate step, after RNAse and DNAse traetment, and after each of the ammonium sulfate precipitations (data not shown). Dialysis of the active enzyme solution against 1 mM MES-NaOH pH 5.9, followed by concentration of the dialysate, showed that the catalytic agent was present in both the the dialysate and the dialyzed enzyme (Figure VI-5), suggesting a very small (dialyzable) factor or factors (MW < 8000). Precipitation of PGK at pH 4.3 resulted in loss of the mutase activity in the pellet as well as in the supernatant (Figure VI-6). The activity could be re-constituted to a limited degree in the pellet fraction by the addition of DNA (data not shown). Re-constitiution of the activity in the supernatant by the addition of DNA was not attempted. When the low pH precipitation step was omitted, the activity was found to remain associated with the PGK fractions following passage through the Sephacryl HR-200S column.

Exhaustive dialysis of active PGK solution (against a total of several liters of buffer) completely removed the activity from the PGK solution. However, the active factor(s) did not survive in the dialysate in these experiments. Also, it was observed in separate NMR experiments that the inclusion

of Mg^{2+}, EDTA, and 20 mM sulfate had no observable effect on the activity; however, the presence of 2 mM sodium pyrophosphate seemed to inhibit the reaction as observed by ^{31}P NMR (data not shown).

3. *Preliminary Analysis of the Active Dialysate*

A sample of the concentrated dialysate, which contained the mutase activity, was fractionated by passage through a Sephadex G-10 column (1 X 45 cm) which had been pre-equilibrated with 5 mM MES-NaOH pH 5.9. The resulting 0.5 ml fractions were analyzed with respect to their absorbance at 260 nm (Figure VI-7). The fractions were pooled as follows: fractions 15-20 were pooled into a single fraction, as were fractions 21-29, fractions 30-35, fractions 36-40, fractions 40-45, and fractions 46-57. None of these pooled fractions alone was found to contain the mutase activity; however, activity was restored upon mixing them all together (data not shown). The UV/visible absorbance of the pooled fractions was analyzed between 230 and 340 nm; the resulting spectra are shown in Figure VI-8. These spectra show varying absorbance at 260 and 280 nm in the different fractions, suggesting at least a partial fractionation of components by the Sephadex G-10 treatment. The low pH supernatant was passed through the same column chromatographic procedure; the resulting fractions exhibited similar absorbances to the fractionated dialysate (data not shown), although the low pH supernatant was inactive

in the mutase assay. A sample of the concentrated, unfractionated dialysate was also analyzed via ^{1}H NMR; the resulting spectrum showed the presence of peaks in the chemical shift region of 1.0 - 2.6 ppm which are indicative of the H2′ and H2″ protons of the ribose ring of deoxyribonucleic acid, and also in the region from 7.0 - 9.5 at positions typical for nucleotide protons (Figure VI-9).

D. Discussion and Conclusions

The NMR data shows that the reaction being catalyzed in these experiments uses 3PGA as a substrate, as evidenced by the lack of any other phosphorylated species which could act as a phosphoryl donor, by the absence of any change in the spectrum of the added DNA, and most convincingly, by the concomitant loss of 3PGA as the product is formed. The identification of the product as "1PGA" is based on the coincident chemical shift of the product ^{31}P NMR resonance to that of the 1-phosphoryl group of 1,3-bisPGA, and also to that of acetyl phosphate, a chemically similar species to the proposed product. The possibility that the reaction being observed was the formation of 1,3-bisPGA was ruled out based on a couple of observations. First, the product of this reaction is more stable than 1,3-bisPGA, which decomposes by 50% after 27 minutes at pH 7.2 and 38°C (much faster at pH

6)(84). In contrast, the product of this reaction remains fairly stable (not more than 30% hydrolysis) for periods of 5-6 hours in aqueous solution at pH 5.9 and 27°C. Second, upon formation of 1,3-bisPGA as monitored by NMR, a shift of the position of the 3-phosphoryl resonance has been observed in these and other experiments (33). No such shift was seen for the reaction being studied here.

The appearance and gradual increase in intensity of a peak corresponding to inorganic phosphate would be expected, since although the proposed product is more stable than 1,3-bisPGA, a phosphoryl group at this position is inherently susceptible to hydrolysis. The appearance of this peak, and, at long time points, the fact that virtually all phosphate present is represented by this peak, has been interpreted as evidence that the reaction follows a course of production of 1PGA from 3PGA, followed by the irreversible hydrolysis of 1PGA to form inorganic phosphate, thus pulling the reaction to completion. However, it is perhaps equally likely that the 3→1 phosphoryl transfer is not always cleanly accomplished, resulting in the production of inorganic phosphate and 1PGA by the same process. It is also impossible to rule out the possibility that completely different processes are competing for 3PGA simultaneously, with one process catalyzing the 3→1 transfer and another process hydrolyzing 3PGA.

Quantitative evaluation of the various steps of the PGK purification in terms of specific activity of the mutase

reaction proved very difficult due to the necessity of dialyzing after the steps of interest and prior to assaying for mutase activity, in order to remove the high concentrations of protamine sulfate, ammonium sulfate, and other substances which might affect observed activity. Also it is likely that a severe problem in the reproducibility of the degree of activity observed in various experiments was due to inconsistency in the composition of the sonicated DNA. The reaction being observed could be a DNA-dependent reaction of a contaminating enzyme, with the observed slow rates reflecting the fact that it is present in very small quantities, or that the conditions are not optimized for the observation of this activity. Phosphoglycerate mutase, an enzyme which catalyzes the conversion of 3PGA to 2PGA, was found not to have the herein described activity. Also, it is significant to note that the activity was not present in PGK purchased from Boehringer. Additionally, it is not clear why the active factor(s) could be removed from PGK solution by dialysis, yet remained associated with the PGK fraction after passage through a meter long Sephacryl HR-200S column, although this could be evidence of an extremely tight association of the active factor(s) with PGK. Such tight association might also explain why DNAse and protease treatment had no observable effect on the activity; if the active factor(s) is a tightly-bound protein or DNA molecule, the tight association might offer protection from digestion.

Regardless of the responsible factor(s), this represents a reaction of 3PGA that has not been described in the literature, either through organic chemical processes or through catalysis by factors of biological origin. Recent results in the laboratory of Vishwanatha have shown that PGK is involved in the DNA replication process, filling the role of a primer recognotion protein (85). In light of this, the discovery of a seemingly DNA-dependent chemical process catalyzed by a factor or factors that co-purify (and therefore may associate closely) with PGK takes on added significance. Clearly, a great deal of work must be done in order to answer the many questions that remain concerning the nature of this activity.

List of References

List of References

1. Bucher, T. (1942) *Naturwissenschaften* **30**, 756-757.

2. Watson, H. C., Walker, N. P. C., Shaw, P. J., Bryant, T. N., Wendell, P. L., Fothergill, L. A., Perkins, R. E., Conroy, S. C., Dobson, M. J., Tuite, M. F., Kingsman, A. J. and Kingsman, S. M. (1982) *EMBO J.* **1**, 1635-1640.

3. Banks, R. D., Blake, C. C. F., Evans, P. R., Haser, R., Rice, D., Hardy, G. W., Merreit, M., and Phillips, A. W. (1979) *Nature* **279**, 773-777.

4. LaDine, J. R., and Cross, R. L. (1991) *J. Biol. Chem.* **266**, 7194-7198.

5. Mori, N., Singer-Sam, J., and Riggs, A. D. (1986) *FEBS Lett.* **204**, 313-317.

6. Blake, C. C. F., and Rice, D. W. (1981) *Phil. Trans. R. Soc. London A* **293**, 93-104.

7. Harlos, K., Vas, M., and Blake, C. F. (1992) *Proteins* **12**, 133-144.

8. Mas, M. T., Resplandor, Z. E., and Riggs, A. D. (1987) *Biochemistry* **26**, 5369-5377.

9. Minard, P., Bowen, D. J., Hall, L., Littlechild, J. A., and Watson, H. C. (1990) *Protein Engineering* **3**, 515-521.

10. Webb, M. R. and Trentham, D. R. (1980) *J. Biol. Chem.* **255**, 1775-1779.

11. McDonald, R. C., Steitz, T. A., and Engelman, D. M. (1979) *Biochemistry* **18**, 338-342.

12. Bennett, W. S., and Steitz, T. A. (1978) *Proc. Natl. Acad. Sci. U.S.A.* **75**, 4848-4852.

13. Pickover, C. A., McKay, D. B., Engelman, D. M. and Steitz, T. A. (1979) *J. Biol. Chem.* **254**, 11323-11329.

14. Larsson-Raznikiewicz, M. (1967) *Biochim. Biophys. Acta* **132**, 33-40.

15. Scopes, R. K. (1978) *Eur. J. Biochem.* **91**, 119-129.

16. Khamis, M. M. and Larsson-Raznikiewicz, M. (1981) *Biochim. Biophys. Acta* **657**, 190-194.

17. Wrobel, J. A. and Stinson, R. A. (1978) *Eur. J. Biochem.* **85**, 345-350.

18. Rao, B. D. N., Cohn, M. and Scopes, R. K. (1978) *J. Biol. Chem.* **253**, 8056-8060.

19. Dryden, D. T. F., Varley, P. G., and Pain, R. H. (1992) *Eur. J. Biochem.* **208**, 115-123.

20. Adams, B., Burgess, R. J., and Pain, R. H. (1985) *Eur. J. Biochem.* **152**, 715-720.

21. Betton, J., Desmadril, M., and Yon, J. M. (1989) *Biochemistry* **28**, 5421-5428.

22. Sachsenheimer, W., and Schulz, G. E. (1977) *J. Mol. Biol.* **114**, 23-36.

23. Evans, P. R., and Hudson, P. J. (1979) *Nature (Lond.)* **279**, 500-504.

24. Dunaway-Mariano, D. and Cleland, W. W. (1980) *Biochemistry* **19**, 1496-1505.

25. Jaffe, A. K., Nick, J., and Cohn, M. (1982) *J. Biol. Chem.* **257**, 7650-7656.

26. Dunaway-Mariano, D. and Cleland, W. W. (1980) *Biochemistry* **19**, 1506-1515.

27. Ray, B. D. and Rao, B. D. N. (1988) *Biochemistry* **27**, 5579-5585.

28. Moore, J. M. and Reed, G. H. (1985) *Biochemistry* **24**, 5328-5333.

29. Pineda, T., Kwon, O. S., Serpersu, E. H., and Churchich, J. E. (1993) *Eur. J. Biochem.* **212**, 719-726.

30. Fairbrother, W. J., Graham, H. C., and Williams, R. J. P. (1990) *Eur. J. Biochem.* **190**, 161-169.

31. Janson, C. A., and Cleland, W. W. (1974) *J. Biol. Chem.* **249**, 2567-2571.

32. Scopes, R. K. (1978) *Eur. J. Biochem.* **85**, 503-516.

33. Rao, B. D. N., Cohn, M. and Scopes, R. K. (1978) *J. Biol. Chem.* **253**, 8056-8060.

34. McClaugherty, S. H., and Grisham, C. M. (1982) *Inorg. Chem.* **21**, 4133-4138.

35. Yount, R. G., Babcock, D., Ballantyne, W., and Ojala, D. (1971) *Biochemistry* **10**, 2484-2489.

36. Schierbeck, B. and Larsson-Raznikiewicz, M. (1979) *Biochim. Biophys. Acta* **568**, 195-204.

37. Serpersu, E. H., Summitt, L., and Gregory, J. D. (1992) *J. Inorg. Biochem.* **48**, 203-215.

38. Mildvan, A. S., and Cohn, M. (1965) *J. Biol. Chem.* **240**, 238.

39. Mildvan, A. S., and Cohn, M. (1966) *J. Biol. Chem.* **241**, 1178-1193.

40. Karlik, S. J., Elgavish, G. A., and Eichorn, G. L. (1983) *J. Am. Chem. Soc.* **105**, 602-609.

41. Shulman, R. G., Sternlicht, H., and Wyluda, B. J. (1965) *J. Chem. Phys.* **43**, 3116-3122.

42. Agey, M. W., and Dunn, S. M. J. (1989) *Biochemistry* **28**,

4200-4208.

43. Al-Shawi, M. K., Parsonage, D., and Senior, A. E. (1989) *J. Biol. Chem.* **264**, 15376-15383.

44. Wuthrich, K. "NMR of Proteins and Nucleic Acids", Wiley, New York (1986).

45. Jardetzky, O., and Roberts, G. C. K. "NMR in Molecular Biology", Academic, New York (1981).

46. Serpersu, E. H., Kirch, U., and Schoner, W. (1982) *Eur. J. Biochem.* **122**, 347-354.

47. Penefsky, H. S. (1977) *J. Biol. Chem.* **252**, 2891-2899.

48. Mildvan, A. S. and Engle, J. L. (1972) *Methods Enzymol.* **26C**, 654-682.

49. Serpersu, E. H., Shortle, D. and Mildvan, A. S. (1987) *Biochemistry* **26**, 1289-1300.

50. Carr, H. Y. and Purcell, E. M. (1954) *Phys. Rev.* **94**, 630.

51. Mildvan, A. S. and Cohn, M. (1970) *Advan. Enzymol.* **33**, 1-70.

52. Reed, G. H., Cohn, M. and O'Sullivan, W. J. (1970) *J. Biol. Chem.* **245**, 6547-6552.

53. Eckstein, F. (1985) *Ann. Rev. Biochem.* **54**, 367-402.

54. Cornelius, R. D., and Cleland, W. W. (1978) *Biochemistry* **17**, 3279.

55. Farber, G. K., Glasfield, A., Tiraby, G., Ringe, D., and Petsko, G. A. (1989) *Biochemistry* **28**, 7289-7297.

56. Lolis, E., and Petsko, G. A. (1990) *Biochemistry* **29**, 6619-6625.

57. Fry, D. C., Kuby, S. A., and Mildvan, A. S. (1985) *Biochemistry* **24**, 4680-4694.

58. Melamud, E., and Mildvan, A. S. (1975) *J. Biol. Chem.* **250**, 8193-8201.

59. Serpersu, E. S., Hibler, D. W., Gerlt, J. A., and Mildvan, A. S. (1989) *Biochemistry* **28**, 1539-1548.

60. Smith, G. M., Mildvan, A. S., and Harper, E. T. (1980) *Biochemistry* **19**, 1248-1255.

61. James, T. L. (1976) *Biochemistry* **15**, 4724-4730.

62. Ferrin, L. J., and Mildvan, A. S. (1985) *Biochemistry* **24**, 6904-6913.

63. Redfield, A. G. (1957) *IBM J. Res. Dev.* **19**, 1.

64. Kalk, A., and Berendsen, H. J. C. (1976) *J. Magn. Reson.* **24**, 343-366.

65. LeMaster, D. M. (1990) *Quarterly Rev. Biophys.* **23**, 133-174.

66. Shibata, C. G. (1992) Master's Thesis, University of Tennessee, Knoxville.

67. Gregory, J. D., and Serpersu, E. H. (1993) *J. Biol. Chem.* **25**, 3880-3888.

68. Freeman, R., and Hill, H. D. W. (1971) *J. Chem. Phys.* **54**, 3367-3377.

69. Wolkers, W. W., Gregory, J. D., Churchich, J. E., and Serpersu, E. H. (1991) *J. Biol. Chem.* **266**, 20761-20766.

70. Mildvan, A. S., Granot, J., Smith, G. M., and Liebman, M. N. (1980) *Adv. Inorg. Biochem.* **2**, 211-236.

71. Mildvan, A. S. and Gupta, R. K. (1978) *Methods Enzymol.* **49**, 322-359.

72. Mildvan, A. S. (1977) *Acc. Chem. Res.* **10**, 246-252.

73. Koshland, D. E. (1959) *The Enzymes* **1**, 305-346.

74. Anderson, C. M., Zucker, F. H., and Steitz, T. A. (1979) *Science* **204**, 375-380.

75. Walker, P. A., Littlechild, J. A., Hall, L., and Watson, H. C. (1989) *Eur. J. Biochem.* **183**, 49-55.

76. Campbell, A. P., and Sykes, B. D. (1993) *Ann. Rev. Biophys. Biomol. Struct.* **22**, 99-122.

77. Fry, D. C., Byler, D. M., Susi, H., Brown, E. M., Kuby, S. A., and Mildvan, A. S. (1988) *Biochemistry* **27**, 3588-3598.

78. Mildvan, A. S. (1981) *Phil. Trans. R. Soc. Lond.* **B293**, 65-

79. Saenger, W. "Principles of Nucleic Acid Structure", Springer-Verlag, New York (1984).

80. Mildvan, A. S. (1989) *FASEB J.* **3**, 1705-1714.

81. Kuntz, G. W. K., and Krietsch, K. G. (1982) *Methods Enzymol.* **90**, 103-130.

82. Scopes, R. K. (1971) *Biochem. J.* **122**, 89-92.

83. Ames, B. N. (1967) *Methods Enzymol.* **8**, 115.

84. Negelein, E., and Bromel, H. (1939) *Biochem. Z.* **301**, 135.

85. Jindal, H. K., and Vishwanatha, J. K. (1990) *J. Biol. Chem.* **265**, 6540-6543.

Appendices

Appendix A

Figures

Figure II-1: Double reciprocal plot of initial velocity vs. MgATP concentration at different 3PGA concentrations, showing substrate activation. 3PGA concentrations were 0.126 (○), 0.253 (□), and 0.474 (△) mM. The assay medium also contained 50 mM MES-NaOH pH 5.90, 120 mM NaCl, 150 μg GAPDH, $MgCl_2$ in 1 mM excess of ATP concentration, and NADH sufficient to give 1-1.3 absorbance at 340 nm. The reaction in a total volume of 1 ml at 25°C was started by the addition of 0.25 μg PGK.

Figure II–1

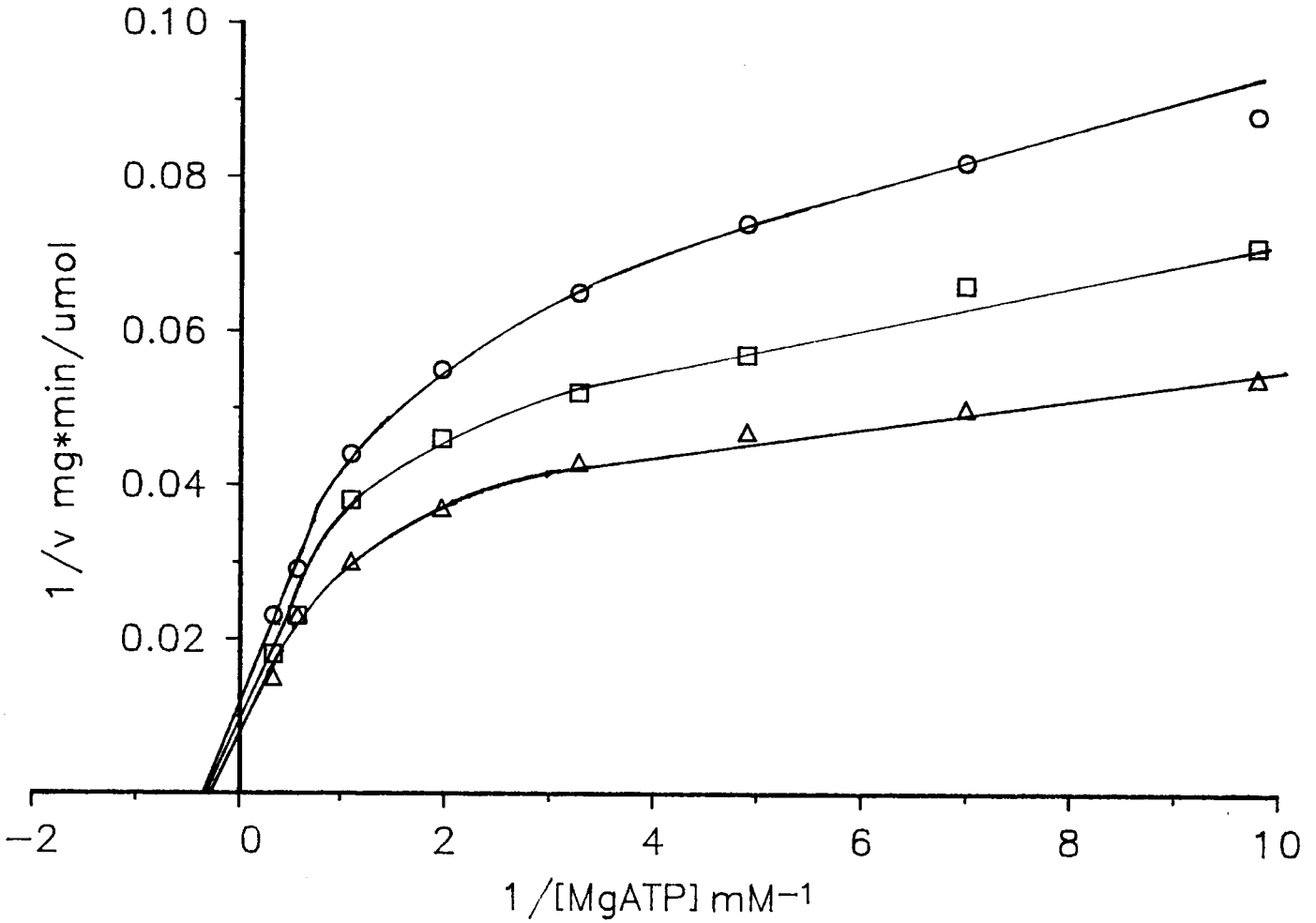

Figure II-2: Double reciprocal plot of initial velocity vs. MgATP concentration at different 3PGA concentrations in the "high affinity" region of MgATP concentration. 3PGA concentrations were 0.105 (○), 0.210 (□), and 0.420 (△) mM. The assay medium also contained 50 mM MES-NaOH pH 5.90, 150 μg GAPDH, $MgCl_2$ in 1 mM excess of ATP concentration, and NADH sufficient to give 1-1.3 absorbance at 340 nm. The reaction in a total volume of 1 ml at 25°C was started by the addition of 0.25 μg PGK.

Figure II–2

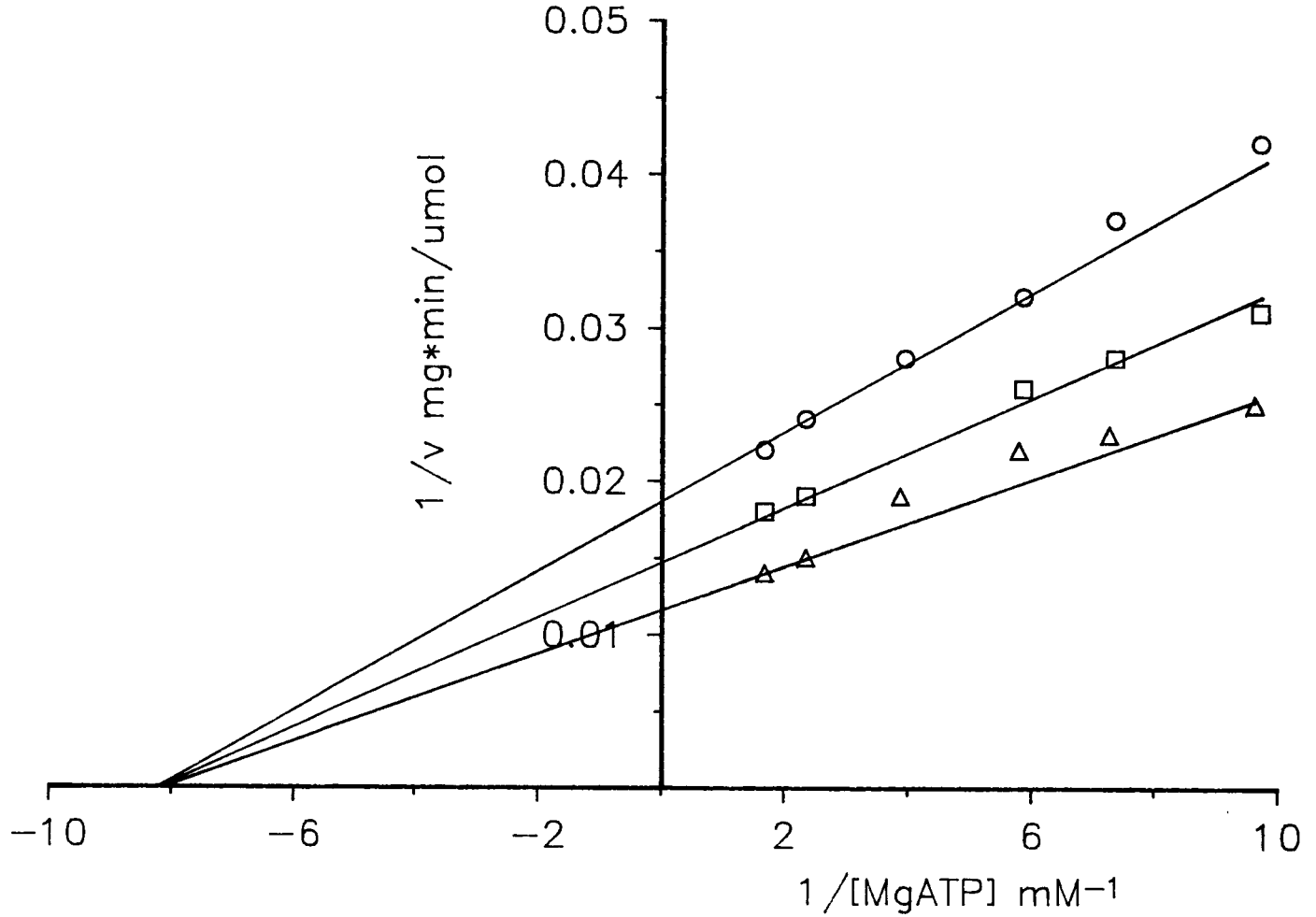

Figure II-3: Double reciprocal plot of initial velocity vs. MgATP concentration at different 3PGA concentrations in the presence of 40 mM sulfate, showing loss of substrate activation. 3PGA concentrations were 0.081 (◇), 0.121 (○), 0.268 (△), and 0.536 (□) mM. The assay medium also contained 50 mM MES-NaOH pH 5.90, 150 μg GAPDH, $MgCl_2$ in 1 mM excess of ATP concentration, and NADH sufficient to give 1-1.3 absorbance at 340 nm. The reaction in a total volume of 1 ml at 25°C was started by the addition of 0.25 μg PGK.

Figure II–3

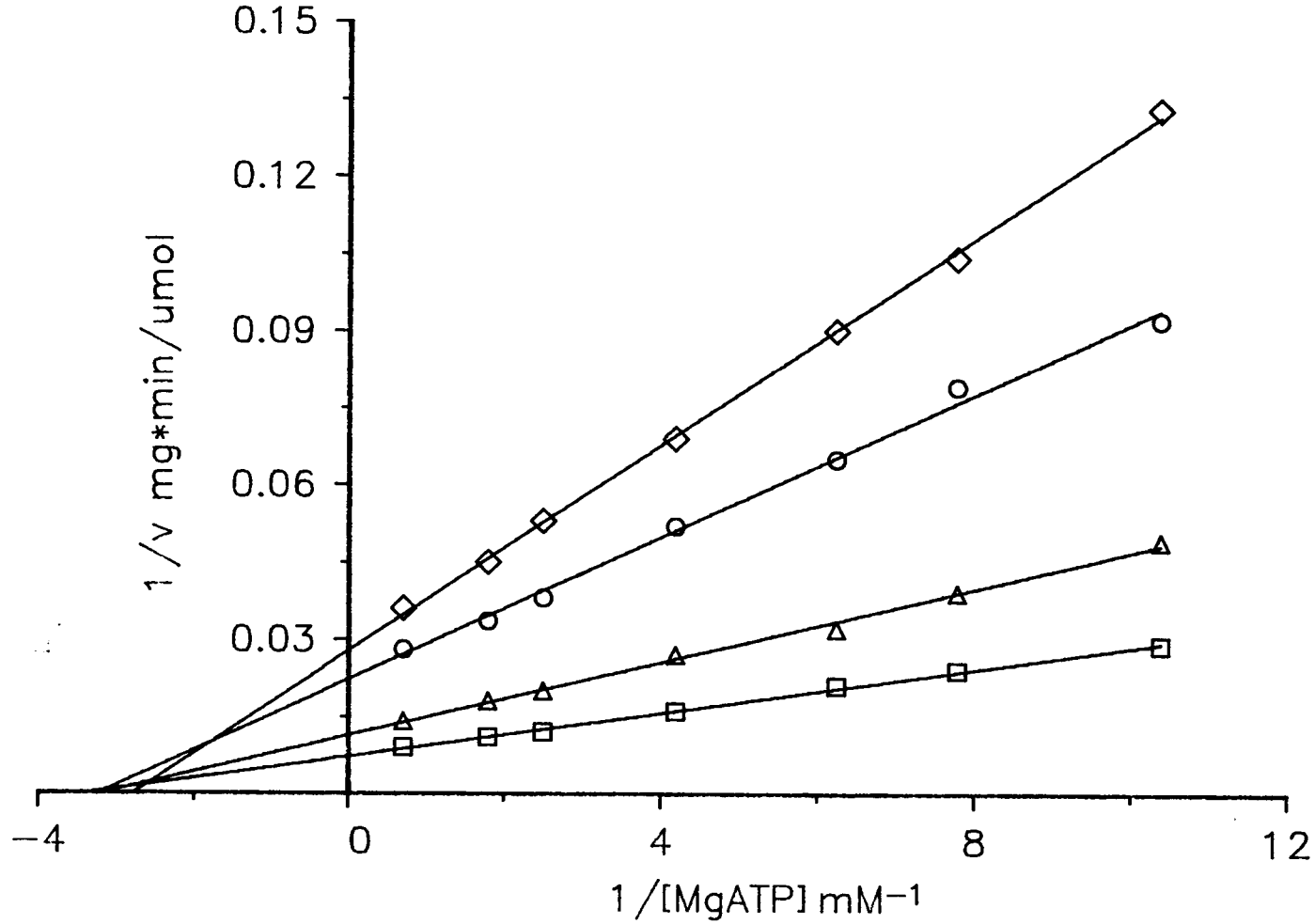

Figure II-4: Double reciprocal plot of initial velocity vs. MgATP concentration at different CrATP concentrations, showing inhibition of phosphoglycerate kinase by CrATP. CrATP concentrations were 0.25 (□), 0.13 (▵), 0.08 (▿), and 0.0 (○) mM. The assay medium also contained 50 mM MES-NaOH pH 5.90, 120 mM NaCl, 0.07 mM 3PGA, 150 μg GAPDH, $MgCl_2$ in 1 mM excess of ATP concentration, and NADH sufficient to give 1-1.3 absorbance at 340 nm. The reaction in a total volume of 1 ml at 25°C was started by the addition of 0.25 μg PGK. (Inset) Secondary plot of slopes vs. CrATP concentration, which yielded K_i^{CrATP}=0.069 ± 0.008 mM.

Figure II–4

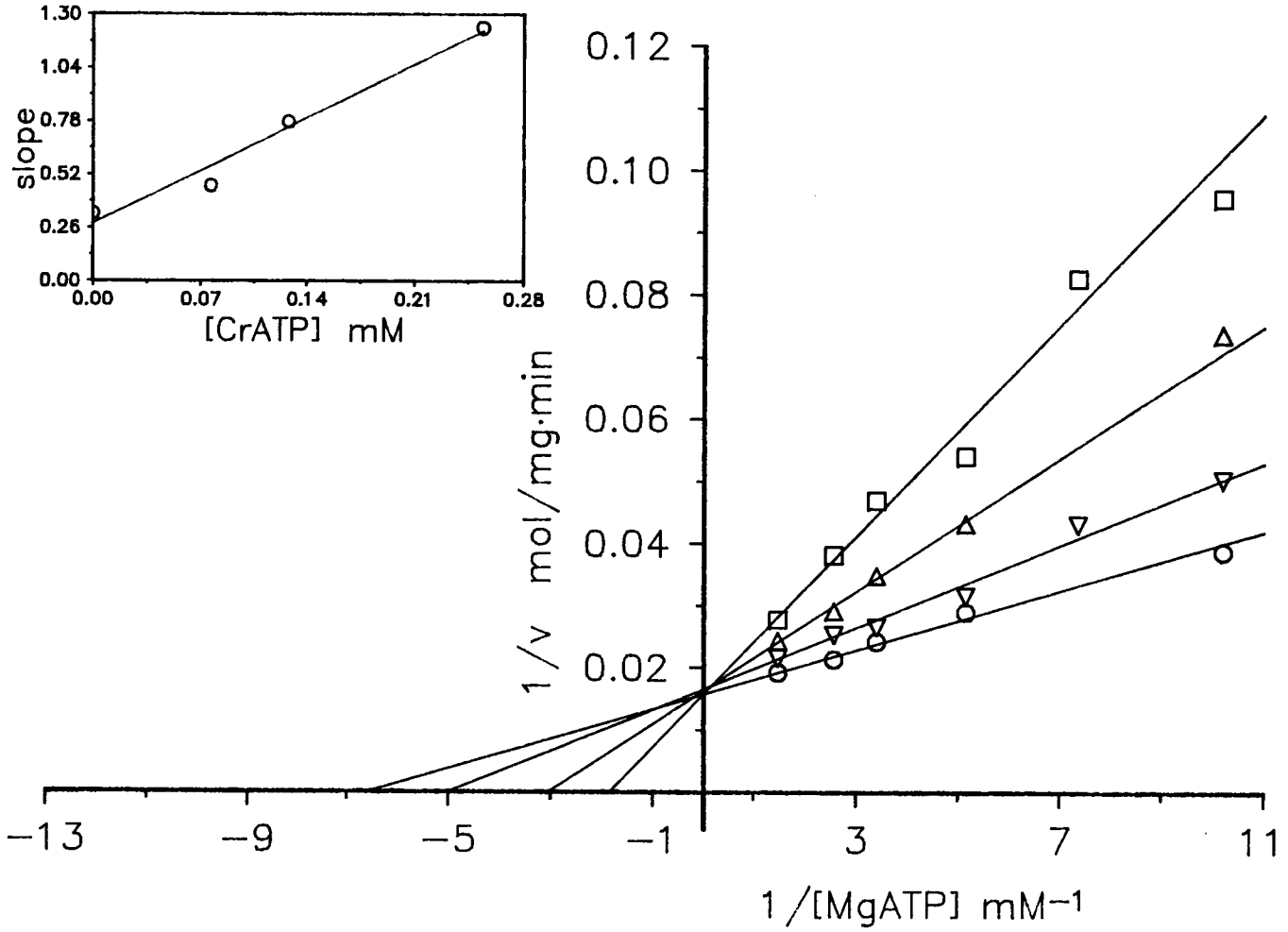
1.30
1.04
0.78
0.52
0.26
0.00
slope
0.00
0.07
0.14
0.21
0.28
[CrATP] mM
0.12
0.10
0.08
0.06
0.04
0.02
1/v mol/mg·min
−13
−9
−5
−1
3
7
11
1/[MgATP] mM−1

Figure II-5: Plot of K_{iapp} for CrATP vs. 3PGA concentration obtained from eight different kinetic experiments. This analysis yielded K_i^{CrATP}=0.070 ± 0.014 mM in the absence of sulfate (O) and 0.725 ± 0.178 mM in the presence of sulfate (□).

Figure II–5

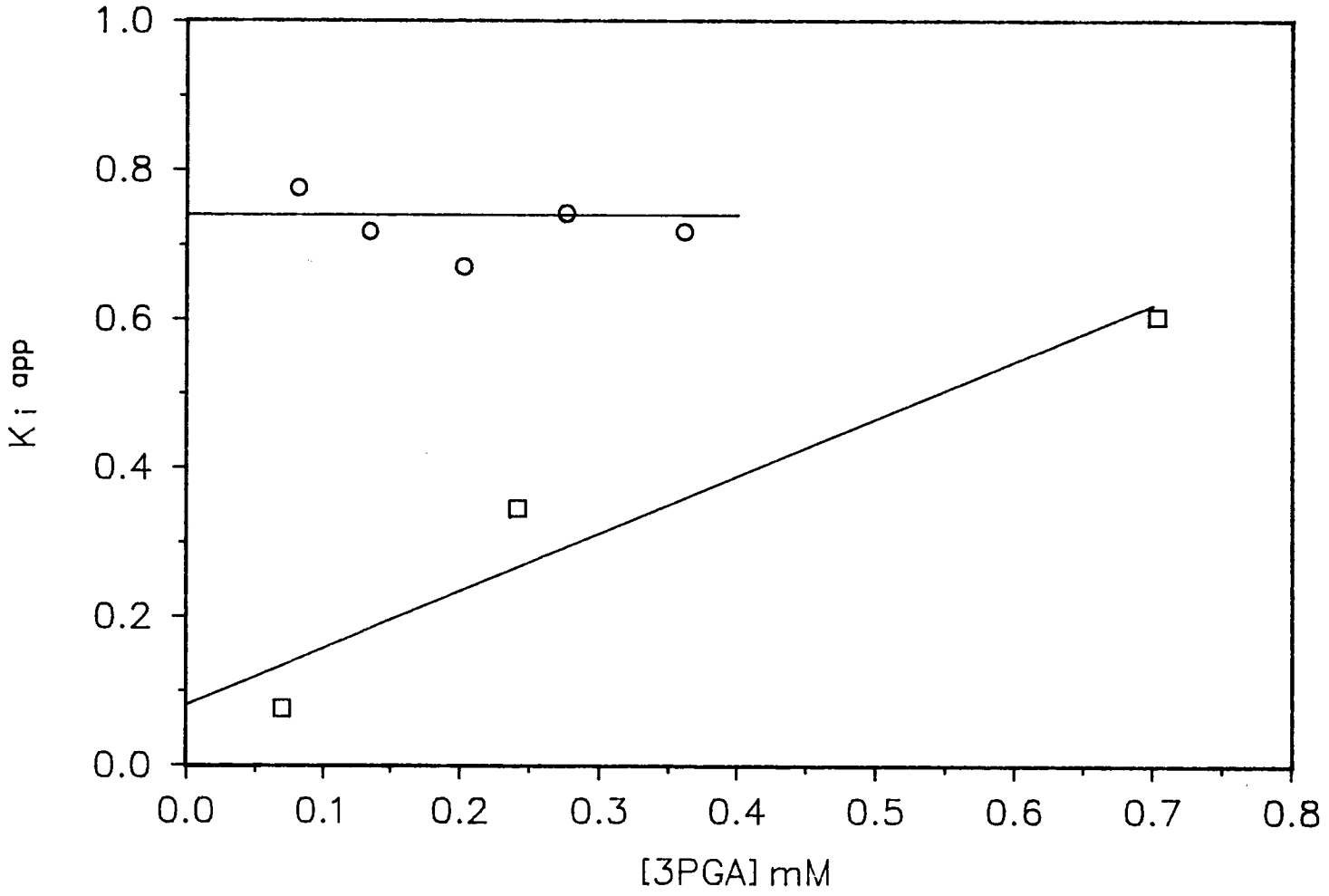

Figure II-6: Double reciprocal plot of initial velocity vs. MgATP concentration at different CrATP concentrations in the presence of 40 mM sulfate. CrATP concentrations were 0.0 (O), 0.306 (Δ), 0.612 (□) mM. The assay medium also contained 50 mM MES-NaOH pH 5.90, 0.134 mM 3PGA, 150 μg GAPDH, $MgCl_2$ in 1 mM excess of ATP concentration, and NADH sufficient to give 1-1.3 absorbance at 340 nm. The reaction in a total volume of 1 ml at 25°C was started by the addition of 0.25 μg PGK.

Figure II–6

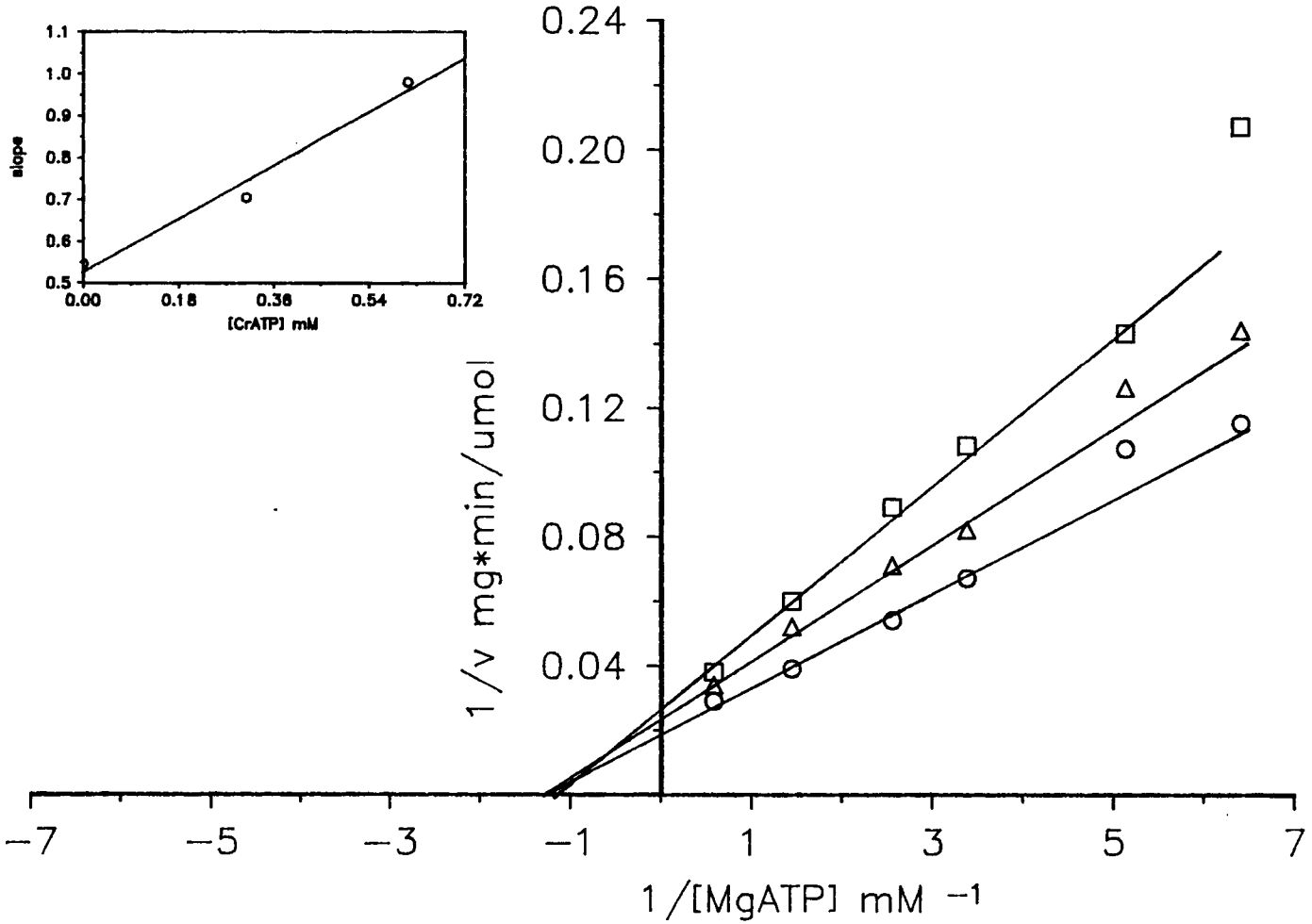
1.1
1.0
0.9
0.8
0.7
0.6
0.5
slope
0.00
0.18
0.36
0.54
0.72
[CrATP] mM
0.24
0.20
0.16
0.12
0.08
0.04
1/v mg*min/umol
−7
−5
−3
−1
1
3
5
7
1/[MgATP] mM −1

Figure II-7: Double reciprocal plot of initial velocity vs. 3PGA concentration at different CrATP concentrations showing mixed-type inhibition. CrATP concentrations were 0.0 (○), 0.126 (△), 0.237 (□), and 0.472 (▽) mM. The assay medium also contained 50 mM MES-NaOH pH 5.90, 0.116 mM MgATP, 150 μg GAPDH, and NADH sufficient to give 1-1.3 absorbance at 340 nm. The reaction in a total volume of 1 ml at 25°C was started by the addition of 0.25 μg PGK.

Figure II–7

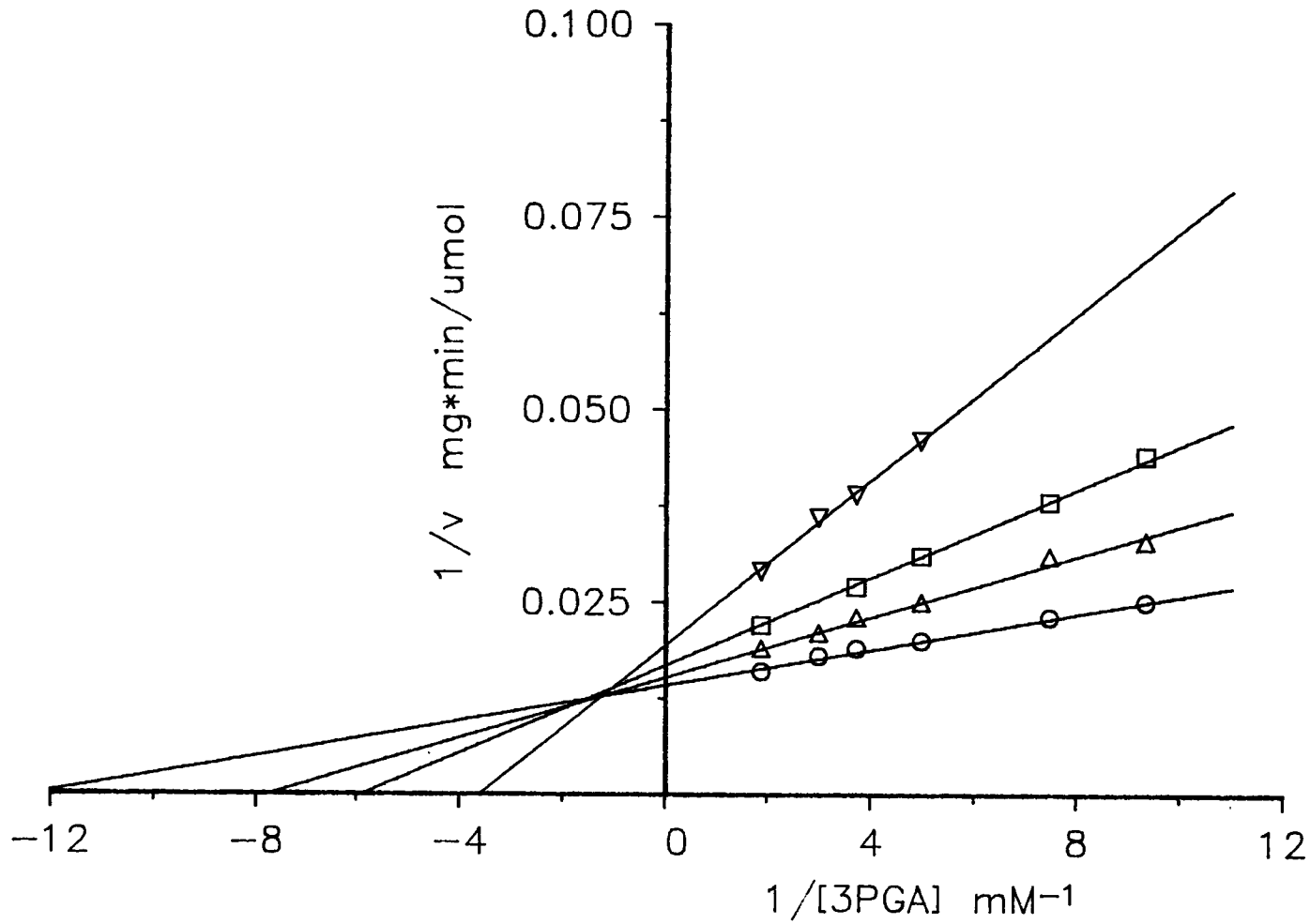

Figure II-8: Double reciprocal plot of initial velocity vs. 3PGA concentration at different CrATP concentrations in the presence of 40 mM sulfate, showing noncompetitive inhibition. CrATP concentrations were 0.0 (○), 0.511 (□), 1.022 (△), and 1.752 (▽) mM. The assay medium also contained 50 mM MES-NaOH pH 5.90, 0.202 mM MgATP, 150 μg GAPDH, and NADH sufficient to give 1-1.3 absorbance at 340 nm. The reaction in a total volume of 1 ml at 25°C was started by the addition of 0.25 μg PGK.

Figure II–8

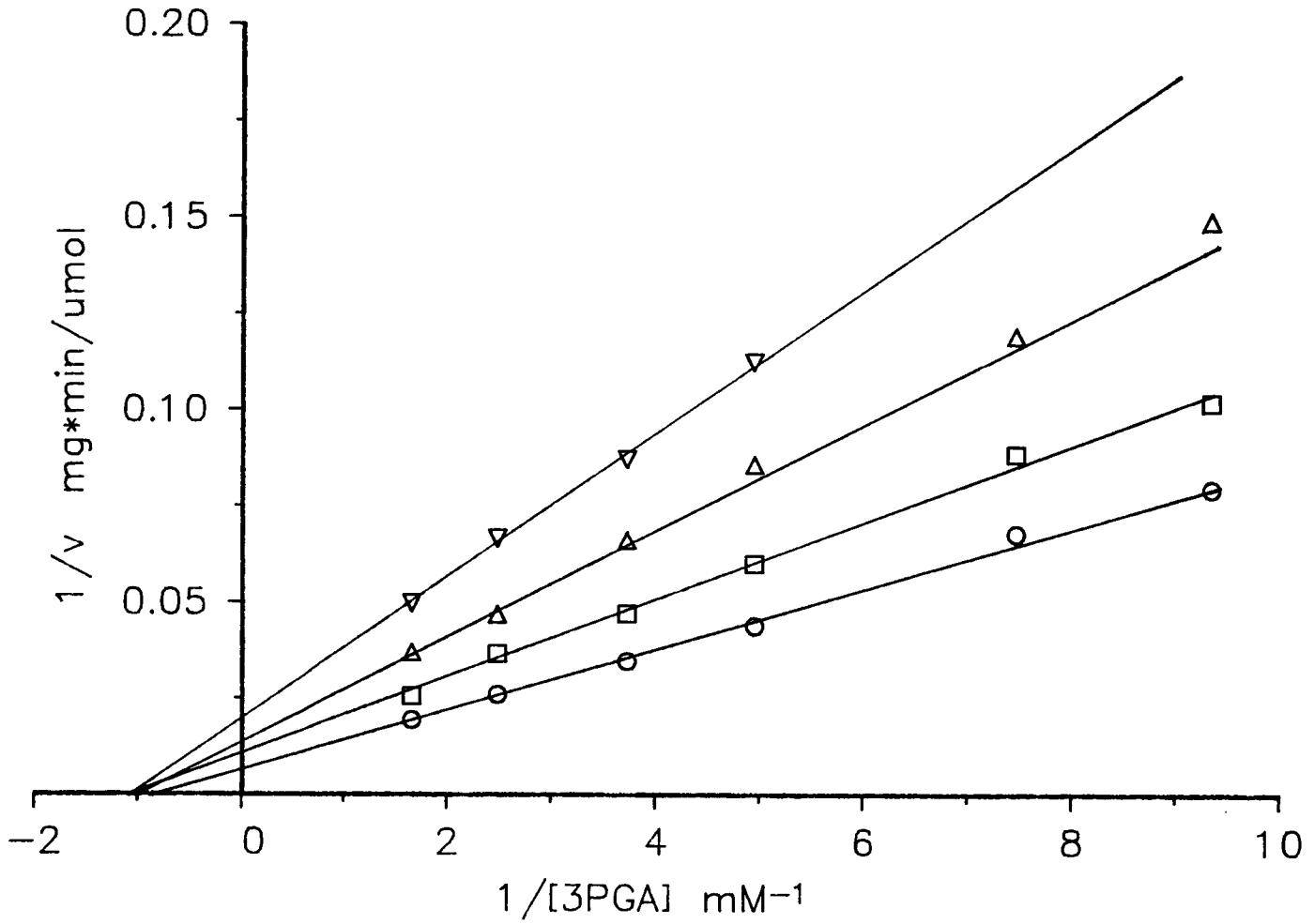

Figure II-9: Proposed model for the observed effects of sulfate ion on the ligand binding and catalysis by phosphoglycerate kinase. The binding of sulfate results in a more open active site (top right). CrATP is represented by a larger rectangle to signify the presence of slowly exchanging ligands in the coordination sphere of Cr^{3+}.

Figure II–9

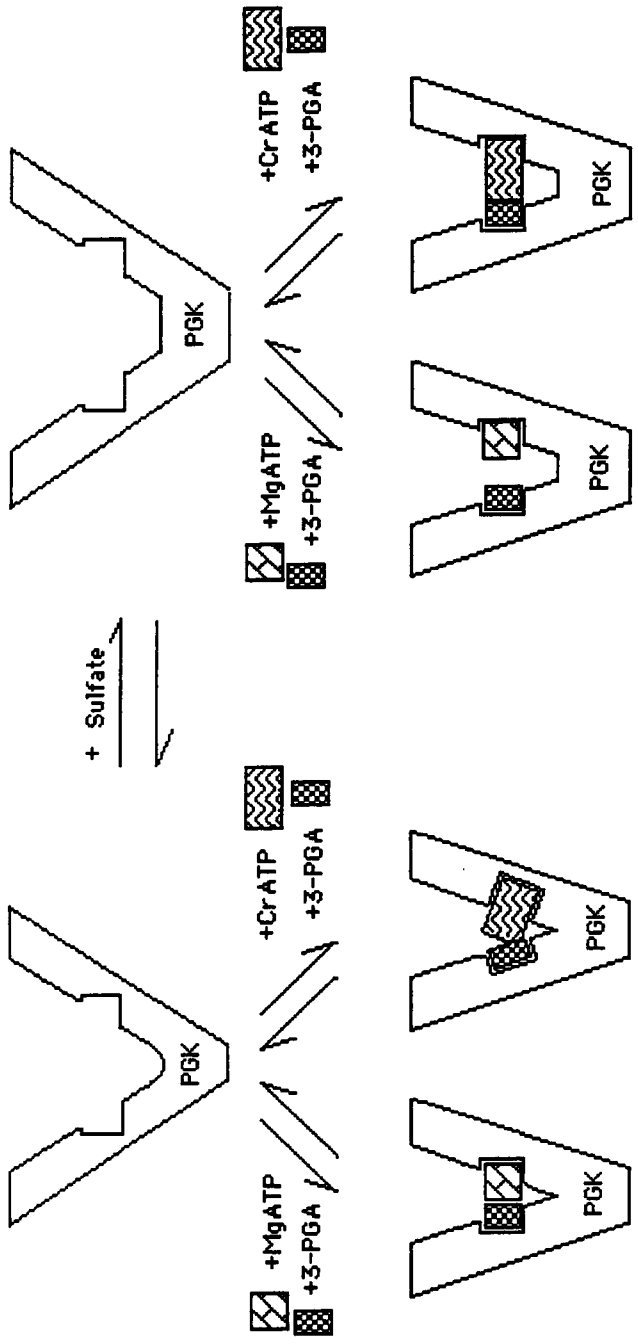
PGK
+CrATP
+3-PGA
+MgATP
+3-PGA
+ Sulfate
PGK
+CrATP
+3-PGA
+MgATP
+3-PGA
PGK
PGK
PGK
PGK

Figure III-1: Scatchard plots of CrATP binding to PGK in the absence (O) and presence (Δ) of 40 mM sulfate. Other components present were 120 mM NaCl, 145 μM PGK, 4.43 mM 3PGA, 0.13-5.2 mM γ-^{32}P labelled CrATP in 50 mM MES-NaOH pH 5.9. When sulfate was present, NaCl was omitted from the mixture to maintain a constant ionic strength. Solid lines represent computer fitted curves to the data; in the presence of sulfate, the data was fit by assuming two types of independent sites. Dashed lines represent the calculated contributions of the low and high affinity CrATP sites to the biphasic binding curve observed in the presence of sulfate.

Figure III–1

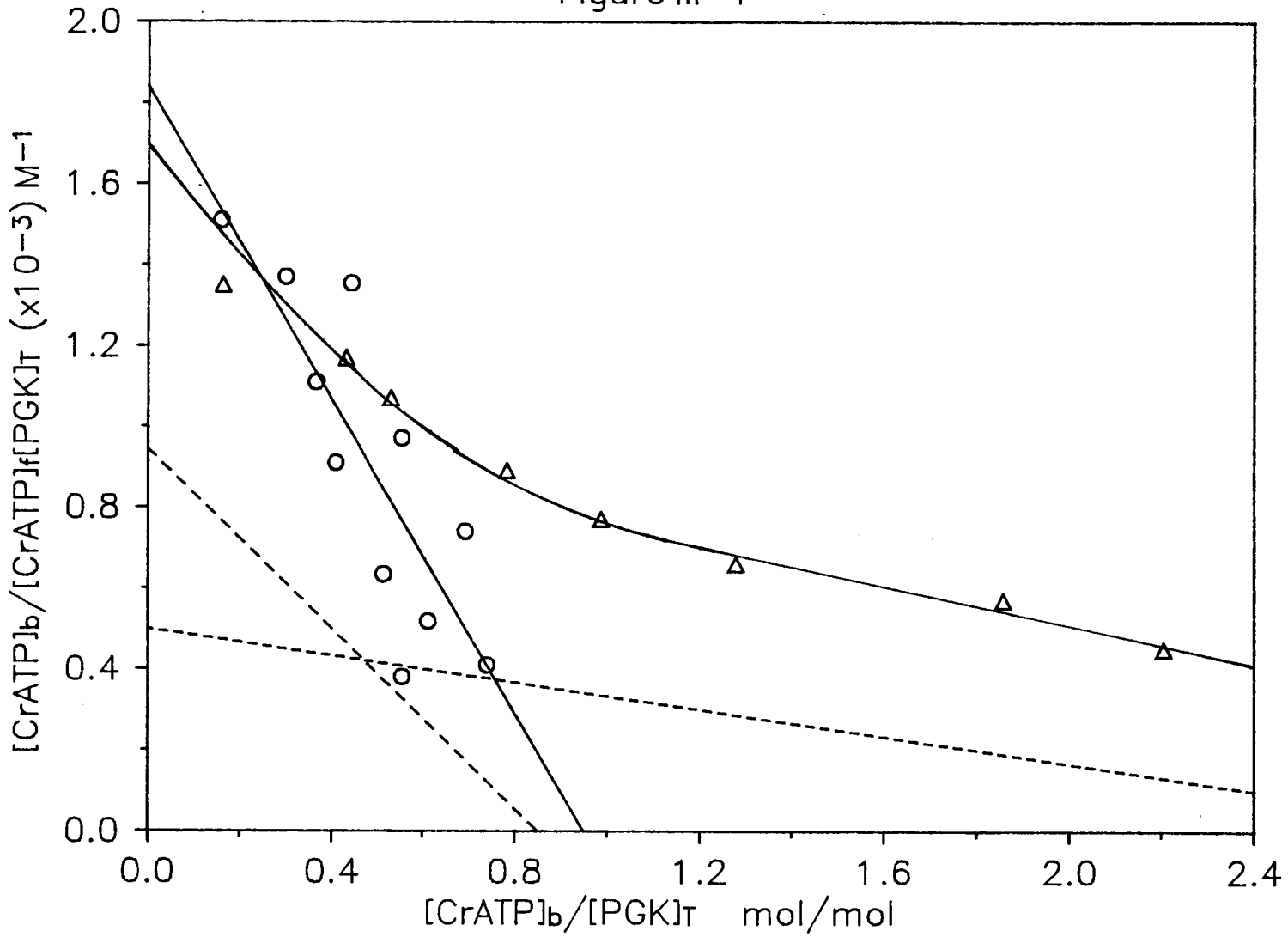
2.0
1.6
1.2
0.8
0.4
0.0
[CrATP]b/[CrATP]f[PGK]T (x10-3) M-1
0.0
0.4
0.8
1.2
1.6
2.0
2.4
[CrATP]b/[PGK]T mol/mol

Figure III-2: Titration of CrATP with PGK, plotted as the double reciprocal of the observed enhancement (ε^*) vs. enzyme concentration. CrATP concentrations were 0.242 mM (△) and 0.053 mM (○). Samples also contained 50 mM MES-NaOH pH 5.90 and 120 mM NaCl. The ordinate intercept yielded ε_b=1.46 ± 0.12. The determined ε_b, together with the observed enhancements, were used to calculate the concentration of free and bound CrATP in the solutions of enzyme and CrATP according to the equation given in the text.

Figure III--2

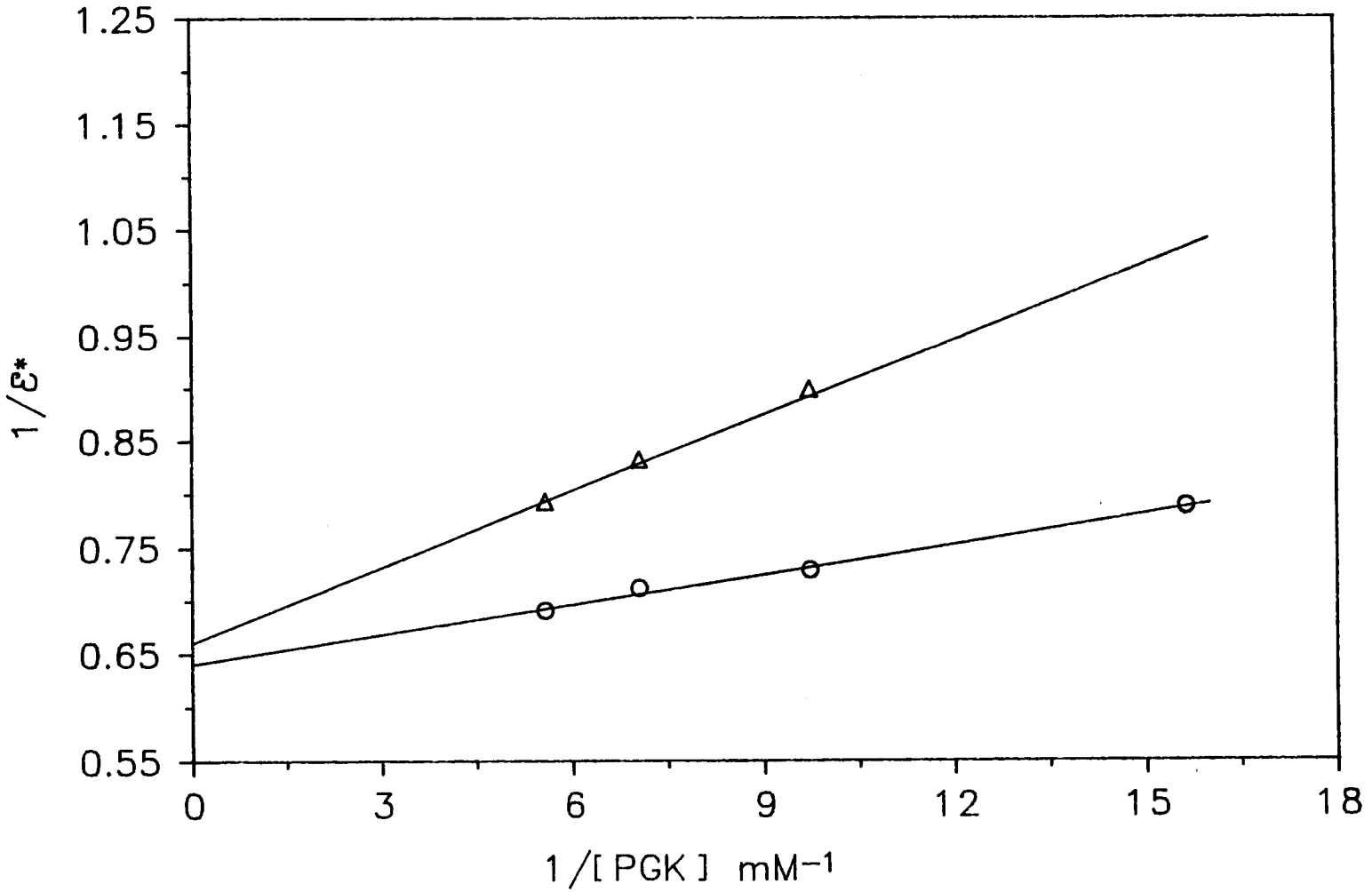

Figure III-3: Scatchard analysis of ε_b titration data from Figure III-2, which yielded K_D=60 ± 19 μM and stoichiometry of 1.2 ± 0.4 CrATP/PGK (mol/mol).

Figure III–3

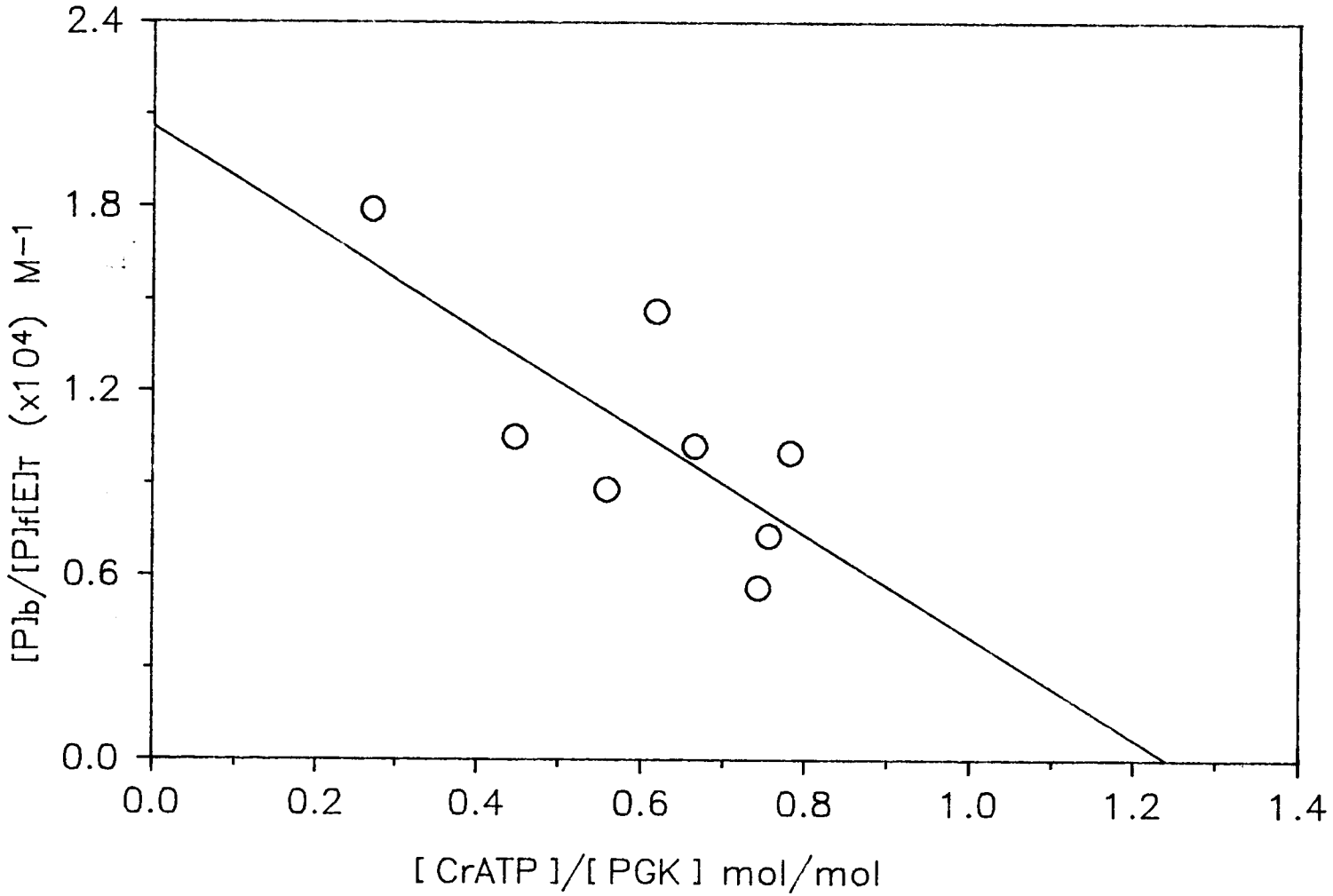
2.4
1.8
1.2
0.6
0.0
[P]b/[P]f[E]T (x10 04) M-1
0.0
0.2
0.4
0.6
0.8
1.0
1.2
1.4
[CrATP]/[PGK] mol/mol

Figure III-4: Binding studies of 3PGA to binary PGK·CrATP complex at three CrATP/PGK ratios, showing the changes in the observed enhancement (ε^*) of the paramagnetic effects of CrATP on $1/T_1$ of water protons. The concentrations of CrATP used were 0.058 mM (△), 0.12 mM (□), and 0.229 mM (○). Solutions also contained 0.17 mM PGK, 50 mM MES-NaOH pH 5.90, and 120 mM NaCl. The inset shows an expanded view of the region from 0.0 to 0.06 mM 3PGA.

Figure III-4

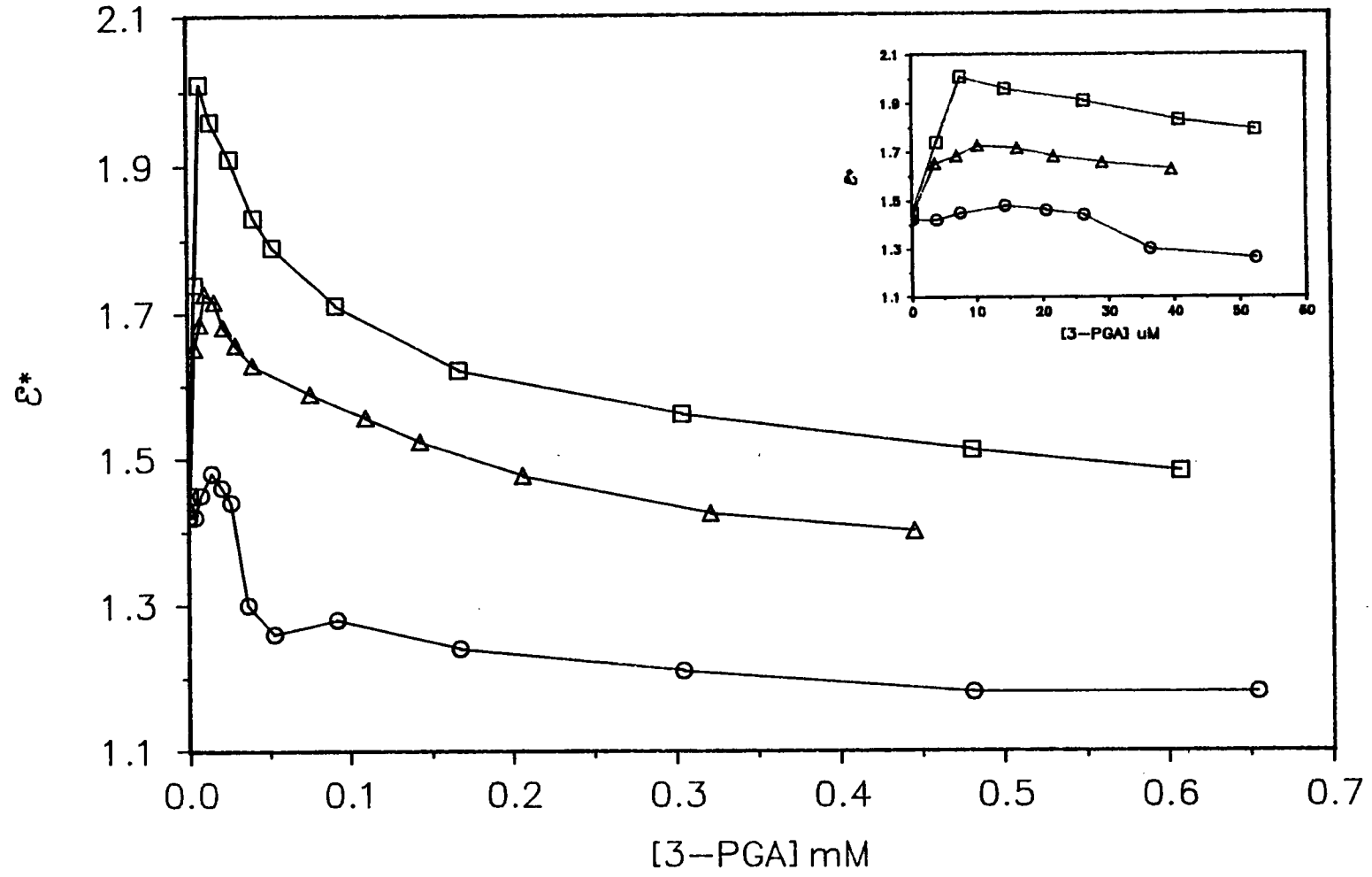

Figure III-5: Binding studies of 3PGA to binary PGK·CrATP complex at three CrATP/PGK ratios in the presence of sulfate. The concentrations of CrATP used were 0.056 mM (○), 0.112 mM (□), and 0.225 mM (△). The samples also contained 0.322 mM PGK, 50 mM MES-NaOH pH 5.90, and 40 mM sulfate. The inset shows an expanded view of the region from 0.0 to 0.3 mM 3PGA.

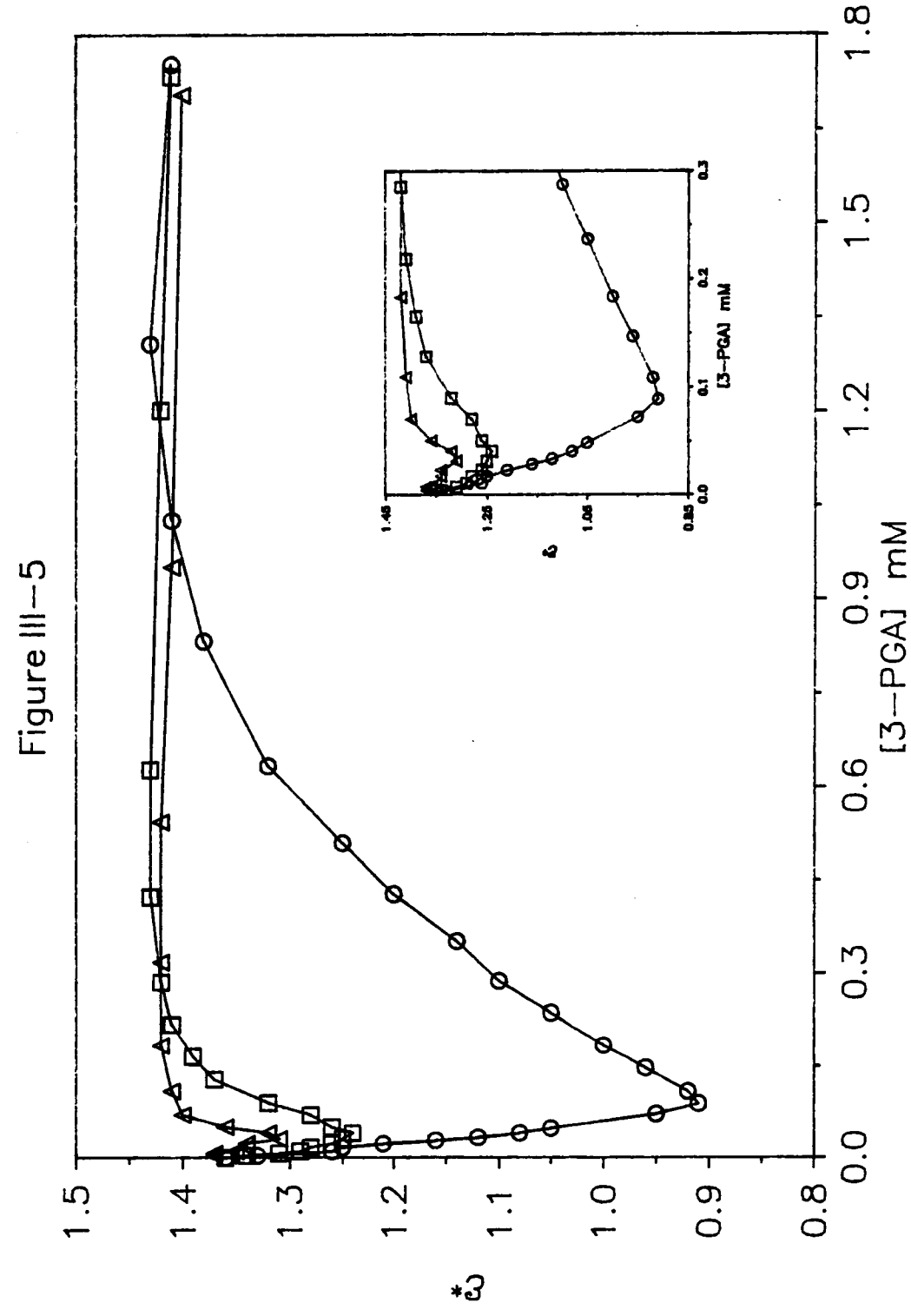
Figure III–5
*ϑ
[3–PGA] mM
1.5
1.4
1.3
1.2
1.1
1.0
0.9
0.8
0.0
0.3
0.6
0.9
1.2
1.5
1.8
[3–PGA] mM
0.0
0.1
0.2
0.3
1.45
1.25
1.05
0.85

```
;JT1PS.AU
;T1 MEASUREMENT VIA PROGRESSIVE SATURATION

1  ZE                  ;ZERO MEMORY
2  WR #1               ;CREATE FILE
3  IF #1               ;INCREMENT FILE #
4  LO TO 2 TIMES C     ;FIRST C = #OF FILES = NE
   VC                  ;SELECT SECOND C
5  RF #1.001           ;RESET FILE EXTENSION, BEGIN CYCLE
6  RE #1               ;READ CURRENT FID
7  VD                  ;VARIABLE DELAY FROM CURRENT VD LIST
8  GO=7                ;ACQUIRE DATA, LOOP TO 7 "NS" TIMES
9  WR #1               ;STORE CURRENT FID
10 IF #1               ;INCREMENT FILE EXTENSION
11 IN=7                ;LOOP TO 7 AND INCREMENT VD VALUE
12 LO TO 5 TIMES C     ;REPEAT CYCLE THROUGH DELAY LIST
                       ;C IS SECOND IN VC LIST
13 EXIT

;PROGRAM REQUESTS FILENAME FOR FIDS
;NE DEFINES # OF VALUES IN VD LIST (= # OF FIDS)
;RD=0, PW=90 DEGREE PULSE
;NS=MULTIPLE OF 8, DS=0
;CURRENT VC LIST MUST CONTAIN AN ENTRY WHICH DEFINES THE
;NUMBER OF FILES (=NE) AND A SECOND ENTRY WHICH DEFINES THE
;NUMBER OF CYCLES TO BE MADE THROUGH THE VD LIST FOR LONG-TERM
;SIGNAL AVERAGING
;TOTAL TRANSIENTS PER FILE = SECOND C * NS
```

Figure IV-1: Pulse program for the automated acquisition of data for analysis of the longitudinal relaxation rates of ^{13}C nuclei via the progressive saturation method. The syntax of the pulse program is compatible with Bruker AC NMR instruments equipped with an ASPECT-3000 processor and utilizing the ADACOS operating system.

Figure IV-2: ^{1}H- and ^{13}C-NMR spectra ("a" and "b,c" respectively) of 3PGA and [U-^{13}C]3PGA. Sample composition and data acquisition parameters were: (a) 20 mM 3PGA in 99+% $^{2}H_2O$, spectrum obtained at 400 MHz using 16 transients, a spectral width of 3200 Hz, 5 s acquisition time, and a 90° pulse with 10 s delay; (b) 150 mM 3PGA in 20% $^{2}H_2O$, spectrum obtained at 100 MHz using 3800 transients, 17 KHz spectral width, .95 s acquisition time, a 45° pulse with 12 s delay, and bi-level proton decoupling for NOE enhancement of signals; (c) 10 mM [U-^{13}C]3PGA in 20% $^{2}H_2O$, spectrum obtained at 400 MHz using 3300 transients, 26 KHz spectral width, .6 s acquisition time, a 45° pulse with 15 sec delay, and proton decoupling. All spectra were recorded with 32K data points and 16 bit A-D conversion at 27°C.

Figure IV–2

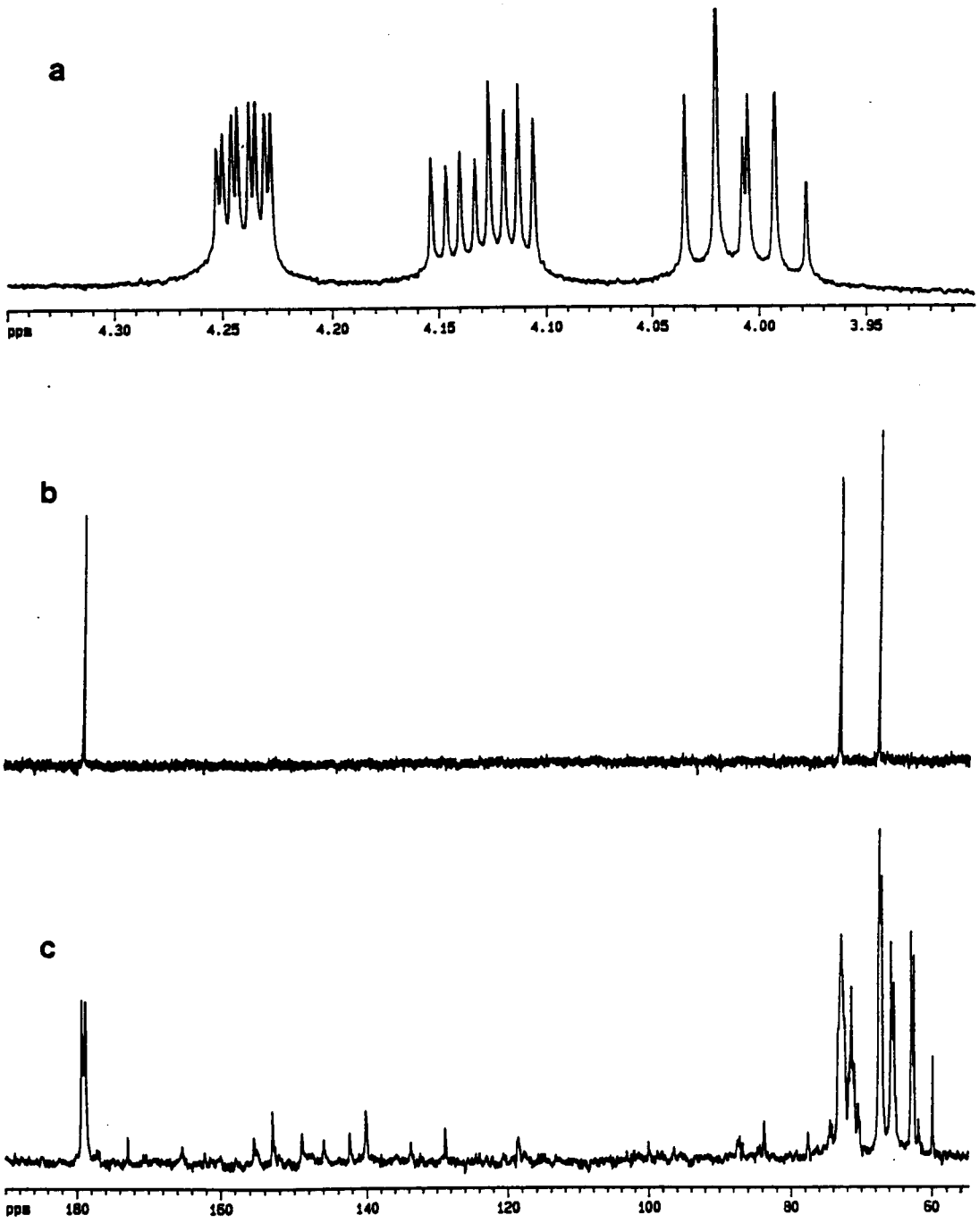
a
ppm
4.30
4.25
4.20
4.15
4.10
4.05
4.00
3.95
b
c
ppm
180
160
140
120
100
80
60

Figure IV-3: Two-dimensional heteronuclear ^{1}H-^{13}C correlation spectrum of 3PGA, showing single-bond proton-carbon connectivities. The sample consisted of 150 mM 3PGA in 99.9+% $^{2}H_2O$, pH 6.

Figure IV–3

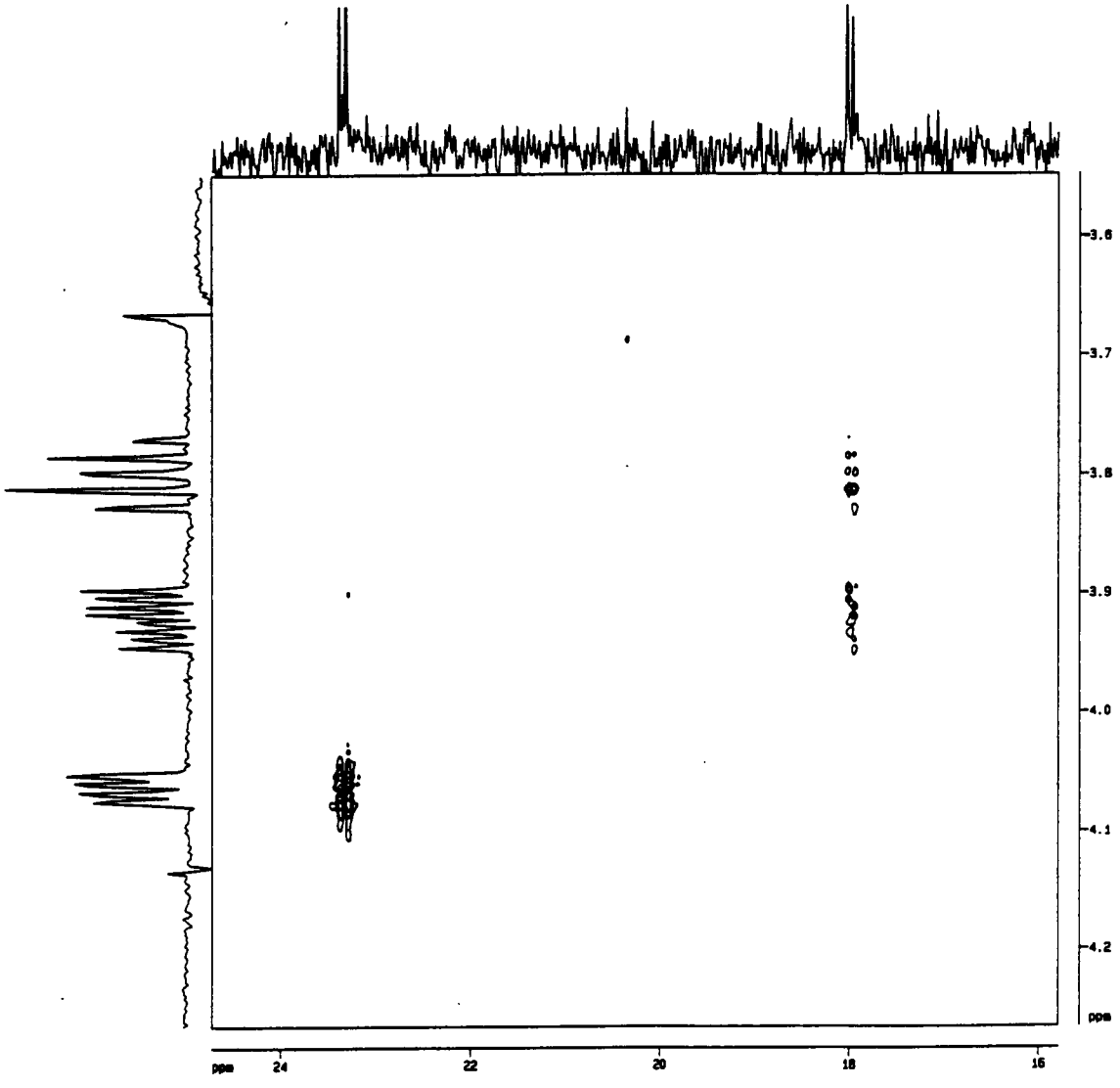

Figure IV-4: Paramagnetic effects of CrATP on the protons of free and enzyme-bound 3PGA in the absence of sulfate. The samples contained 0.108 mM PGK, 10 mM 3PGA, and 60 mM NaCl, in Na^+-acetate buffer pH 5.9 and 99+% ^2H_2O, with a total volume of 500 μl. ▽, H3´; □, H3 and ○, H2 protons of 3PGA. *Lines* represent the least squares fit to the data points; *dashed lines* represent the contributions from the binary CrATP·3PGA interaction. T_1 values were determined at 200 MHz using the inversion recovery method as described in the text.

Figure IV–4

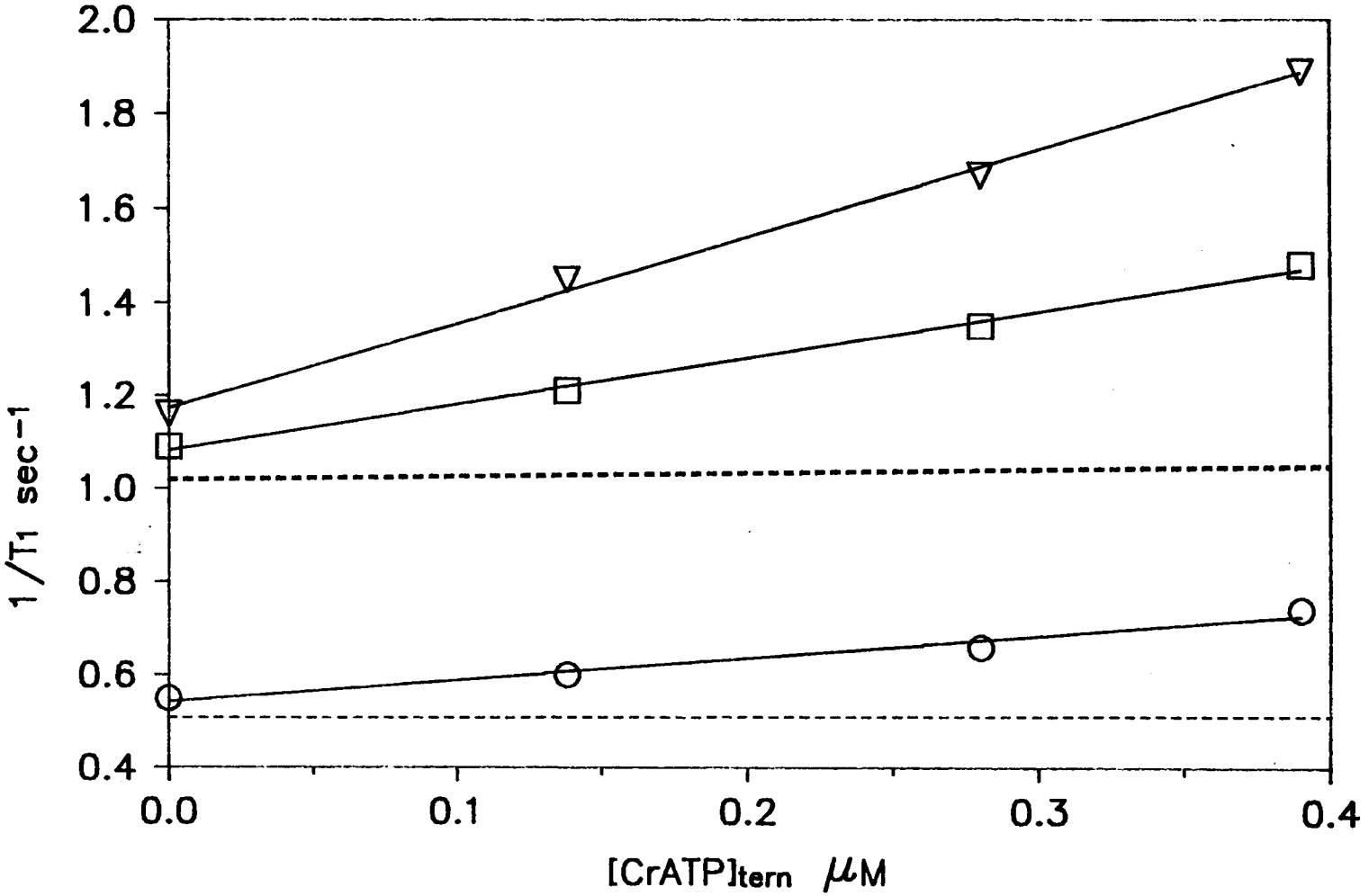

Figure IV-5: Paramagnetic effects of CrATP on the protons of enzyme-bound 3PGA in the presence of sulfate. The samples contained 0.338 mM PGK, 7 mM 3PGA, and 20 mM Na_2SO_4, in Na^+-acetate buffer pH 5.9 and 99+% ^2H_2O, with a total volume of 500 μl. ▽, H3´; □, H3 and ○, H2 protons of 3-PGA. *Lines* represent the least squares fit to the data points. Identical binary contributions were used as in Figure IV-4. T_1 values were determined at 250 MHz using the inversion recovery method as described in the text.

Figure IV–5

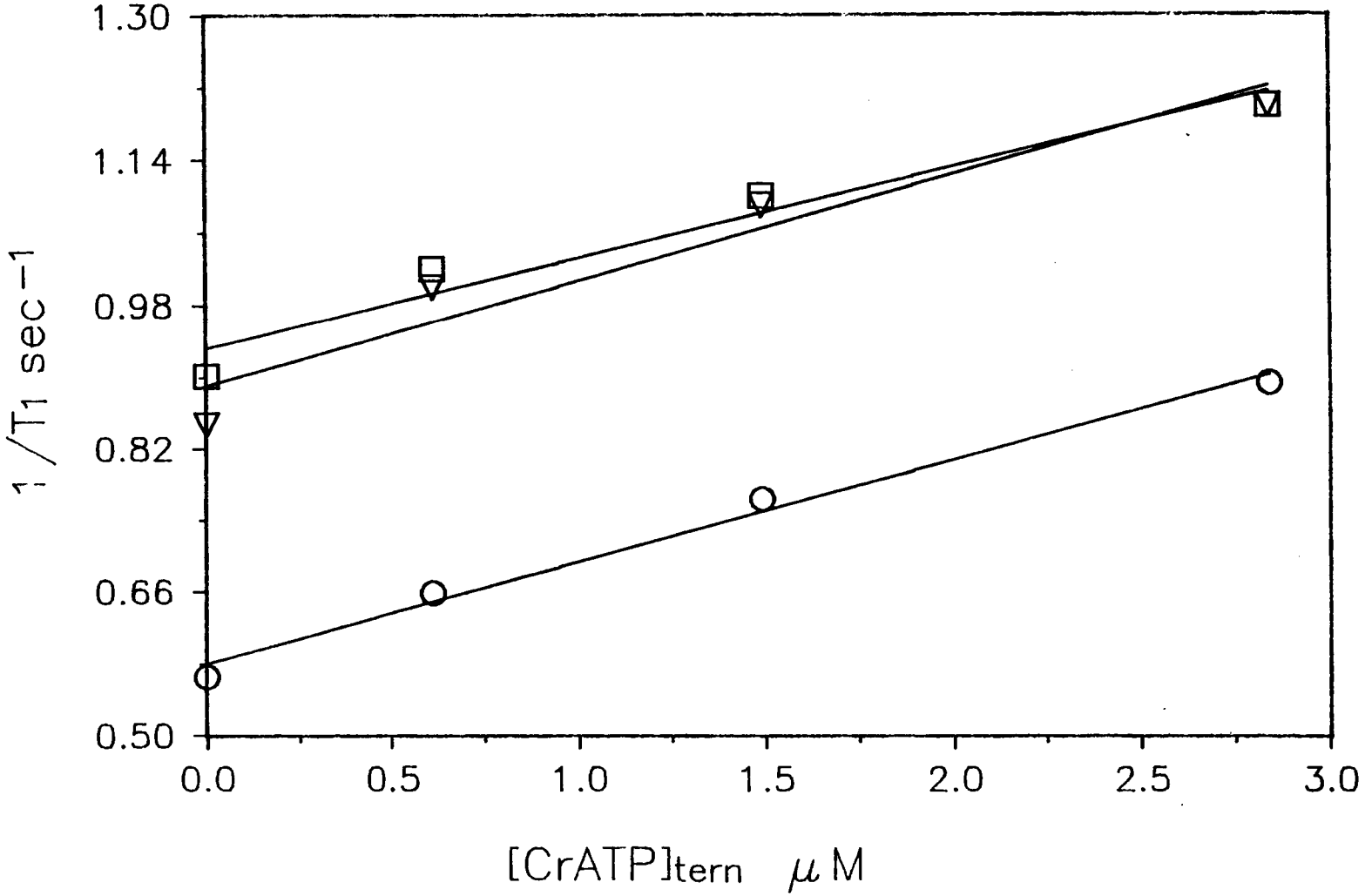
1.30
1.14
0.98
0.82
0.66
0.50
1/T1 sec−1
0.0
0.5
1.0
1.5
2.0
2.5
3.0
[CrATP]tern μM

Figure IV-6: Paramagnetic effects of CrATP on the phosphorous of free and enzyme-bound 3PGA in the absence and presence of sulfate. The samples contained 8.3 mM 3PGA, 50 mM MES-NaOH pH 5.9, and either 0.35 mM PGK and 60 mM NaCl (○) or 0.45 mM PGK and 20 mM sulfate (△) in 500 μl total volume, with 20% ^2H_2O for locking. *Lines* represent the least squares fit to the data points; the *dashed line* represents the binary contribution. T_1 values were determined at 161 MHz using the inversion recovery method as described in the text.

Figure IV–6

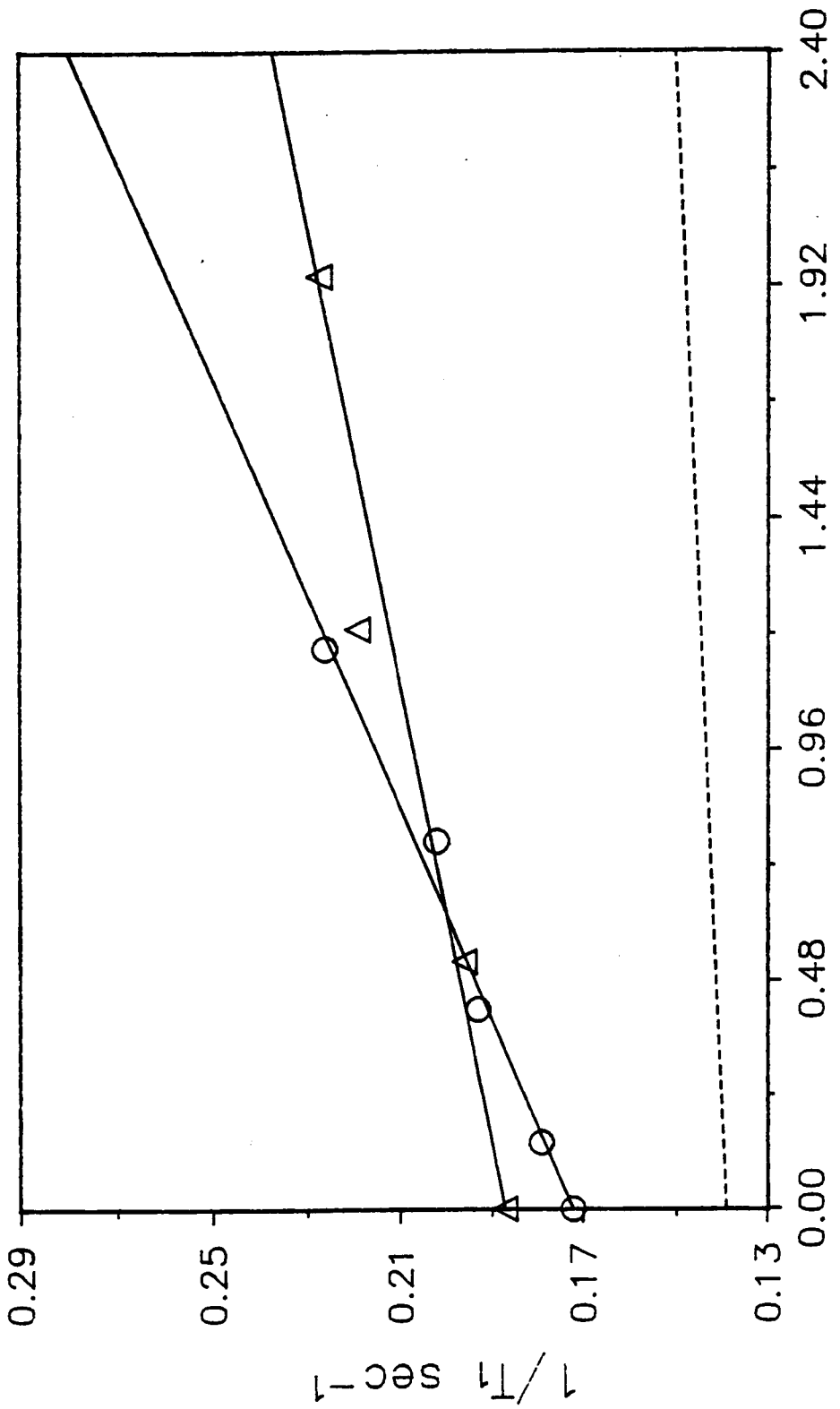
0.29
0.25
0.21
0.17
0.13
1/T1 sec−1
0.00
0.48
0.96
1.44
1.92
2.40
[CrATP]tern μ M

Figure IV-7: Paramagnetic effects of CrATP on the carbons of free and enzyme-bound 3PGA in the absence and presence of sulfate. The figure shows the paramagnetic effect of CrATP on C1 of 3PGA; the inset shows the paramagnetic effect of CrATP on C2 of 3PGA. Samples contained 9.9 mM [U-^{13}C]3PGA, 50 mM MES-NaOH pH 5.9, and either 0.3 mM PGK and 60 mM NaCl (□) or 0.4 mM PGK and 20 mM sulfate (○) in 425 μl total volume, with 20% $^{2}H_2O$ for locking. *Lines* represent the least squares fit to the data points; the *dashed line* represents the binary contribution. T_1 values determined at 62 MHz using the method of progressive saturation as described in the text.

Figure IV–7

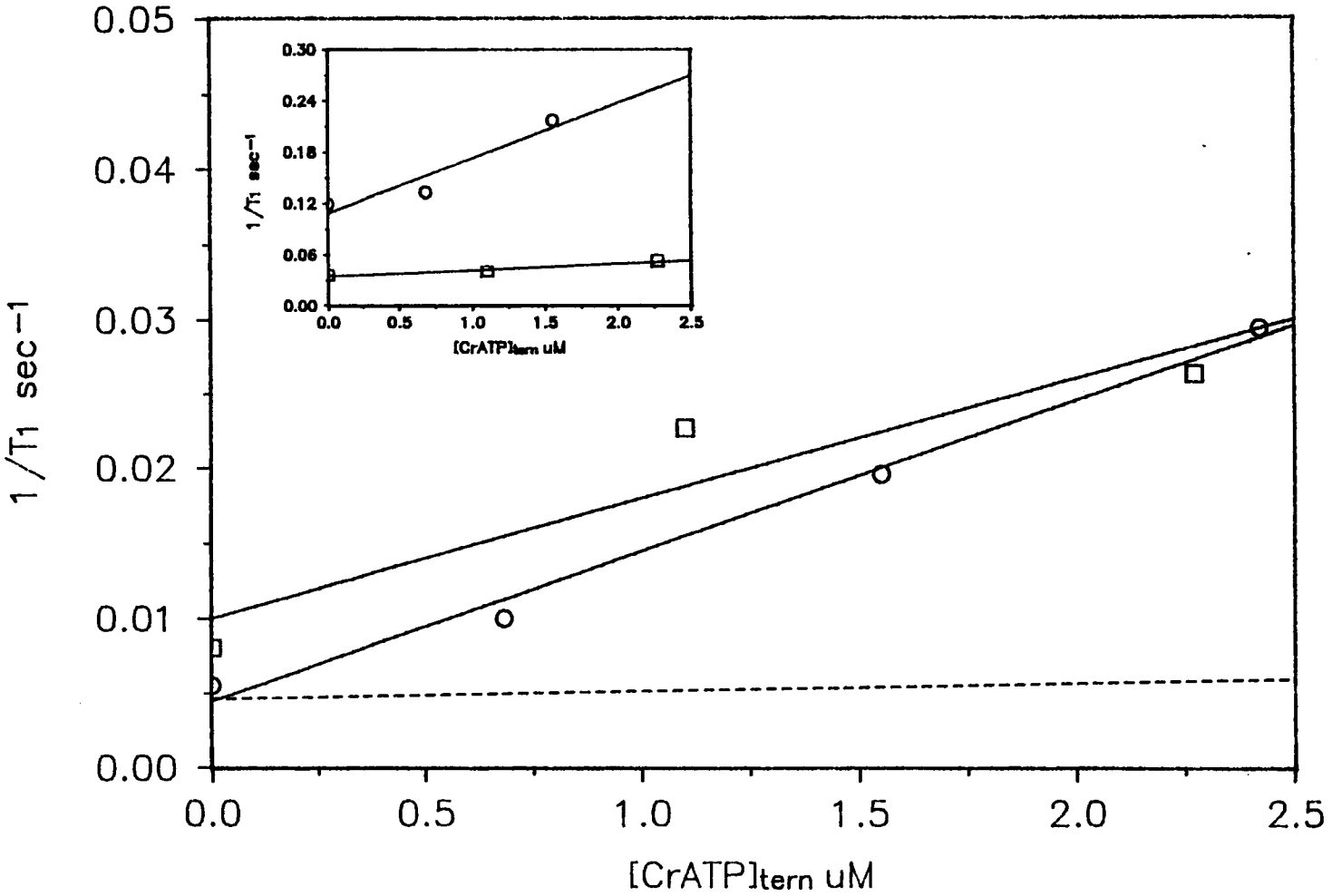
0.05
0.04
0.03
0.02
0.01
0.00
1/T1 sec−1
0.0
0.5
1.0
1.5
2.0
2.5
[CrATP]tern uM
0.30
0.24
0.18
0.12
0.06
0.00
1/T1 sec−1
0.0
0.5
1.0
1.5
2.0
2.5
[CrATP]tern uM

Figure IV-8: Temperature dependence of $1/fT_{1\rho}$ of 3PGA protons in the ternary PGK·CrATP·3PGA complex. The sample contained 0.108 mM PGK, 10 mM 3PGA, 2.37 μM CrATP, and 60 mM NaCl in Na^+-acetate buffer pH 5.9 and 99+% ^2H_2O, with a total volume of 500 μl. $\triangle$, H2; $\square$, H3; and $\circ$, H3´ protons of 3PGA. NMR spectra were collected at 200 MHz, as described for Figure IV-4.

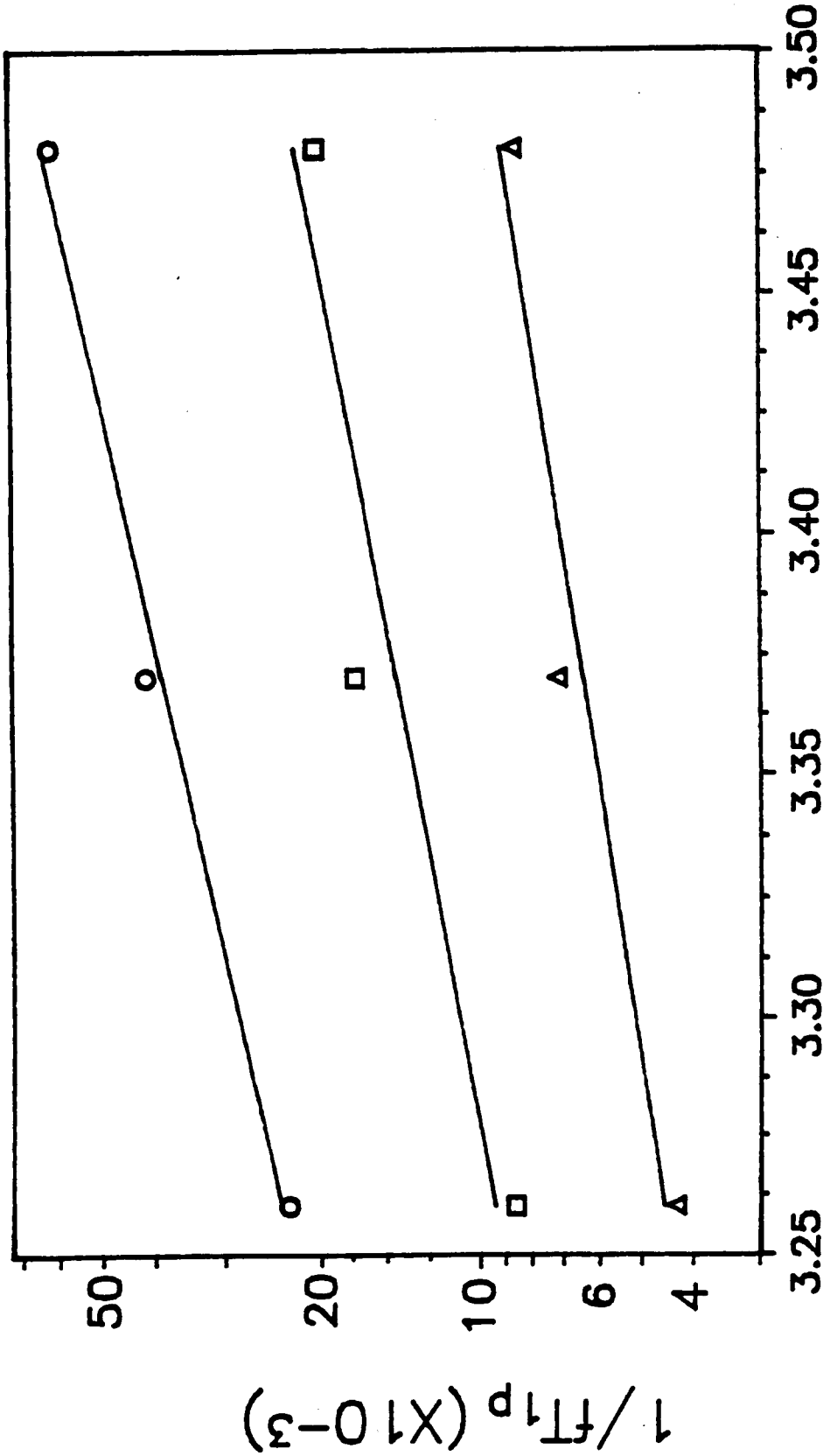

Figure IV–8

Figure IV-9: Bond-only models of the arrangement of 3PGA and CrATP at the active site of PGK in the absence and presence of sulfate. The models were built by aligning one of the carboxyl oxygens of 3PGA in line with the γ-phosphoryl group of CrATP; no van der Waals overlap was allowed. Modelling was done using the Desktop Molecular Modeller software from Oxford University Press.

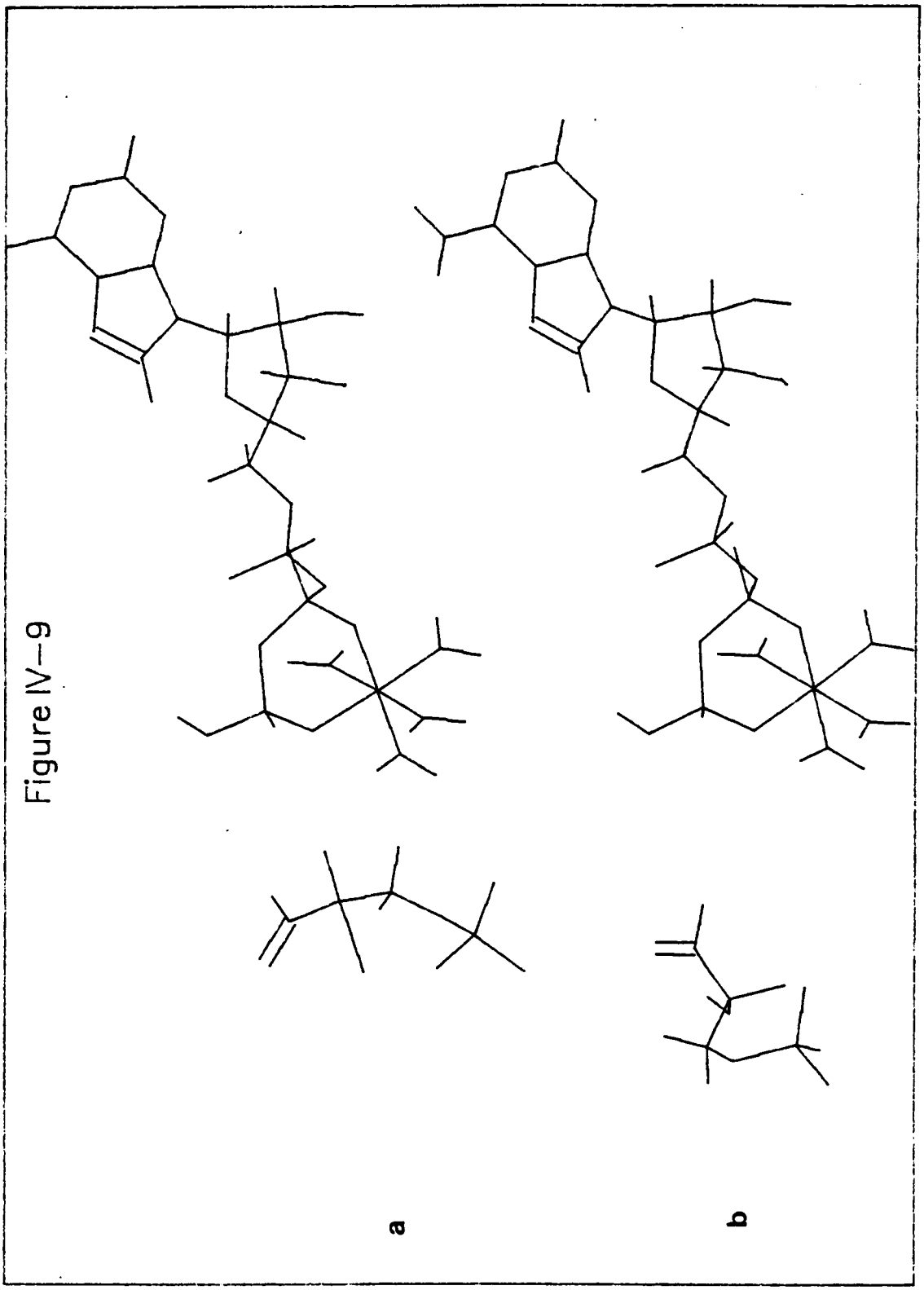

Figure IV–9

Figure IV-10: CPK space-filling models of the arrangement of 3PGA and CrATP in the absence and presence of sulfate. The models were built as described for Figure IV-9; the space-filling representation is included here because it gives a more graphic representation of the overall increase in 3PGA-to-metal distances in the presence of sulfate.

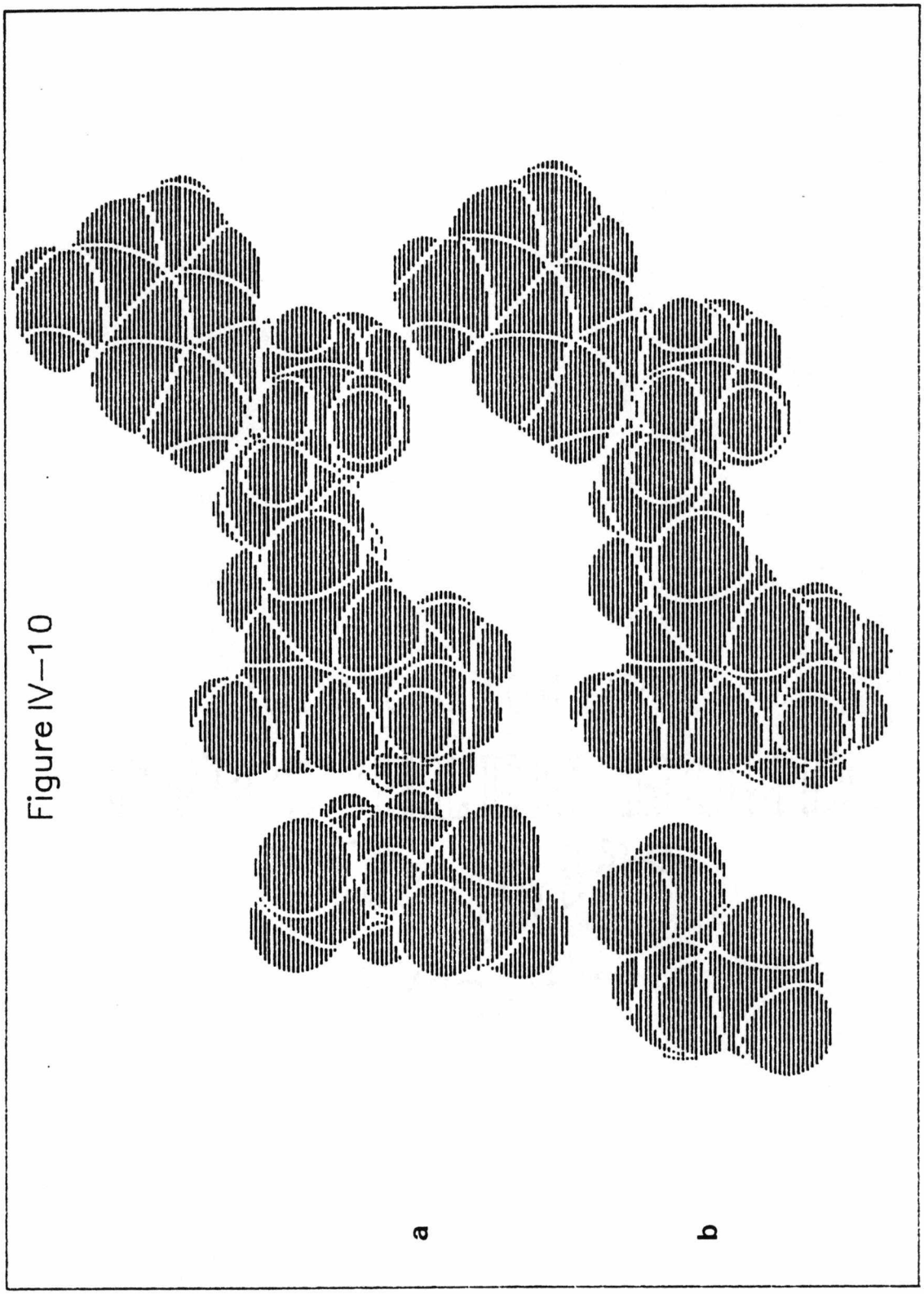

Figure IV–10

Figure IV-11: Contour plot of 2DTRNOESY spectrum of 2'deoxy-ATP in the ternary ^{2}HPGK·dATP·G-3-P complex, taken at a [MgdATP]/^{2}PGK ratio of 18:1. The data was acquired using a mixing time of 15 msec. The sample contained 0.383 mM ^{2}HPGK, 7 mM dATP, 8.2 mM $MgCl_2$, and 3 mM (D)glycerol-3-phosphate in 50 mM deuterated Na^{+}-acetate buffer, pH 5.9, and >99.9+ $^{2}H_2O$.

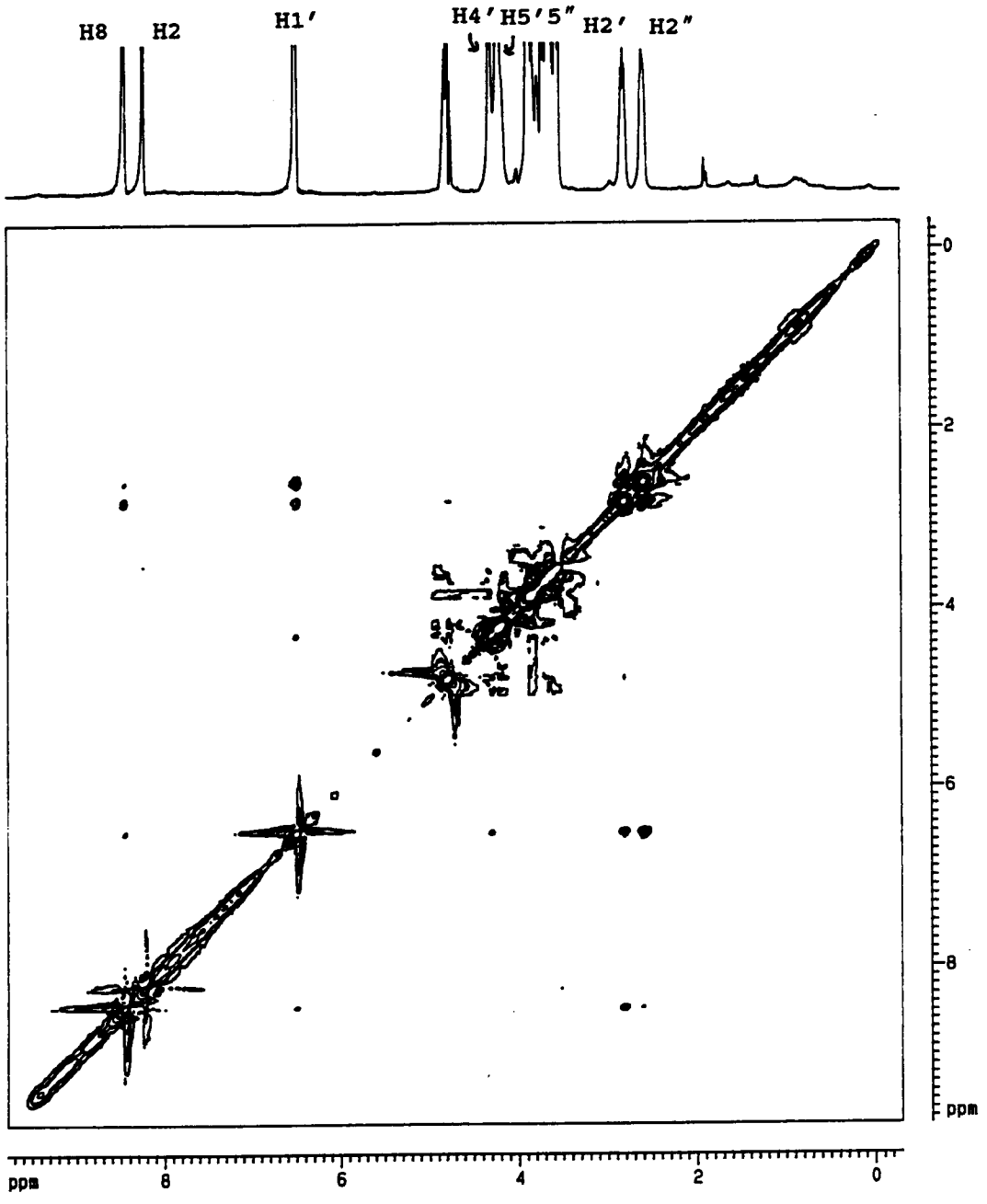
H8
H2
H1′
H4′ H5′5″
H2′
H2″
0
2
4
6
8
ppm
ppm
8
6
4
2
0

Figure IV-12: Contour plot of 2DTRNOESY spectrum of 2'deoxy-ATP in the ternary ^{2}HPGK·dATP·G-3-P complex, taken at a [MgdATP]/^{2}PGK ratio of 18:1. The data was acquired using a mixing time of 70 msec. The sample contained 0.383 mM ^{2}HPGK, 7 mM dATP, 8.2 mM $MgCl_2$, and 3 mM (D)glycerol-3-phosphate in 50 mM deuterated Na^{+}-acetate buffer, pH 5.9, and >99.9+ $^{2}H_2O$.

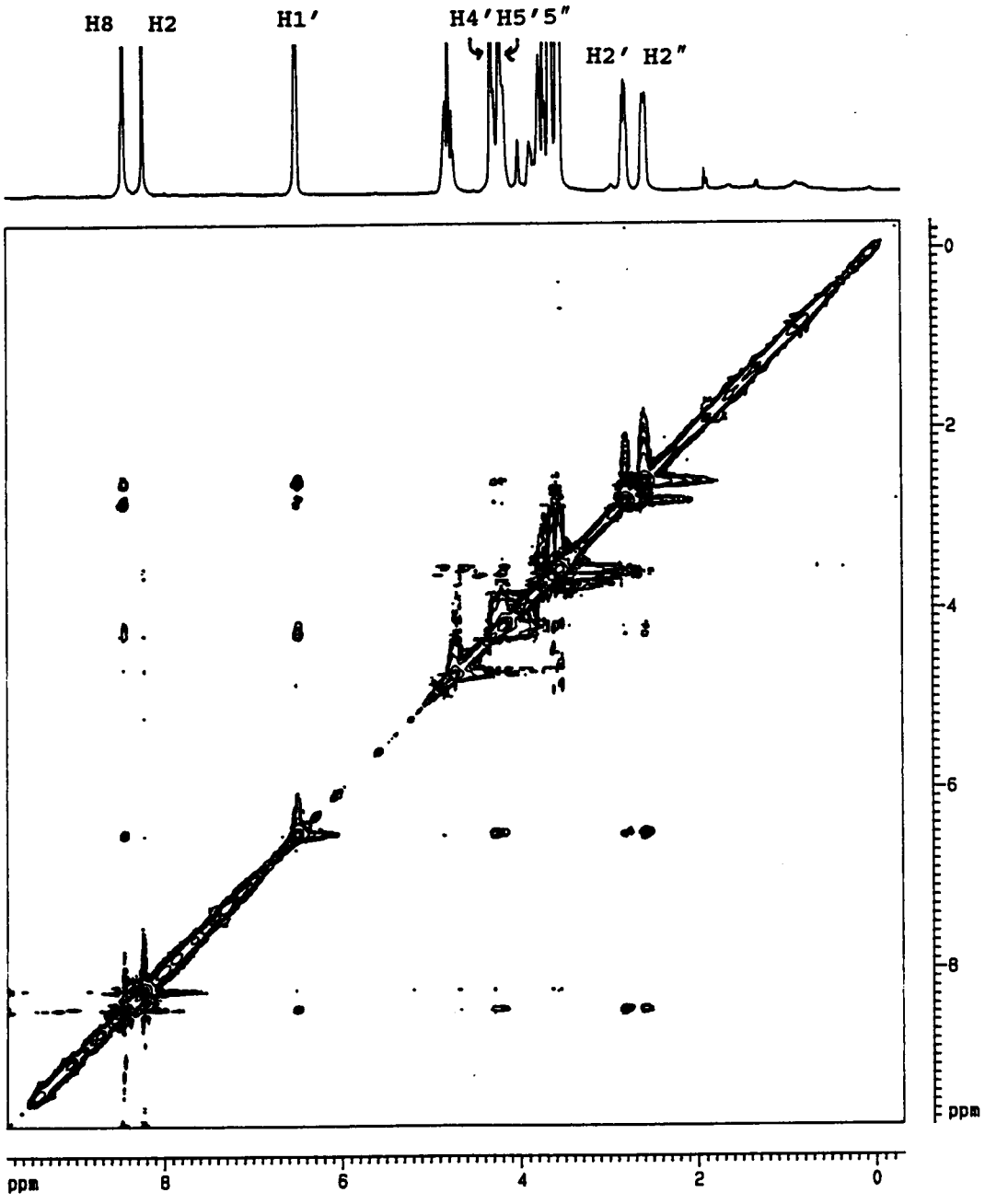
H8
H2
H1′
H4′H5′5″
H2′ H2″
0
2
4
6
8
ppm
ppm
8
6
4
2
0

Figure IV-13: Contour plot of 2DTRNOESY spectrum of 2'deoxy-ATP in the ternary ^{2}HPGK·dATP·G-3-P complex, taken at a [MgdATP]/[^{2}PGK] ratio of 22:1. The data was acquired using a mixing time of 70 msec. The sample contained 0.273 mM ^{2}HPGK, 6.1 mM dATP, 7.4 mM $MgCl_2$, and 1 mM (D)glycerol-3-phosphate in 50 mM deuterated Na^{+}-acetate buffer, pH 5.9, and 99.9+% $^{2}H_2O$.

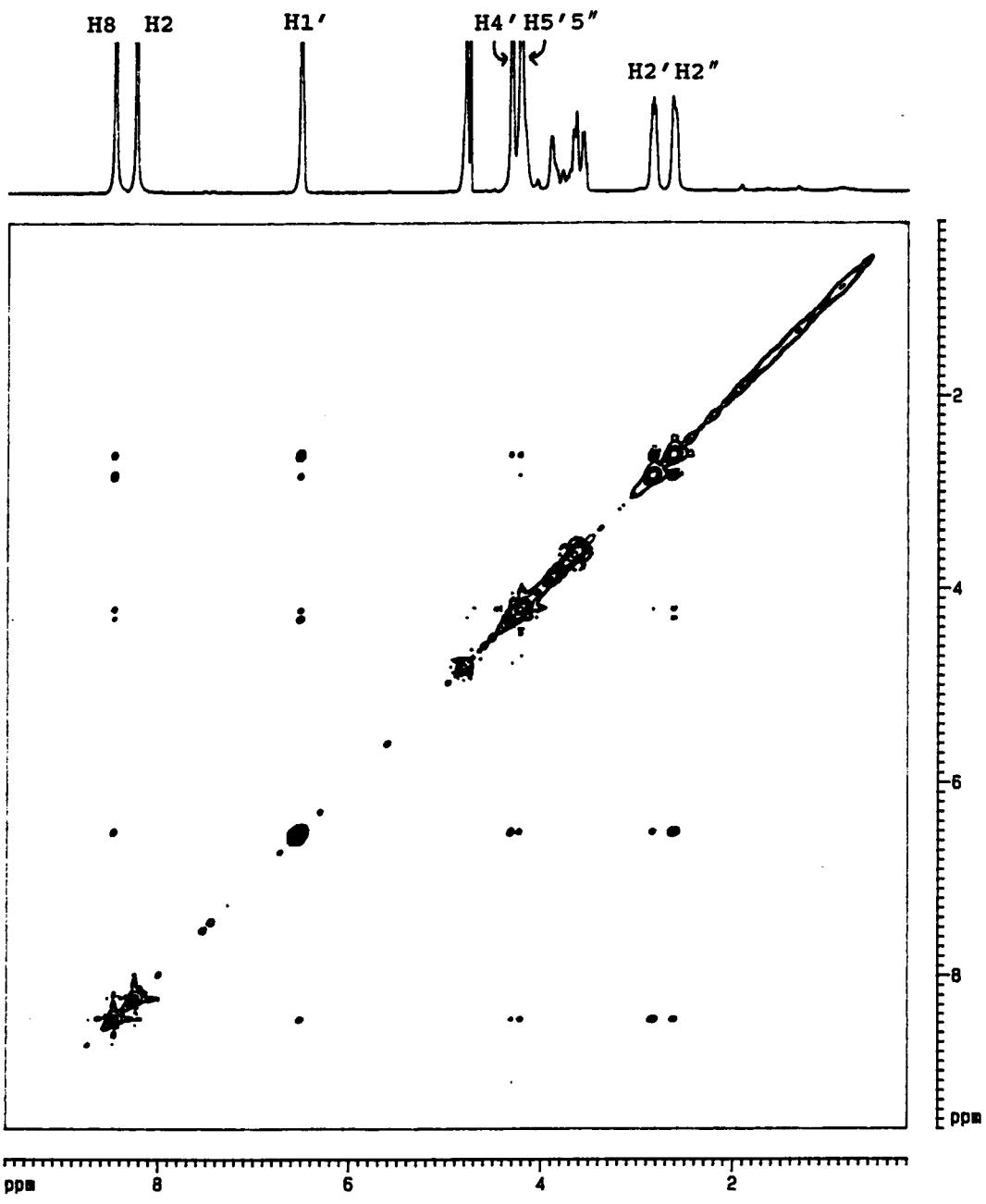
H8
H2
H1'
H4'
H5'5"
H2'H2"
ppm
8
6
4
2
2
4
6
8
ppm

Figure IV-14: Dependence of %NOE on mixing time for the 2DTRNOESY data collected at a [MgdATP]/[^{2}PGK] ratio of 18:1. NOE interactions represented are H2′-H2″ (▽), H2″-H1′ (✱), H2′-H1′ (◇), H2′-H8 (□), H1′-H4′ (○), H2″-H4′ (△), and H2′-H5′5″ (+). Sample composition was as described in Figure IV-11.

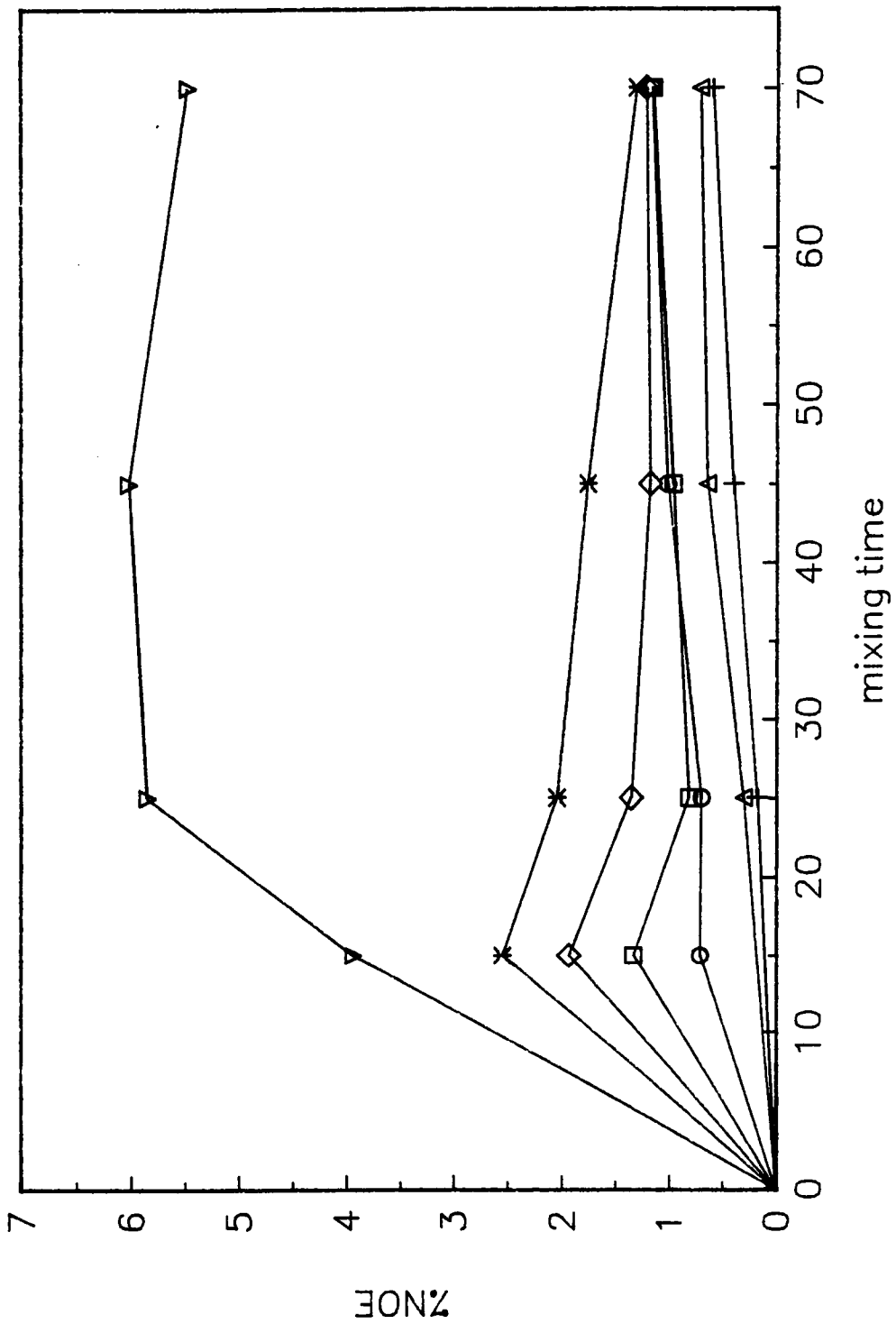

Figure IV–14

Figure IV-15: Dependence of %NOE on mixing time for the 2DTRNOESY data collected at a [MgdATP]/[^{2}PGK] ratio of 22:1. NOE interactions represented are H2′-H2″ (○), H2″-H1′ (△), H2′-H1′ (□), H2′-H8 (▽), H1′-H4′ (+), H1′-H8 (✱), H2″-H4′ (◇), and H2′-H5′5″ (✠). Sample composition was as described in Figure IV-13.

Figure IV–15

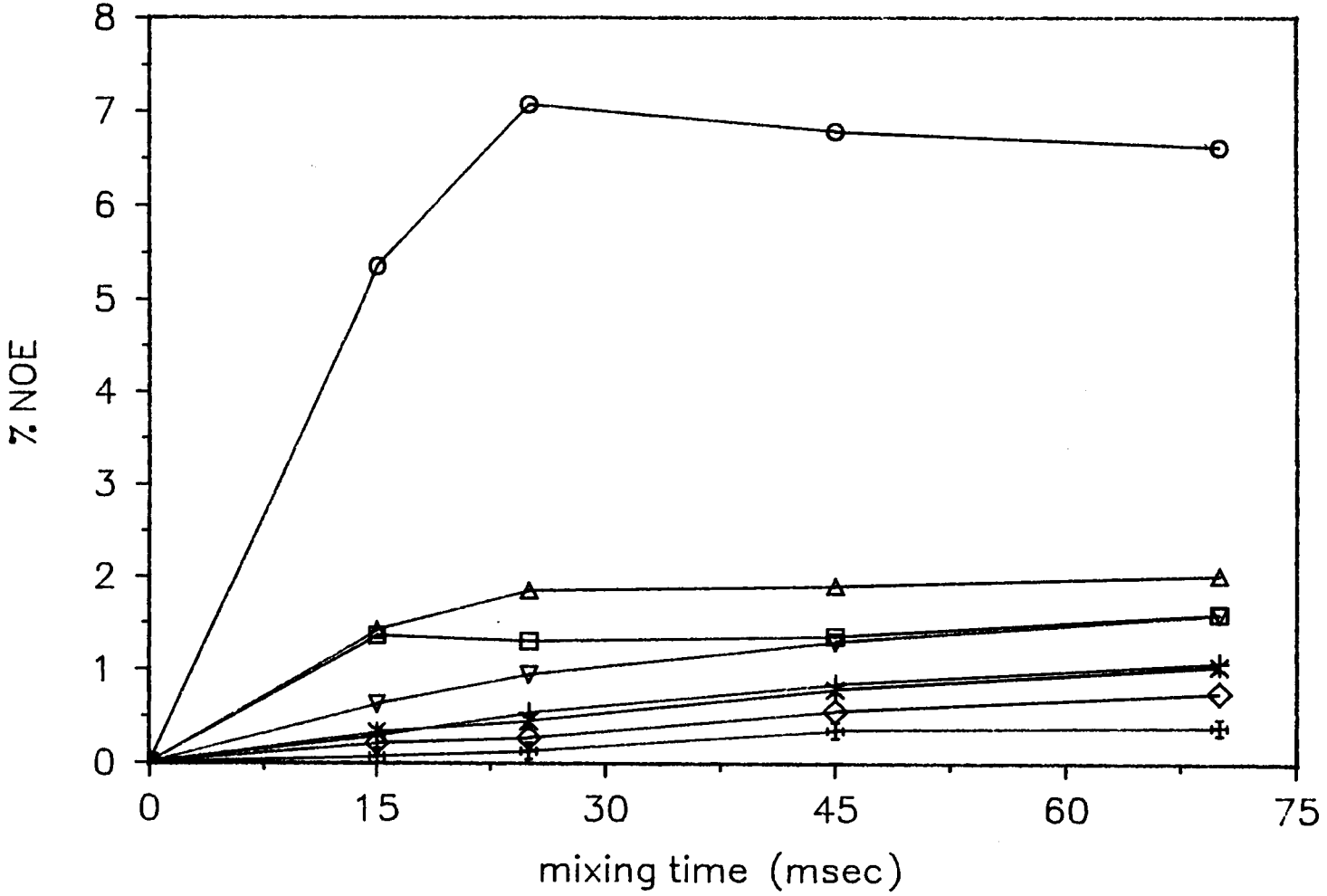

Figure IV-16: Dependence of %NOE on mixing time for the 2DTRNOESY data collected at a [MgdATP]/[^{2}PGK] ratio of 55:1. NOE interactions represented are H2′-H2″ (○), H2″-H1′ (▲), H2′-H8 (▼), H2′-H1′ (□), and H1′-H4′ (◇). Sample was composed of 0.09 mM ^{2}HPGK, 5 mM dATP, 6 mM $MgCl_2$, 1 mM (D)glycerol-3-phosphate, and 50 mM deuterated Na^+-acetate buffer in 99.9+% ^2H_2O.

Figure IV–16

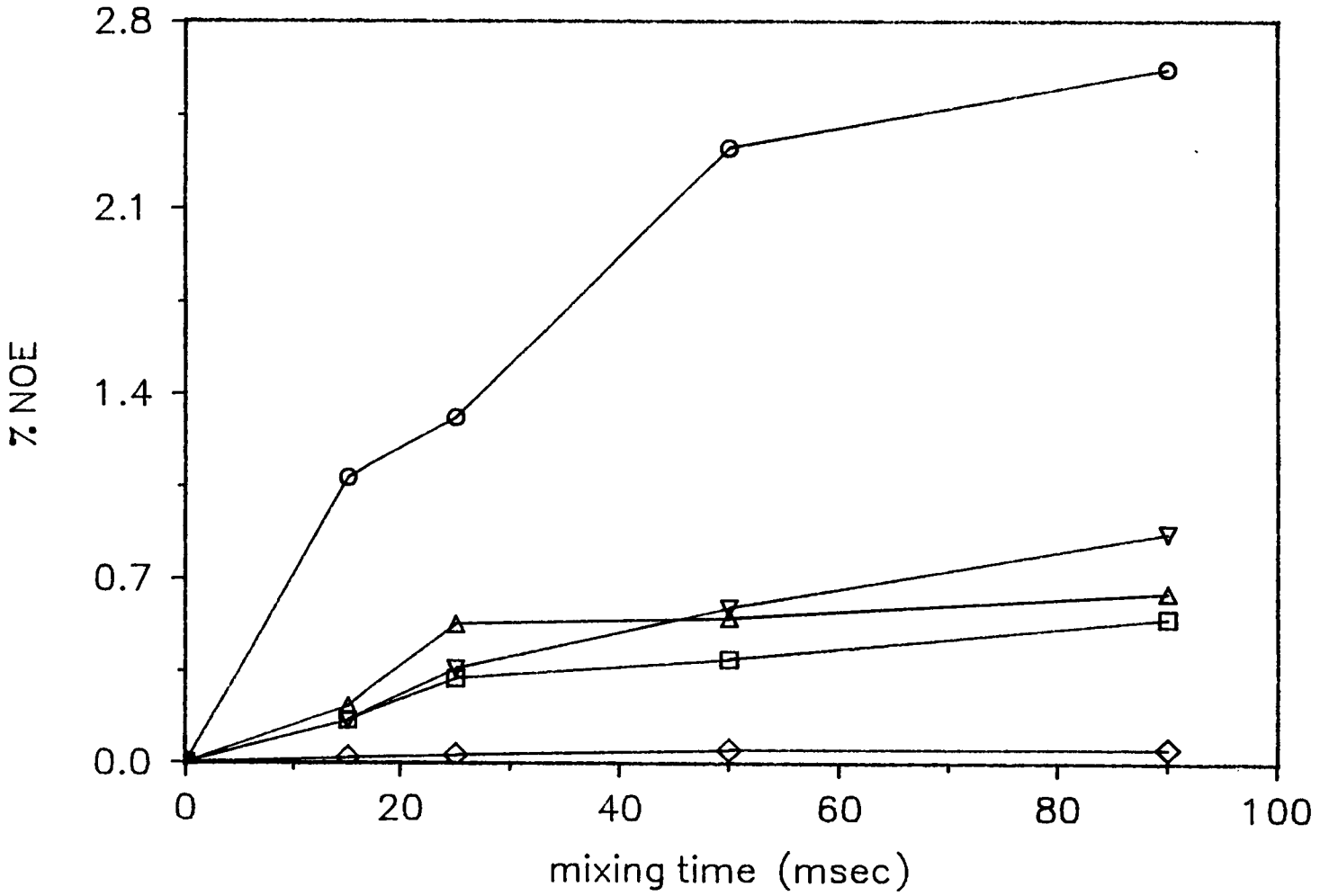

Figure IV-17: Dependence of %NOE on [MgdATP]/[^{2}PGK] ratio at 15 msec. mixing time for three different NOE interactions: H2″-H1′ (□), H2′-H8 (△), and H1′-H4′ (○).

Figure IV–17

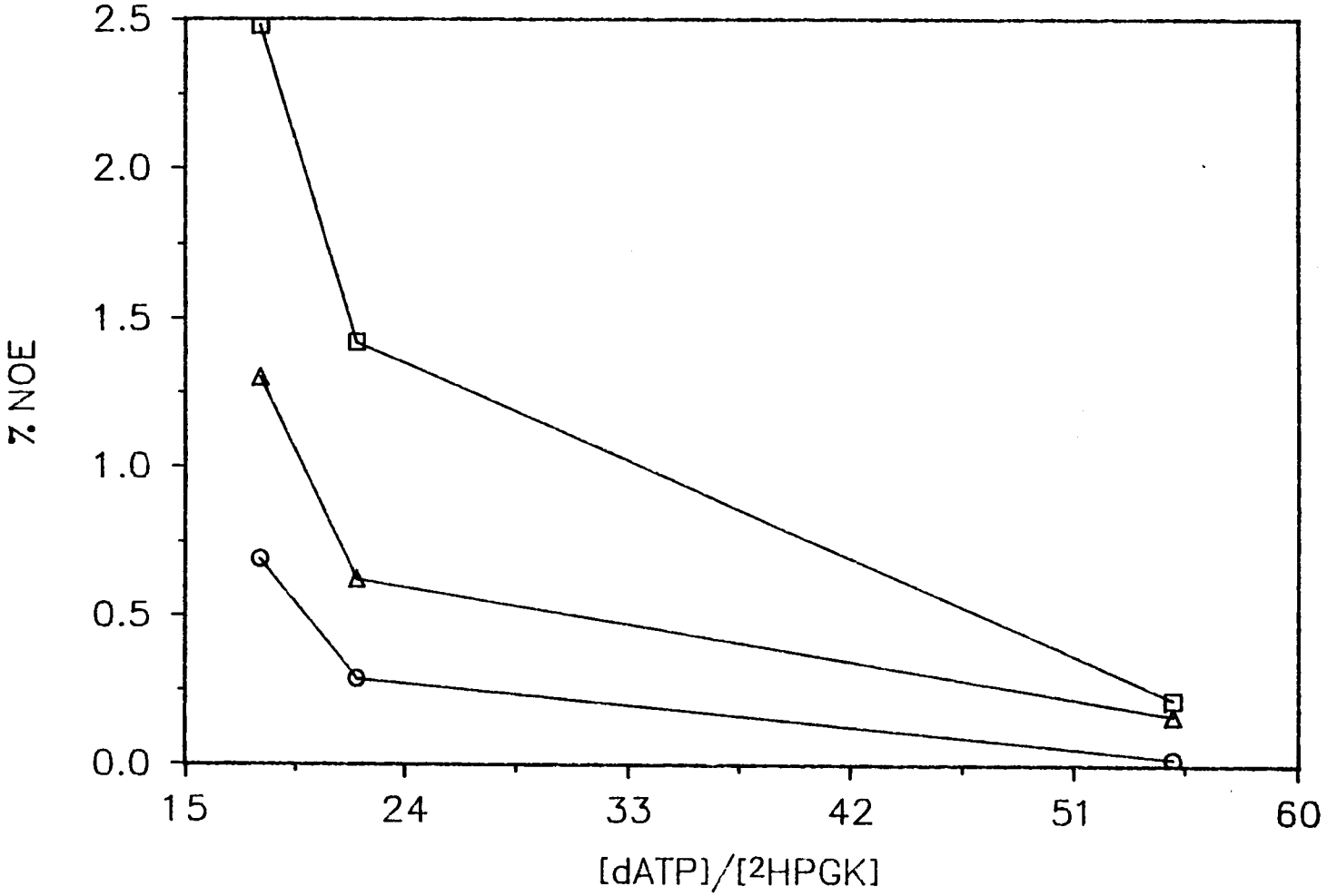

Figure IV-18: Model showing the conformation of the ribose ring and orientation of the adenine moiety of 2'deoxy-ATP at the active site of yeast PGK, as determined by 2DTRNOESY measurement of inter-proton distances. The model was constructed with distance constraints as calculated from NOE data by the MARDIGRAS matrix-relaxation analysis program, using the Desktop Molecular Modeller software.

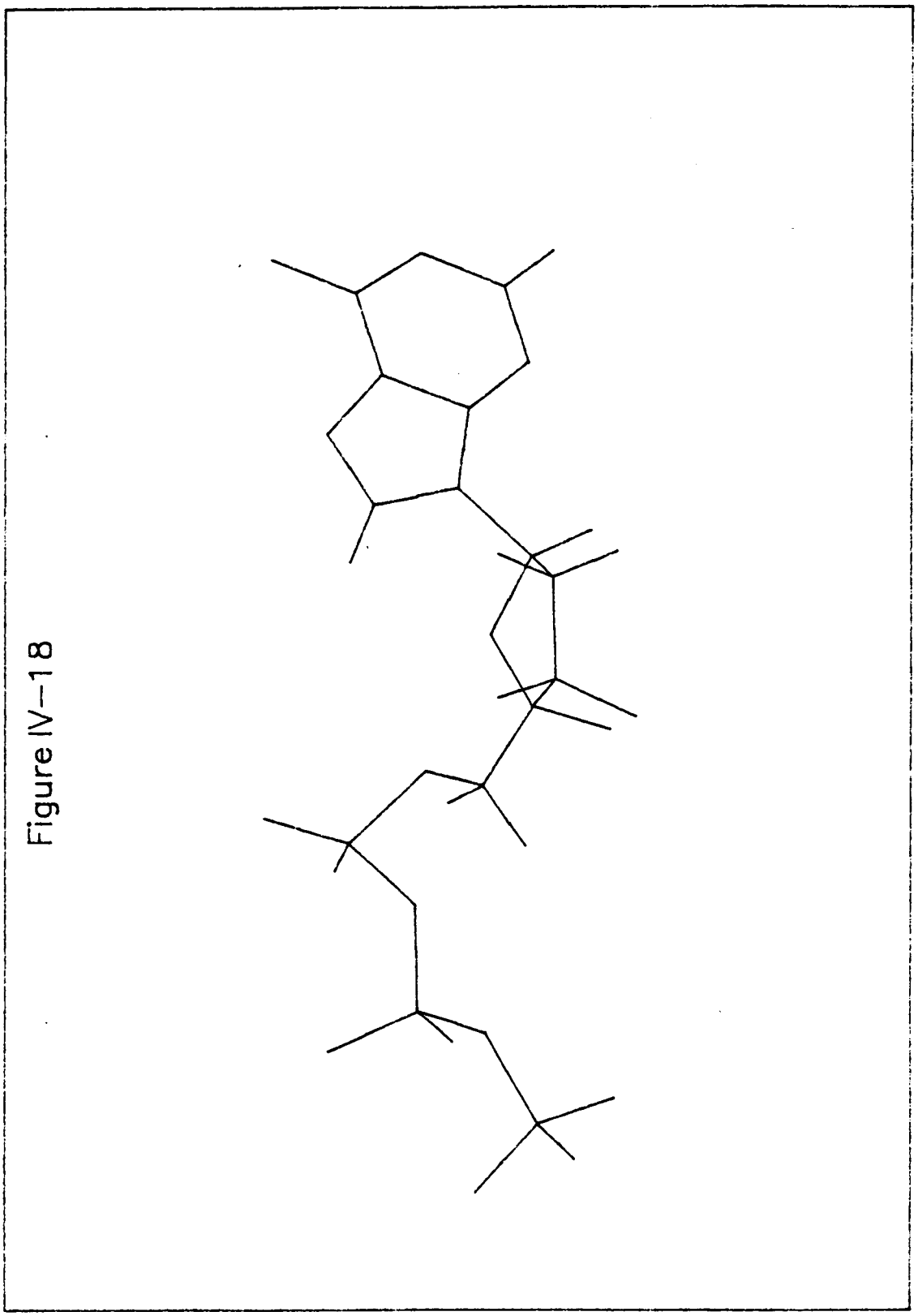

Figure IV—18

Figure IV-19: Alternate views of the bound dATP conformation shown in Figure IV-18, illustrating (a) the 59° glycosidic angle determined for the adenine moiety and (b) the O4′-endo conformation determined for the ribose ring.

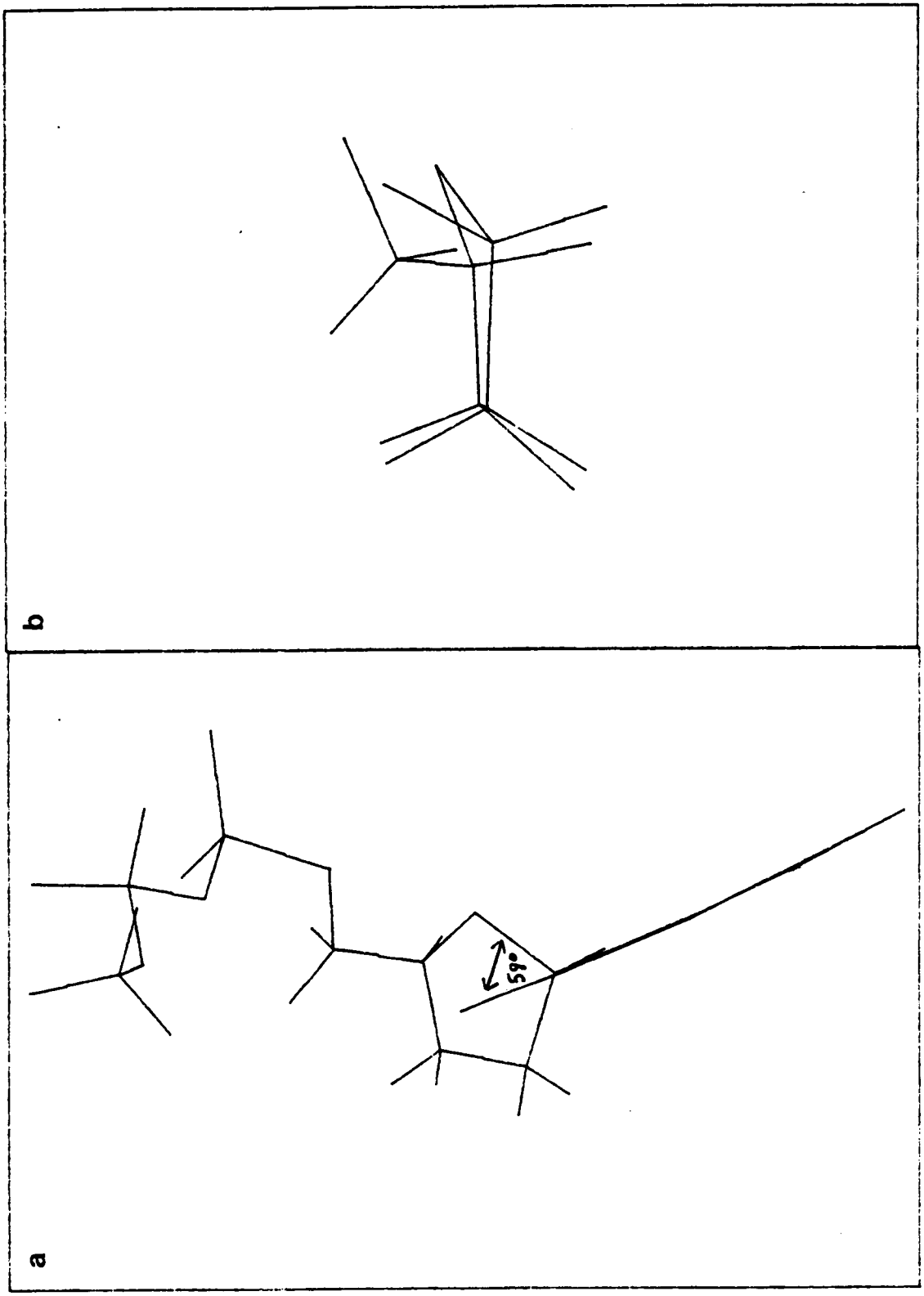
b
a
59°

Figure IV-20: Dependence of the MARDIGRAS-calculated inter-proton distances on mixing time for the 2DTRNOESY data collected at a [MgdATP]/[^{2}PGK] ratio of 18:1. Inter-proton distances represented are H2′-H5′5″ (◇), H2″-H4′ (○), H1′-H4′ (□), H2′-H8 (▽), and H2″-H1′ (△). Sample composition was as described in figure IV-11.

Figure IV—20

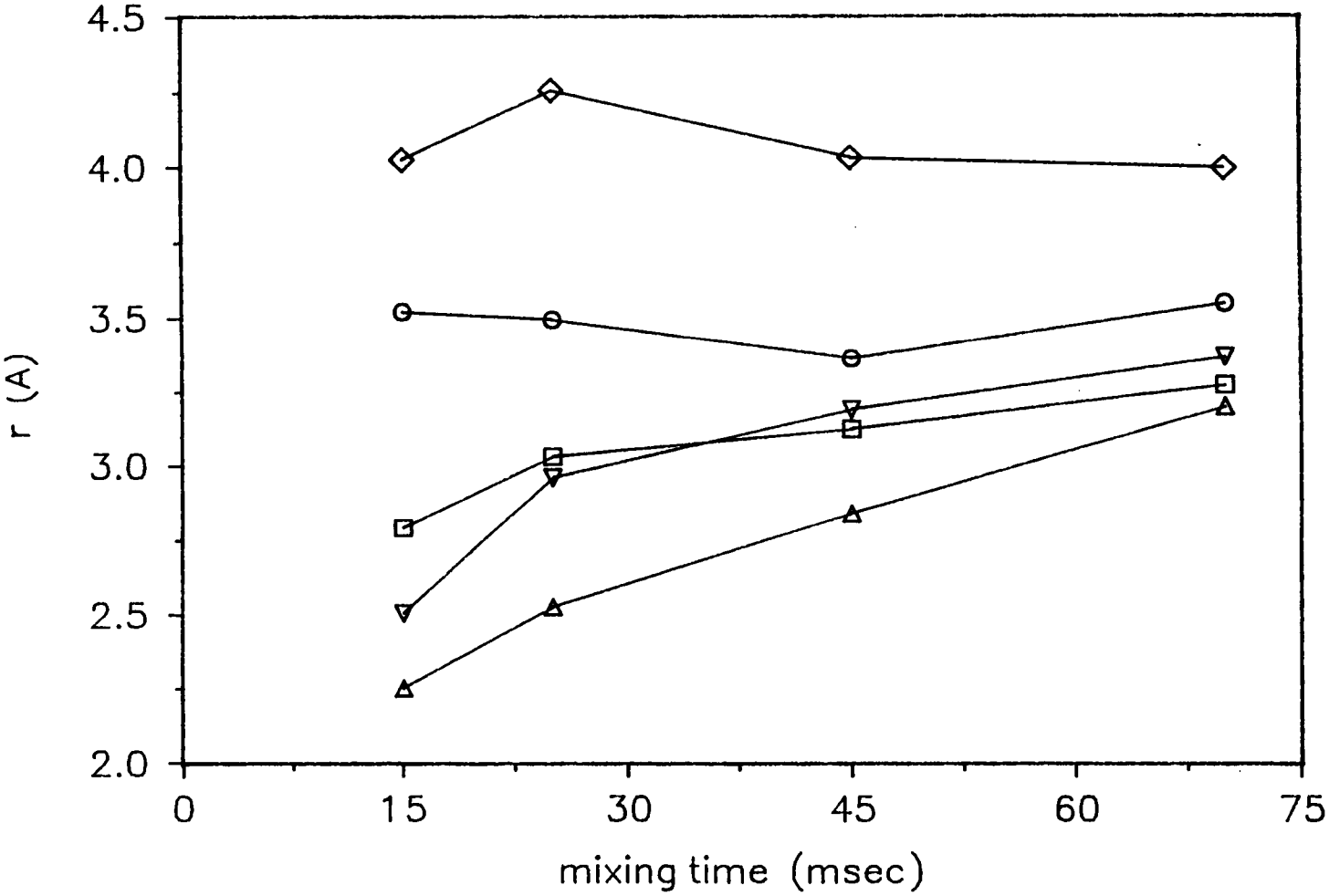

Figure IV-21: Dependence of the MARDIGRAS-calculated inter-proton distances on mixing time for the 2DTRNOESY data collected at a [MgdATP]/[^{2}PGK] ratio of 22:1. Inter-proton distances represented are H2′-H5′5″ (◇), H2″-H4′ (○), H1′-H4′ (□), H1′-H8 (✠), H2′-H8 (▽), and H2″-H1′ (△). Sample composition was as described in figure IV-13.

Figure IV—21

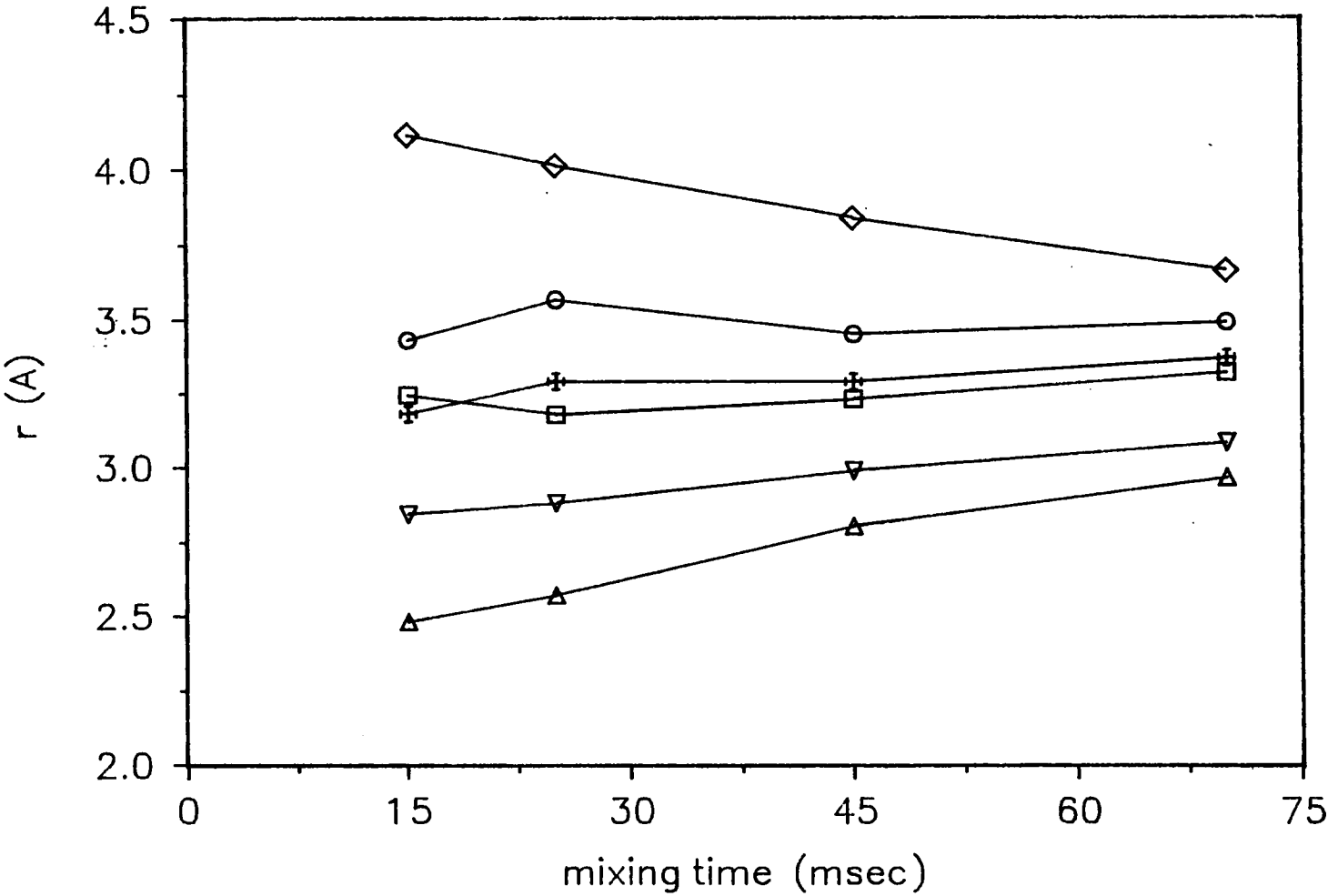

Figure IV-22: Dependence of the MARDIGRAS-calculated inter-proton distances on mixing time for the 2DTRNOESY data collected at a [MgdATP]/[^{2}PGK] ratio of 55:1. Inter-proton distances represented are H2″-H4′ (O), H2′-H8 (Δ), and H1′-H4′ (□). Sample composition was as described in figure IV-16.

Figure IV–22

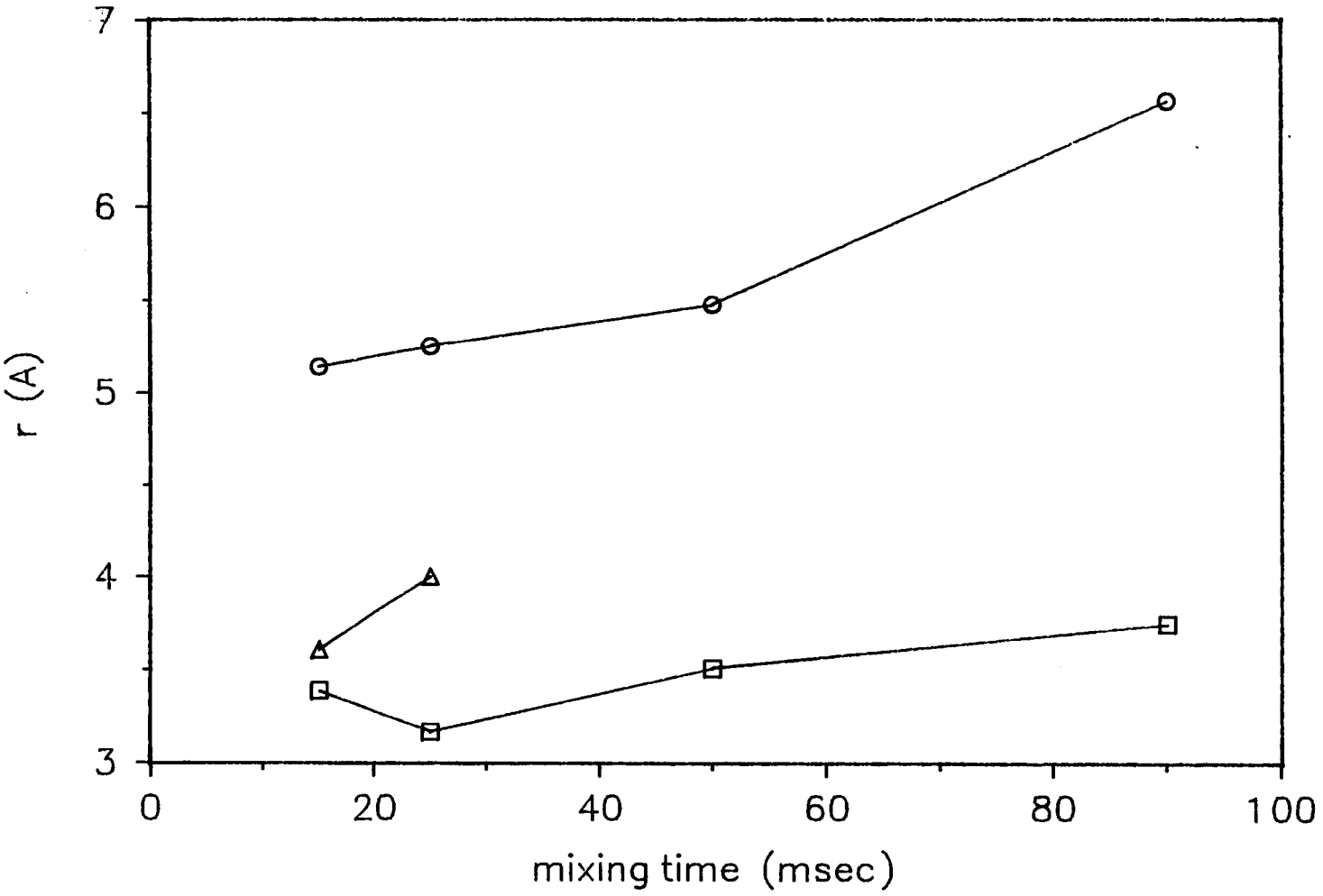

Figure IV-23: Dependence of the MARDIGRAS-calculated inter-proton distances on [MgdATP]/[^{2}PGK] ratio at 15 msec. mixing time for three different inter-proton distances: H1′-H4′ (O), H2′-H8 (△), and H2″-H1′ (□).

Figure IV–23

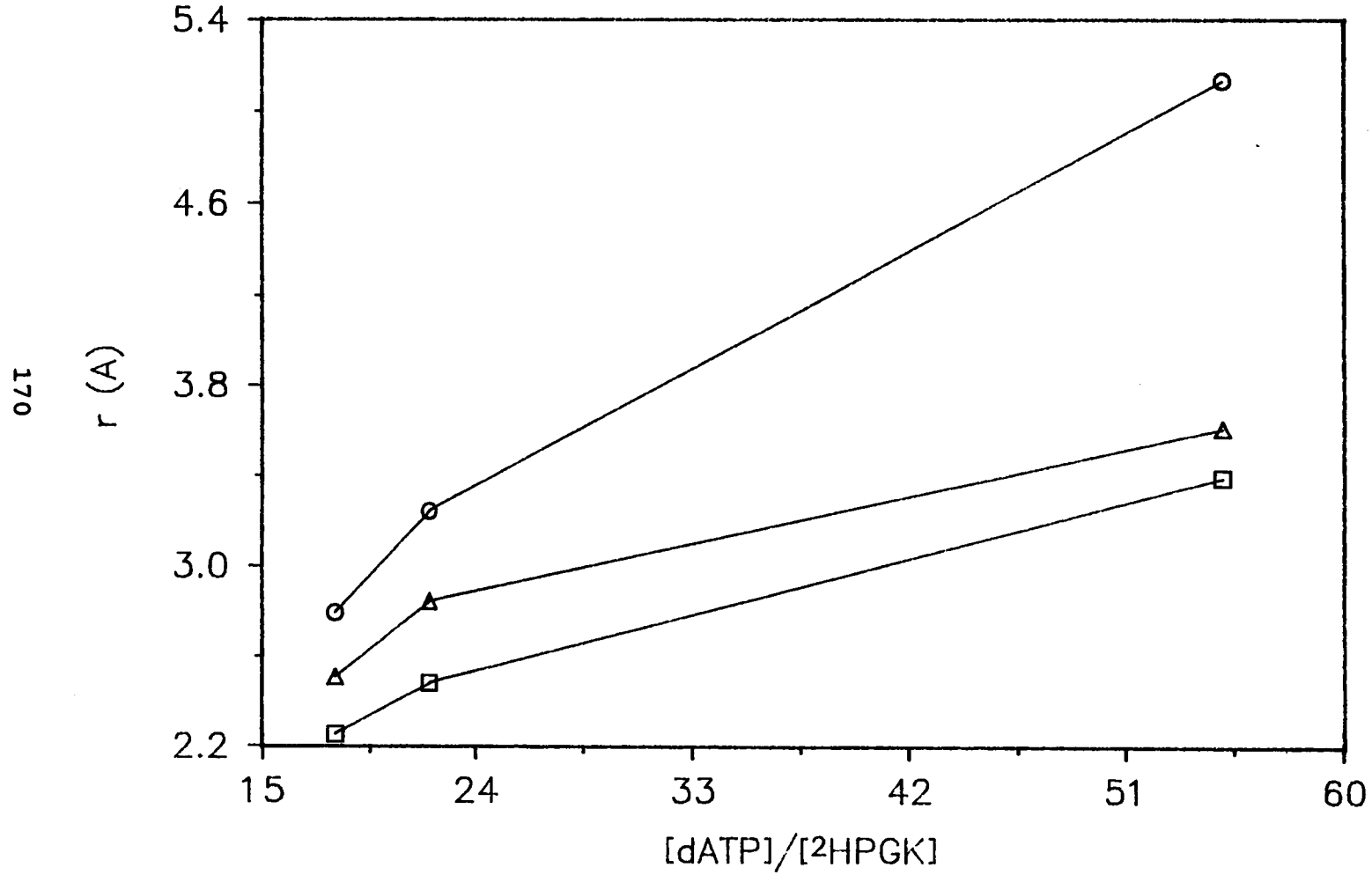

```
;kinet.jdg
;kinetic measurement with variable delay between expts.

1 ze
  vd
2 d1
3 p1 ph2
4 go=2 ph31
  d11 wr #0 if #0 iv
  lo to 1 times l4
5 d11
  exit


ph1=0 2
ph2=0 0 2 2 1 1 3 3
ph31=0 0 2 2 1 1 3 3


;hl1: ecoupler power high level
;p1 : 90 degree transmitter high power pulse
;d1 : relaxation delay
;d11: delay for disk I/O                          [30 msec]
;vd : variable delay (taken from vd list)
;L4 : l4 = number of expts. = number of delays in vd list
;NS : 8 * n
;DS : 2 or 4
;td1: number of expts.
;you MUST define vd list in acquisition parameters
;this pulse program produces a ser-file (PARMOD = 2D)
```

Figure VI-1: Pulse program for sequential acquisition of one-dimensional NMR spectra with a variable delay between experiments. This pulse program can be modified for X-nucleus observation with proton decoupling as follows: add the command "cpd" after the first "d11", add "do" after the second "d11", and set up normal decoupling parameters.

Figure VI-2: 3PGA mutase reaction as monitored by ^{31}P NMR spectroscopy. Samples contained (a) 0.1 mM PGK, 60 mM NaCl, and 50 mM MES-NaOH buffer pH 5.9, with 20% $^{2}H_2O$ for locking; (b) same as in (a), plus 9.8 mM 3PGA, time = 15 hours after 3PGA addition; (c) as in (b), with 0.5 mg sonicated, single-stranded DNA, time = 45 minutes after DNA addition; (d) as in (c), time = 7.5 hours after DNA addition; (e) as in (c), time = 22 hours after DNA addition.

Figure VI--2

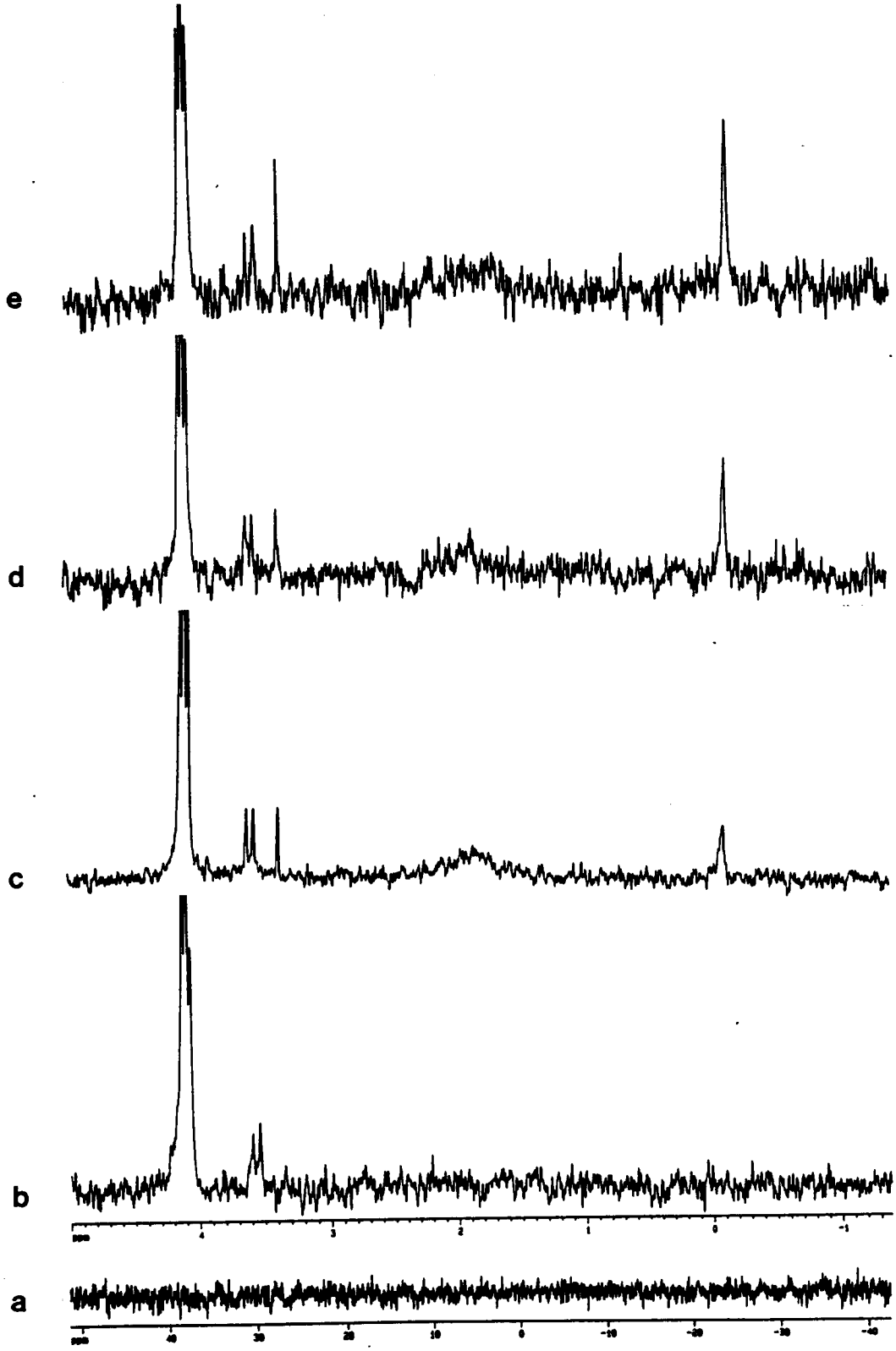

Figure VI-3: 3PGA mutase reaction as monitored by ^{31}P NMR spectroscopy, showing no change in the DNA resonance (centered at 0.9 ppm) during the course of the reaction. Sample contained 0.1 mM PGK, 9.8 mM 3PGA, 60 mM NaCl, 50 mM MES-NaOH buffer pH 5.9, and 3 mg sonicated, single-stranded DNA, with 20% $^{2}H_2O$ for locking.

Figure VI—3

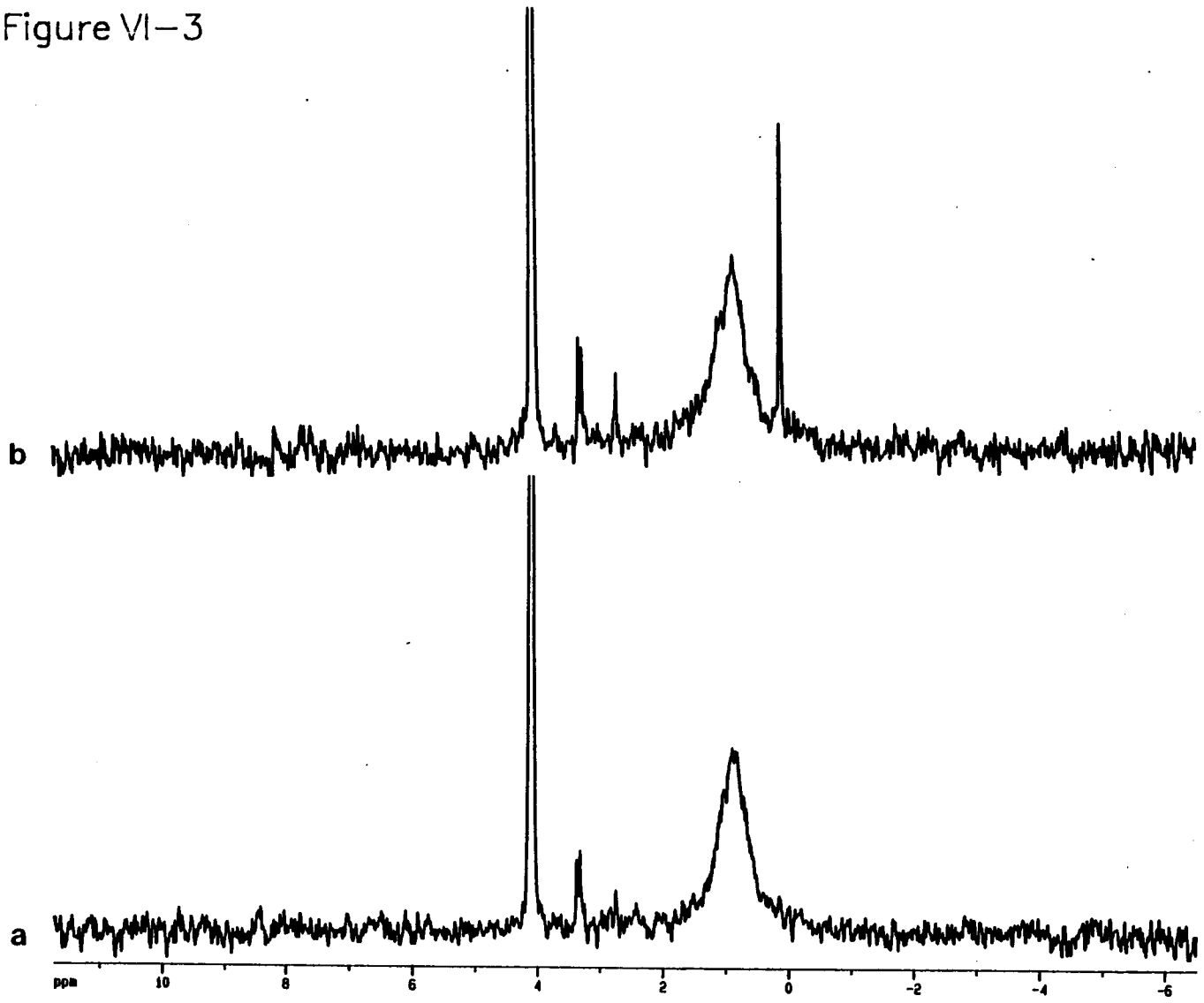

Figure VI-4: 3PGA mutase reaction after 120 hours incubation, showing essentially complete reaction of 3PGA. Sample composition was as described for (c) in Figure VI-2.

Figure VI—4

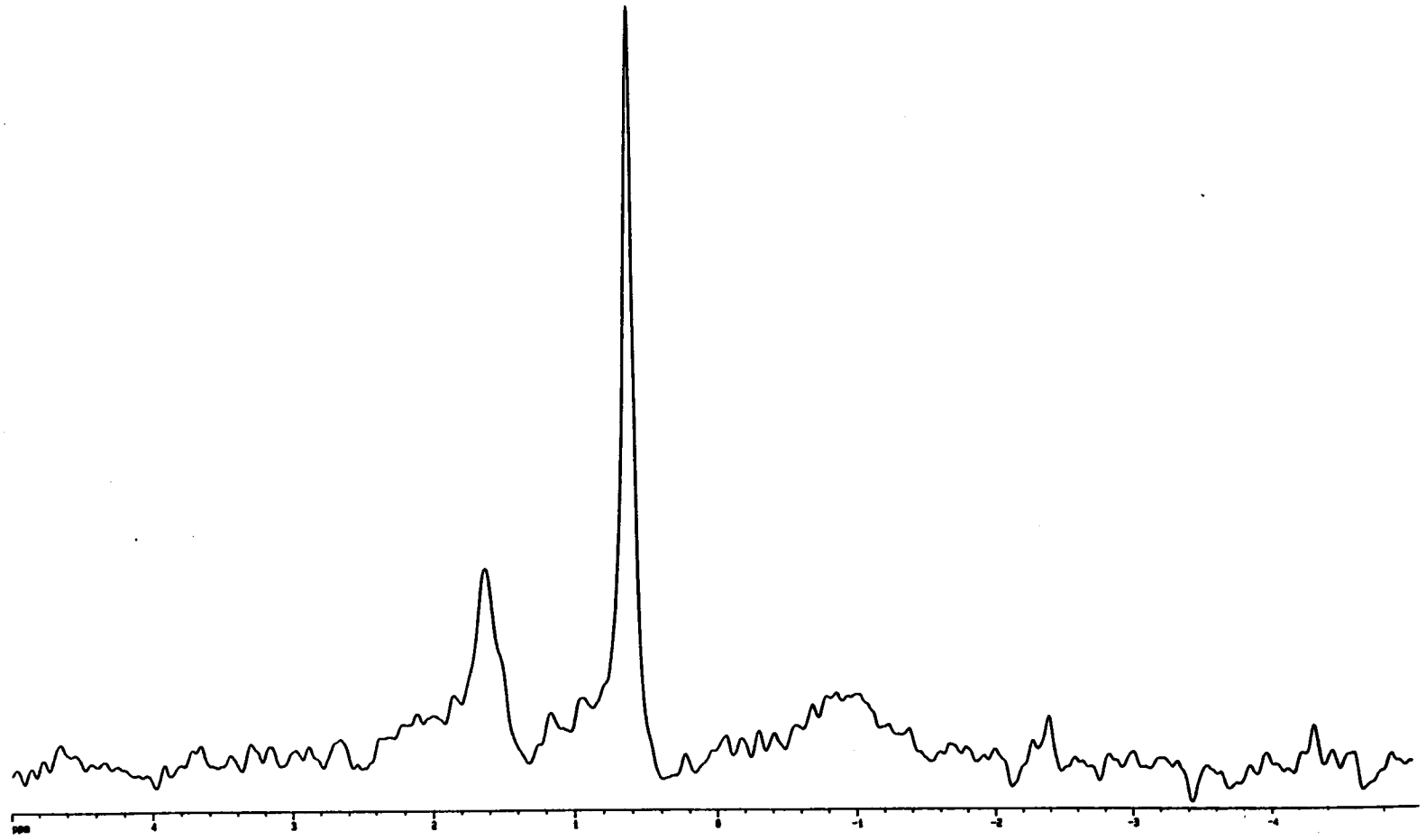

Figure VI-5: 3PGA mutase activity in dialyzed PGK and dialysate as monitored by inorganic phosphate assay. Samples were: dialyzed PGK+dialysate+3PGA (△); dialyzed PGK+3PGA (○); dialysate+DNA+3PGA (▽); dialysate+3PGA (◇); dialyzed PGK+DNA+3PGA (□); and 3PGA alone (⊕).

Figure VI–5

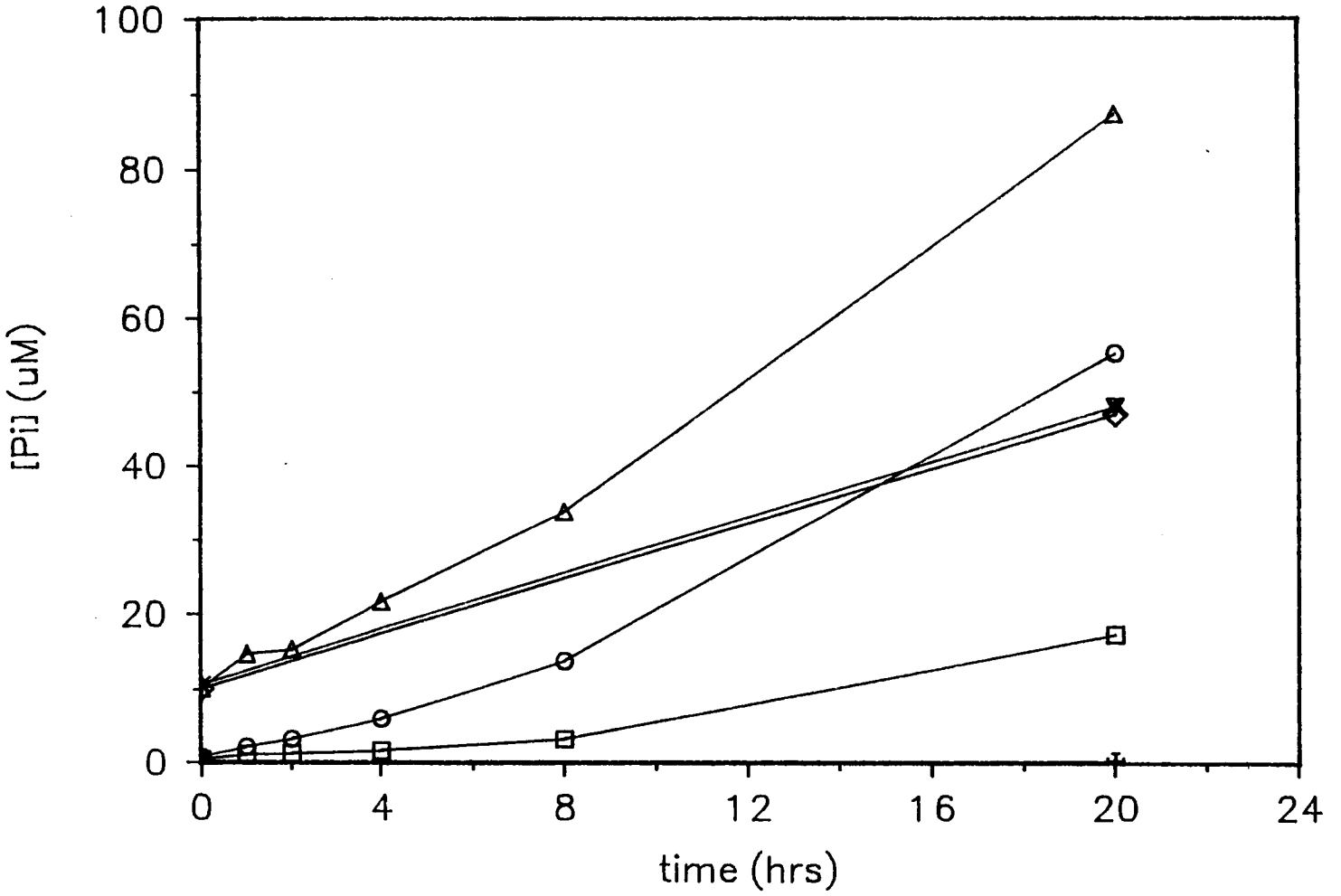

Figure VI-6: 3PGA mutase activity in pH 4.3-precipitated PGK and in the supernatant, as monitored by inorganic phosphate assay. Samples were: supernatant (2x volume)+pellet PGK+3PGA (▲); supernatant (1x volume)+pellet PGK+3PGA (□); supernatant+pellet PGK (2x volume)+3PGA (▼); supernatant+3PGA (○); supernatant+pellet PGK, no 3PGA (+); supernatant, no 3PGA (⊕); pellet PGK+3PGA (◇).

Figure VI–6

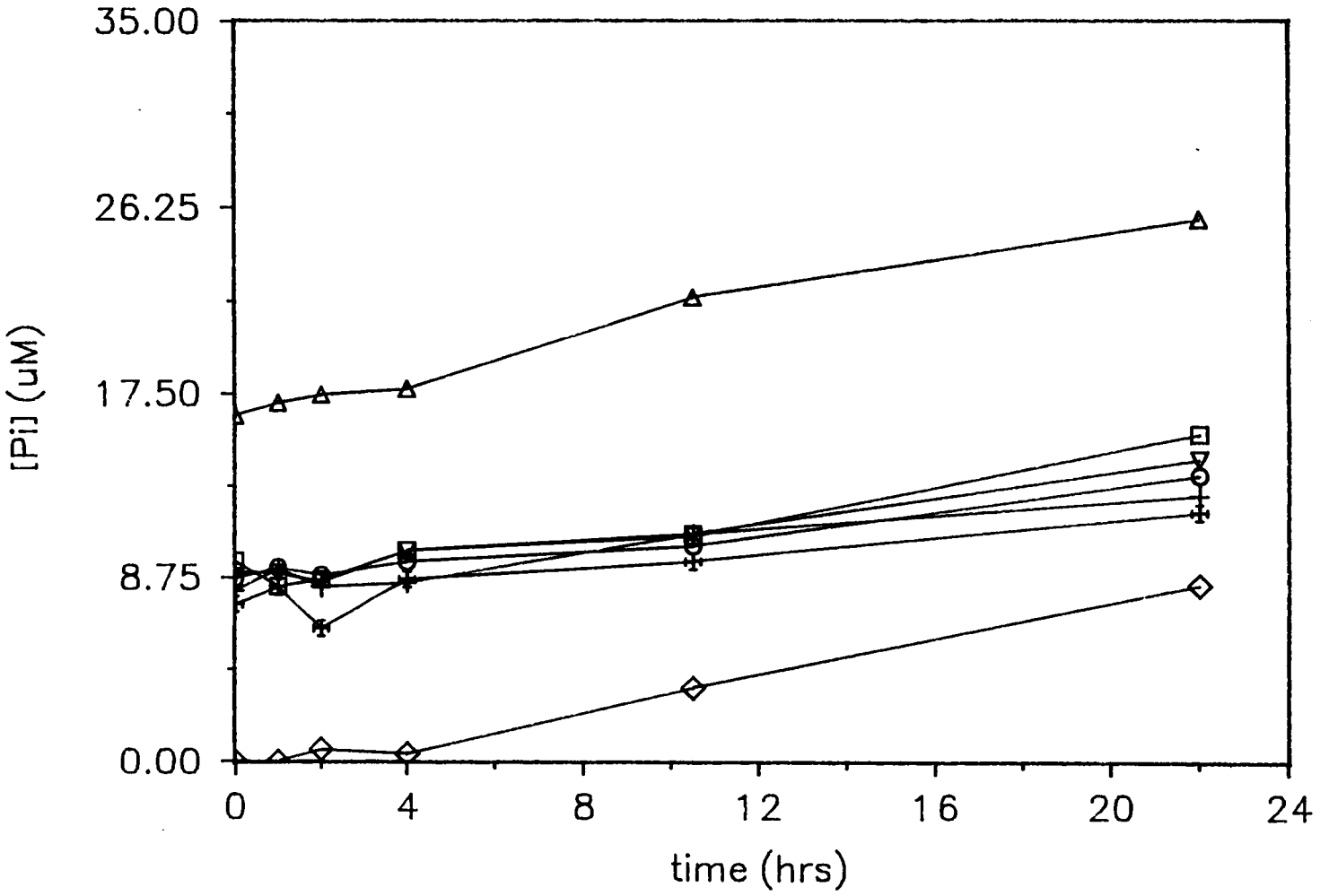

Figure VI-7: Elution profile of dialysate from Sephadex G-10, as monitored by the absorbance of the fractions at 260 nm.

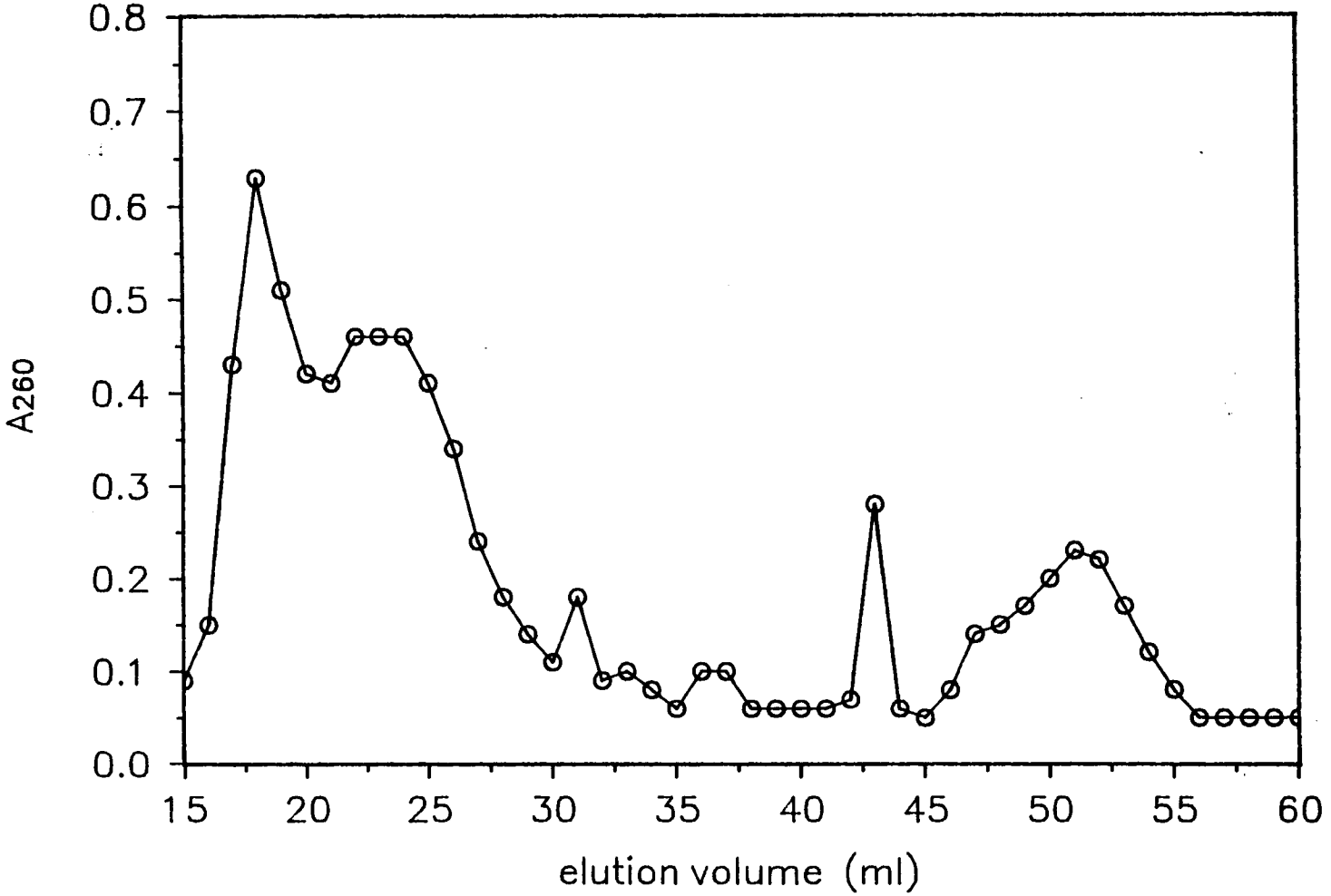
0.8
0.7
0.6
0.5
0.4
0.3
0.2
0.1
0.0
A260
15
20
25
30
35
40
45
50
55
60
elution volume (ml)

Figure VI-8: Analysis of the pooled fractions from Sephadex G-10 treatment of the dialysate shown in Figure VI-7. The fractions were pooled for analysis as follows: fractions 40-44 (a); 45-49 (b); 30-34 (c); 50-56 (d); 21-29 (e); 15-20 (f); and 35-40 (g).

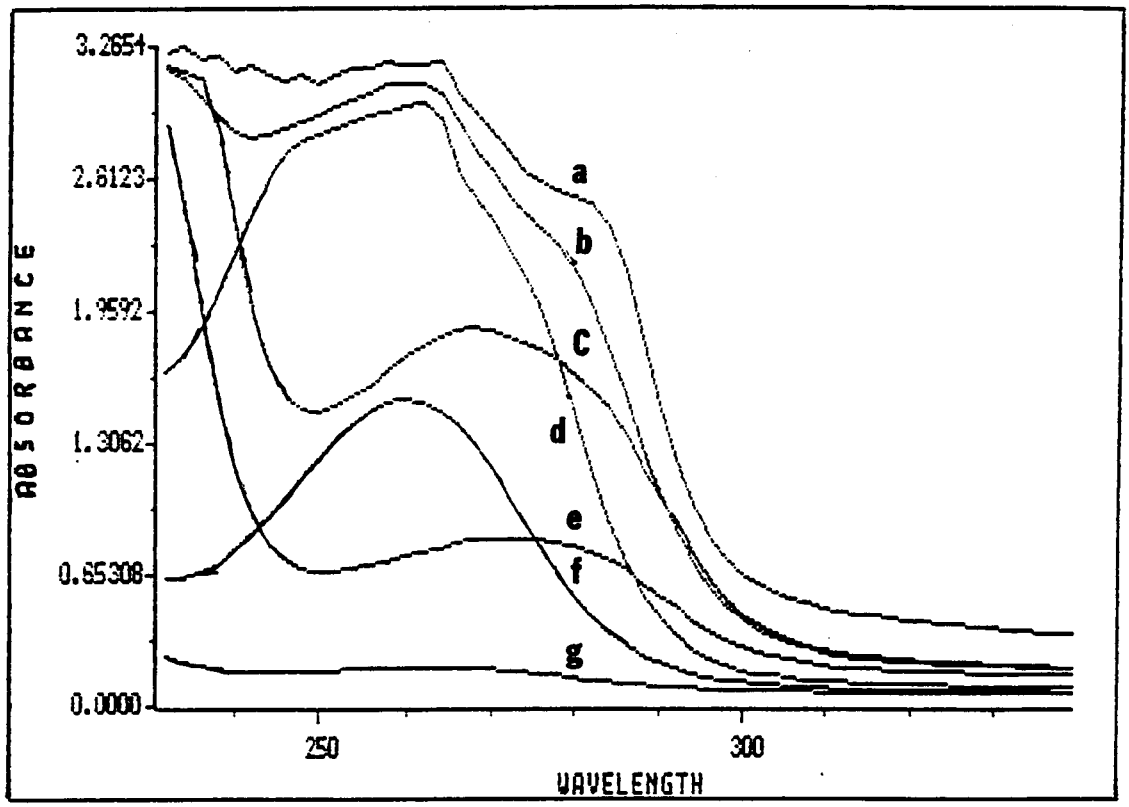
3.2654
2.6123
1.9592
1.3062
0.65308
0.0000
ABSORBANCE
250
300
WAVELENGTH
a
b
C
d
e
f
g

Figure VI-9: ^{1}H-NMR analysis of the PGK dialysate. Resonances in the chemical shift region from 1.0-2.6 ppm are indicative of the H2′ and H2″ protons of the ribose ring of deoxyribonucleic acid; resonances in the chemical shift region 7.0-9.5 are indicative of the aromatic ring protons of deoxyribonucleic acid.

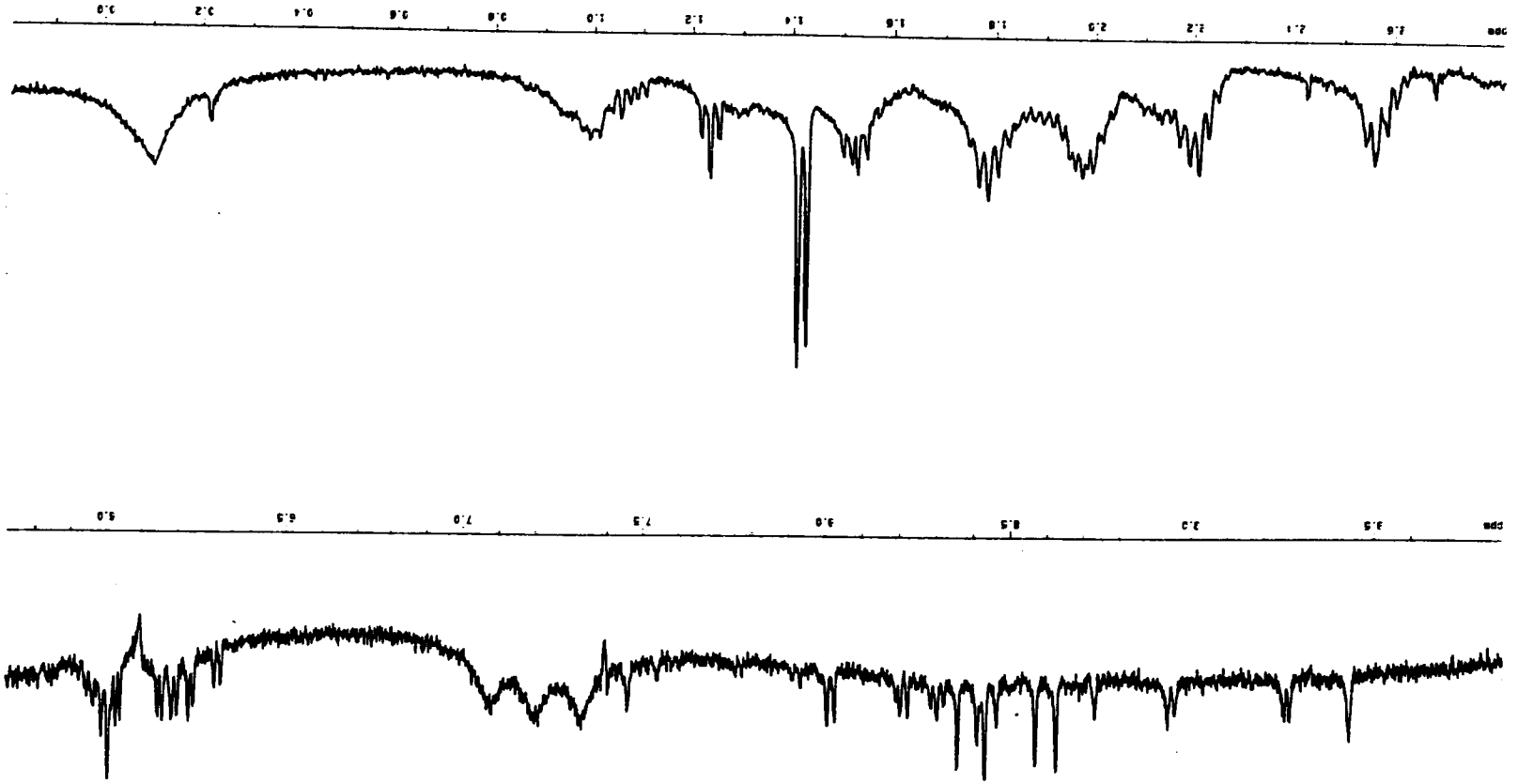

Appendix B

Tables

Table II-1. Kinetic Constants of Yeast Phosphoglycerate Kinase

	High Affinity Site			Low Affinity Site				
	K_m^{MgATP} (μM)	K_m^{PGA} (μM)	V_{max} μmol/min·mg	K_m^{MgATP} (mM)	K_m^{PGA} (mM)	V_{max} μmol/min·mg	K_i^{MgATP}[a] (μM)	K_i^{PGA} (μM)
No SO_4^{2-}	140±19	78±6	120±5	1.1±0.38	3.1±1.0	250±40	70±14	40±20[b] 600±150[c]
+ SO_4^{2-}	500±35	1150±213	230±39	-	-	-	725±178	570±130[b] 450±100[c]

[a] The inhibition constant (K_i) is obtained from the kinetic studies by extrapolating to the "zero" 3-PGA concentration.

[b] K_i values are obtained from the slopes of the secondary plots for noncompetitive and mixed inhibition patterns.

[c] K_i values are obtained from the 1/v axis intercepts for noncompetitive and mixed inhibition patterns.

Table III-1. Dissociation Constants and the Enhancement of Longitudinal Relaxation Rates ($1/T_{1p}$) in the Binary and Ternary Complexes of CrATP, PGK, and 3PGA.

Complex	n (# of binding sites)	K_D, K_I or K_A' [a] (mM)	ε_a or ε_b [b]
CrATP•3PGA	ND[c]	12.2±2.3	1.14±0.05
PGK•CrATP	1.2±0.4	0.060±0.019	1.46±0.12
PGK•CrATP•3PGA	0.95±0.1	0.55±0.12	ND
PGK•CrATP•3PGA + SO_4^{2-} [d]	0.85±0.06	0.90±0.070	ND
PGK•CrATP•3PGA + SO_4^{2-} [e]	3.0±0.38	6.0±0.450	ND

Table III-1 (cont.)

[a] Binary dissociation constants K_I and K_D are defined respectively as:

$K_I = [CrATP]_f[3PGA]_f/[CrATP \cdot 3PGA]$ and

$K_D = [CrATP]_f[Enzyme]_f/[Enzyme \cdot CrATP]$.

The dissociation constant (K_A') of CrATP from the ternary enzyme·CrATP·3PGA complex is defined as : $K_A' = [CrATP]_f[Enzyme \cdot 3PGA]_f/[Enzyme \cdot CrATP \cdot 3PGA]$.

[b] ε_a and ε_b are the enhancement of the paramagnetic effects of CrATP on the longitudinal relaxation rates of water protons in the binary CrATP·3PGA and Enzyme·CrATP complexes respectively.

[c] Due to very small changes in the observed enhancements the data could not be used for Scatchard analysis.

[d] Represents the high affinity site.

[e] Represents the low affinity sites.

Table IV-1. Corrected relaxation rates and Cr^{3+}-nucleus distances in the PGK·CrATP·3PGA complex[a]

Nucleus	No sulfate		With sulfate	
	$1/fT_{1p}$ (s^{-1})	r (Å)[b]	$1/fT_{1p}$ (s^{-1})	r (Å)[b]
H2	6050±551	4.92±.21	571±51	7.26±.21
H3	4030±262	5.27±.21	73±7	10.21±.48
H3′	20,400±1590	4.02±.16	170±20	9.09±.26
P	250±32	6.22±.26	40±3	8.61±.19
C1	78±20	6.46±.39	61±17	6.88±.37
C2	280±140	5.23±.37	48±24	7.02±.55
C3	841±420	4.35±.46	ND[c]	ND[c]

[a] The corrected longitudinal relaxation rates ($1/fT_{1p}$) are given in the table; in addition, the corrected transverse relaxation rates ($1/fT_{2p}$) were calculated for phosphorous only. The values obtained were 55,600 and 54,038 s^{-1} in the absence and presence of sulfate, respectively.

[b] The errors shown in the absolute distances include 4-20% error in the measurement of $1/fT_{1p}$ from the binary PGK·CrATP titration, 6.5-50% error in the measurement of $1/fT_{1p}$ from the ternary titrations, 8.8% error in the estimation of τ_c, and either 21.8% or 7.8% error in the measurement of the dissociation constant of CrATP from the ternary complex in the absence or presence of sulfate, respectively.

[c] ND, not determined.

Table IV-2. Frequency dependence of the corrected and normalized relaxation rates and correlation times in the ternary PGK·CrATP·3PGA complex[a]

Frequency (MHz)	$1/fT_{1p}$[b] ($s^{-1}x10^{-6}$)	τ_c[b] ($sx10^{10}$)	$f(\tau_c)$[b] ($sx10^{10}$)
15.0	1.54	2.83	8.54
24.3	1.92	2.83	8.50
42.0	2.56	2.84	8.48
59.0	2.45	2.85	8.47
250	2.16	3.33	7.84
400	1.71	4.08	5.97

[a] The solution contained 383 μM PGK, 187 μM CrATP, 5.2 mM 3PGA, and 60 mM NaCl in 40 mM MES-NaOH pH 5.9, at 22°C. No difference was detected when the experiment was repeated with sulfate included.

[b] Determined from the frequency dependence of the normalized longitudinal relaxation rates ($1/fT_{1p}$) of water protons at frequencies indicated and analyzed according to the equation $1/\tau_c \sim 1/\tau_s = B[\tau_r/(1+\omega_s^2\tau_r^2) + 4\tau_r/(1+4\omega_s^2\tau_r^2)]$ and equations and given in text where τ_c is dipolar correlation time, ω_s is electron precession frequency, τ_s is the longitudinal electron spin relaxation time, B is the zero field splitting parameter, and τ_r is a time constant for ligand motion that modulates B. The correlation times shown above is from the best fitted curve to the data points which also yielded $B = 3.16x10^{21}$ s^{-2} and $\tau_r = 2.51x10^{-13}$

Table IV-3. MARDIGRAS calculated distances[a] for proton pairs of dATP.

NOE Interaction	r (Å) 18:1 ratio[b]	r (Å) 22:1 ratio[c]
H2″-H4′	3.43	3.43
H2′-H5′5″	3.83	4.12
H1′-H4′	2.96	3.24
H2″-H1′	2.30	2.48
H2′-H8	2.58	2.84

[a] Distances were calculated with while imposing the following distance constraints: H2′-H2″ = 1.78 Å ; H2′-H1′ = 2.92 Å.

[b] The RMS and % errors were 1.0 Å and 20%, respectively.

[c] The RMS and % errors were 1.2 Å and 22%, respectively.

VITA

Jay Dwight Gregory was born on April 10th, 1964 in Huntington Park, California. Soon after, he and his family moved to Arkansas; he grew up in various communities in the central Arkansas area, graduating from Cabot High School in 1982 (alongside his future wife, Donna Goodwin, unbeknownst to the both of them). He began college at the University of Arkansas, Fayetteville, in the fall of 1982. He and Donna were married in the spring of 1984. Following a move to Fairbanks, Alaska, he continued study for a year at the University of Alaska, Fairbanks; the couple ended up in Seattle, Washington, where Jay completed his degree at the University of Washington, receiving a Bachelor of Arts degree in Chemistry in the summer of 1988. He then entered the Ph.D. program in Biochemistry at the University of Tennessee in Knoxville. Midway through his degree program, in November of 1990, Jay and Donna were blessed by the arrival of a beautiful daughter, Emma. He completed his Ph.D. in August of 1993, and has accepted a position as Assistant Professor at Culver-Stockton College in Canton, Missouri, beginning in August of 1993.